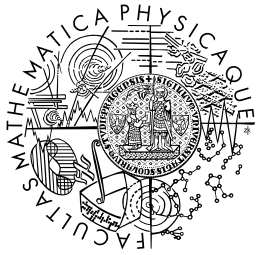

FACULTY
OF MATHEMATICS
AND PHYSICS
Charles University

DOCTORAL THESIS

Jakub Řada

Synthetic geometry in various dimensions

Mathematical Institute of Charles University

Supervisor of the doctoral thesis: Mgr. Lukáš Krump, Ph.D.

Study programme: General Questions of Mathematics and Computer Science

Study branch: General Questions of Mathematics and Computer Science

Prague 2024

I declare that I carried out this doctoral thesis independently, and only with the cited sources, literature and other professional sources. It has not been used to obtain another or the same degree.

I understand that my work relates to the rights and obligations under the Act No. 121/2000 Sb., the Copyright Act, as amended, in particular the fact that the Charles University has the right to conclude a license agreement on the use of this work as a school work pursuant to Section 60 subsection 1 of the Copyright Act.

In ..... date ....

Author's signature

To all,

the invisible helping phantoms

with all our love.

Title: Synthetic geometry in various dimensions

Author: Jakub Řada

Department: Mathematical Institute of Charles University

Supervisor: Mgr. Lukáš Krump, Ph.D., Mathematical Institute of Charles University

Abstract: This doctoral thesis focuses on synthetic geometry in various dimensions. We start with plane geometry to show how synthetic geometry can be used in proofs. We demonstrate the advantages of synthetic geometry on two different geometric proofs of the Pappus–Pascal theorem, the construction of the osculating circles of an ellipse at any point of the ellipse and the graphical solution of a quadratic equation. Moreover, the thesis describes visualisation of the n-dimensional space using the "behind" view method and perpendicular layering. Furthermore, the thesis focuses on visualisation of 4-dimensional space. It describes two possible methods: a generalisation of Monge's projection (orthogonal projection onto two mutually perpendicular subspaces) and a generalisation of linear perspective. Finally, the thesis contains applications of the visualisation of 4-dimensional space. For example, the usage of the generalised Monge's projection and 4-dimensional perspective for representation of the complex number plane. The application for visualisation of shadows in 4-dimensions synthetically and algebraically, and for representation of 4-dimensional objects using 3D printing.

Keywords: algebraic geometry, descriptive geometry, multidimensional geometry, 4D perspective, double orthogonal projection

Contents

Introduction

Geometry is all around us. Even before humans were here, nature played with geometric shapes and patterns. We can find the golden spiral in a sunflower, a mollusc shell or a pineapple. The eggs we eat without noticing are made up of two different ellipsoids, and the filaments of caterpillars form gossamer webs close to hyperbolic paraboloids. Geometry surrounds us in beautiful patterns. Kvasz begins his book on painting (Kvasz [2020]) with the words: "Painting, like geometry, is based on the incomprehensible mystery of seeing. Through seeing, we constantly acquire much information about our surroundings. In addition to this experiential dimension, visual perception has an aesthetic dimension."

It is possible to represent almost any geometry with equations. This is useful with developed computer science, but it is a great pity because we miss out the visual aspect of geometry. Fortunately, with the advent of modern technology, synthetic geometry is making a comeback in computer graphics.

The earliest recorded beginnings of geometry come from ancient Babylon, around 3000 BC. Geometry at that time was a collection of empirical needs to measure lengths, angles, areas and volumes of simple geometric solids. It was based on experience in surveying, construction, astronomy, and various trades. They probably did not deal with proofs and more general generalisations (Kline [1990]). In ancient Greece in the 7th-5th centuries BC, mathematicians built on previous knowledge by trying to generalise and prove. They were no longer just concerned with how to count but why.

Classical geometry focused on constructions using the compass and ruler. Euclid made a revolution in geometry. He introduced the mathematical rigour and axiomatic method that is still used today. His book *The Elements* (Hypsicles and Mocenigo [1482]) is widely regarded as the most influential textbook of all time and was known to all educated people in the West until the mid-20th century (Eves [1964]).

From the 1st century BC, the ground plans of temples, axial sections of columns and pillars or drawings of statues were drawn on paper. Information about ancient drawings is given in the books Kadeřávek [1997], Kadeřávek [1954]. Vitrius used three methods of representing objects on the plane: ichnography, orthography and scenography. Ichnography and orthography correspond to orthogonal projection, while scenography corresponds to perspectivity (Pollio et al. [2001]). These ancient constructions mainly represented exceptional cases and were not unambiguous. As late as the 13th century, orthogonal projections (ground, front and side views) were placed independently and at different scales, see Honnecourt [2012]. Albrecht Dürer in 1525 in his publication *Underweysung der Messung, mit dem Zirckel und Richtscheyt, in Linien, Ebenen unnd gantzen corporen* (Dürer [1966]) presented several constructions in orthogonal projection on two mutually perpendicular planes. Each drawing was still about mapping space onto the plane, not solving spatial problems in the plane. Dürer concentrated, among other things, on plane curves. He constructed conics as cuts of a cone.

Descartes then explored analytic geometry and the Cartesian coordinate system (Descartes [2001]).Brunelleschi introduced the one-point perspective (Janson

[2023]) which will be generalised to 4D in this thesis. Monge's projection (Monge [1847]) will also be generalised to a higher dimension in this thesis. The author of Monge's projection is the French mathematician Gaspard Monge.

A large part of the work will focus on 4D geometry. For this purpose, it is appropriate to start with the essay "What is the fourth dimension?" by Hinton [1880]. A good answer can be found in the novel Flatland by Abbott [2015]. Rucker [2014] and Kaku [1995] are another breathtaking science fiction novel about introduction to four-dimensional space. For a brief history of multidimensional geometry, particularly synthetically constructed four-dimensional geometry, see Manning [1914]. Work on the synthetic visualisation of points and lines of four-dimensional space in planes was written by Lindgren and Slaby [1968], and an analytical approach and differential geometry in four-dimensional space is described in Forsyth [1930]. Stachel [1990] proves an analogue of the right angle theorem in the orthogonal projection of a four-dimensional space onto a plane. There is no need to stop at four-dimensional geometry; Weiss [1997] visualises n-dimensional Euclidean space on a plane.

Most of the work consists of published articles, and this thesis will focus on visual geometry. Of course, analytical geometry is also used in this work, as some constructions and proofs need to be supported by calculations. This thesis aims not to create a complete textbook of synthetic geometry bypassing analytical geometry. This thesis aims to focus on the synthetic approach in some areas of geometry.

The first part of the thesis focuses on plane geometry, where we show some graphical proofs. The inspiration for this part of the thesis was the book *Geometry in figure* by Akopyan [2017], where a proof is demonstrated using only one figure. Descartes (translated by: J. Fiala), R. [2010] and Glaeser et al. [2016] are other authors who use drawings for proofs. The purpose of this chapter is to make the reader wonder whether it is necessary to use analytic geometry directly for proofs, or whether there are other ways of doing proofs. This chapter is based on two articles Řada [2022b] and Řada [2023]. Both articles focus on geometric proofs rather than using algebraic proofs.

The second chapter is an introduction to 4D geometry. It tries to explain how the reader can understand and imagine 4D geometry. The beginning of this chapter is based on a talk *"Walking through a wall using 4D space (Analogies up to 4D space)"* given at Day of Doctoral Students 2021. The presentation is mainly based on the book Flatland (Abbott [2015]).

The third chapter is a summary of the main principles of double orthogonal projection on two perpendicular three-dimensional spaces inspired by Bogdan and Serbanoiu [2021], Zamboj [2018b], Řada and Zamboj [2021], Zamboj [2019].

The fourth chapter explains the 4D perspective in detail. It explains the basic principles of the 4D perspective, followed by a conference paper *3-sphere in a 4-perspective* Řada and Zamboj [2021] which discusses the representation of the 3-sphere in a 4-perspective, including a cut of the 3-sphere with a 3-space.

Chapter five describes the use of 4D visualisations. This chapter includes the article on the complex number plane Řada and Zamboj [2023]. The complex number plane could be a four-dimensional space so that we can visualise it with a double orthogonal projection onto two mutually perpendicular 3-spaces or with a 4D perspective. Another part of the fifth chapter focuses on 3D shadows of a

4D Algebraic hypersurfaces in a 4D perspective. This part is based on the article

It is also essential to be able to imagine and grasp the 4D space. It jumps over two dimensions from paper to 4D space, but from 3D space to 4D space, it is only one dimension. This is why 3D printing is suitable for representing 4D space. This is the subject of the article *3D printed models of a tesseract in double orthogonal projection, and 4D perspective* Řada and Zamboj [2020].

Throughout the text, we use many figures with the same constructions. It is, therefore, pointless to draw all from zero. Therefore, the appendix B gives some hints on how to make the work easier when using GeoGebra. The thesis contains many figures created in GeoGebra Hohenwarter and Hohenwarter [2002] using shortcuts from the article in the appendix. The rest of the figures are programmed in the computer program Mathematica Wolfram [1999].

The thesis begins by demonstrating the strength of the geometry. It is necessary to be able not only to visualise objects but also to work with displayed objects on paper (measuring, cutting, ...). The work then moves on to the main objective of the thesis, which is to introduce the reader to 4D geometry. This shows the reader how to perceive the 4D world and draw 4D space on paper. The work continues with the practical use of virtualising 4D geometry. In my diploma thesis Řada [2019] it was very difficult to imagine the complex number plane. This work gives a way how to visualise and work with the complex number plane. Only a few papers are devoted to visualising the complex number plane. Most papers skip the complex representation and show only the real x, y plane. The work also includes algebraic shading. Many computer programs use point shading. They take a ray of light through each point of the scene and look at where each point is lighted. In this part, we use an algebraic representation of solids and look at their shadows algebraically. The shadows are done in 3D and 4D geometry.

1. Some geometric construction and proofs

1.1 Introduction

The methods of synthetic geometry are powerful, and their use can simplify some proofs compared to analytical ones. Historically, but also nowadays, many proofs of geometric constructions are based on analytical calculations. However, for many analytical proofs, it is possible to find a synthetic geometric proof that additionally develops logical thinking (Molnár [2009], Tomić et al. [2019]). There are even a few authors who sometimes primarily use geometric proofs that are based only on figures. For example, (Bogomolny and Taleb [2020]) in his book uses some proofs based on figures, and (Akopyan [2017]) in his book proved a geometric statement with only one figure. In many countries, geometry in secondary schools has almost disappeared from the curriculum. It was replaced by calculus, and the same efforts were made in the Czech Republic (Moravcová [2016]).

This chapter is divided into three sections. The first part is devoted to the Pappus–Pascal theorem. We prove this theorem using three different proofs (using homogeneous coordinates, using perspective view and using projectivity). The second part describes the construction of the osculating circle of any point of the ellipse. This part is inspired by the book *The Universe of Conics: From the ancient Greeks to 21st-century developments* (Glaeser et al. [2016]). The third section of this chapter is focused on quadratic equations. In this section, we describe how to solve a quadratic equation graphically.

At first glance, the three parts of this chapter have nothing in common. However, all three sections are devoted to planar geometry and allow the reader to look at classical problems through geometric glasses.

1.2 Pappus–Pascal's theorem

The Pappus–Pascal's theorem is one of the fundamental theorems of projective geometry. The theorem was initially stated by *Pappus of Alexandria* in the 4th century in *Pappus's Collection, book VII.* (Jones [2013]) as *Pappus's hexagon theorem.* In the 17th century, the French philosopher and mathematician Blaise Pascal generalized this theorem to the case where points A to F lie on a conic. Pascal formulated his *Pascal's theorem* in 1639 when he was 16 years old and published it as a broadside titled *Essay pour les coniques* (Biggs [1981]). Later, the theorem was generalized into Pappus–Pascal's theorem.

Theorem 1 (Pappus's hexagon theorem) *Let A, B, C be three points on one line and D, E, F be three points on another line. If $\overline{AE}$ intersect $\overline{BD}$ at X, $\overline{AF}$ intersect $\overline{CD}$ at Y, and $\overline{BF}$ intersect $\overline{CE}$ at Z, then the three points X, Y, Z are collinear.*

Theorem 2 (Pascal's theorem) *Let the points A, B, C, D, E, F be given. Morover suppose that the three intersections $X = (\overline{AE} \times \overline{BD})$, $Y = (\overline{AF} \times \overline{CD})$, $Z =$*

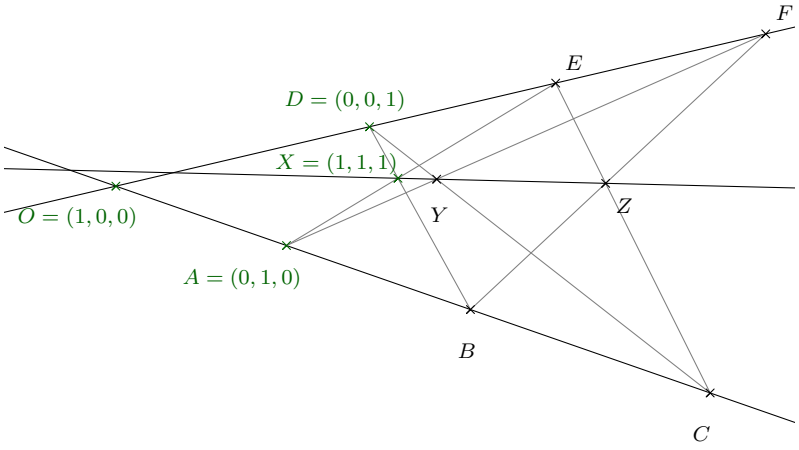

Figure 1.1: Proof of the Pappus's hexagon theorem based on homogeneous coordinates.

$(\overline{BF} \times \overline{CE})$ *exist.*
The three points X, Y, Z *are collinear if and only if the point* A, B, C, D, E, F *lie on the same conic.*

Theorem 1 deals with points on straight lines, theorem 2 deals with points on a conic. We can generalize both theorems into one theorem below.

Theorem 3 (Pappus–Pascal's theorem) *Let* A, B, C, D, E, F *be six different points in a plane. Points* A, B, C, D, E, F *lie on a conic if and only if the three points* $X = (\overline{AE} \times \overline{BD}), \quad Y = (\overline{AF} \times \overline{CD}), \quad Z = (\overline{BF} \times \overline{CE})$ *are collinear.*

Let us start with the most common proof of Pappus's hexagon theorem, which is based on homogeneous coordinates (Mathcam [2013]).

Proof of the Theorem 1. Without loss of generality, let us choose homogeneous coordinates such that:

$$A = (0, 1, 0),\ D = (0, 0, 1),\ X = (1, 1, 1),\ O = (1, 0, 0),$$

where O is intersection of lines $\overline{ABC}$ and $\overline{DEF}$. We have

$$\overline{OA} \cup \overline{DX} = B = (1, 1, 0), \quad \overline{AX} \cup \overline{OD} = E = (1, 0, 1).$$

Assuming that $A \neq C$ and $D \neq F$ we get

$$C = (1, s, 0), \quad F = (1, 0, t),$$

where $s, t \in \mathbb{R}$. Then the remaining points are

$$\overline{AF} \cup \overline{CD} = Y = (1, s, t), \quad \overline{BF} \cup \overline{CE} = Z = (1 - st, s - st, t - st).$$

Points X, Y, Z are collinear because $Y = Z + stX$. The situation is illustrated in figure 1.1. □

Let us introduce the first geometric proof in this paper which is based on a perspective view.

Proof of the Theorem 1. Let the lines between the collinear points ABC and DEF be parallel. In Euclidean space or a perspective, parallel lines intersect at a line at infinity. Parallel lines in a ground plane $\pi(x, y)$ intersect at a point on the horizon line h. In this case, the parallel lines $\overline{AE}$ and $\overline{BF}$ intersect at point X, the parallel lines $\overline{AD}$ and $\overline{CF}$ intersect at point Y, and the parallel lines $\overline{BD}$ and $\overline{EC}$ intersect at point Z. All three intersection points X, Y, Z lie on the horizon h (fig. 1.2b) or at the line at infinity l_∞ (fig. 1.2a).

□

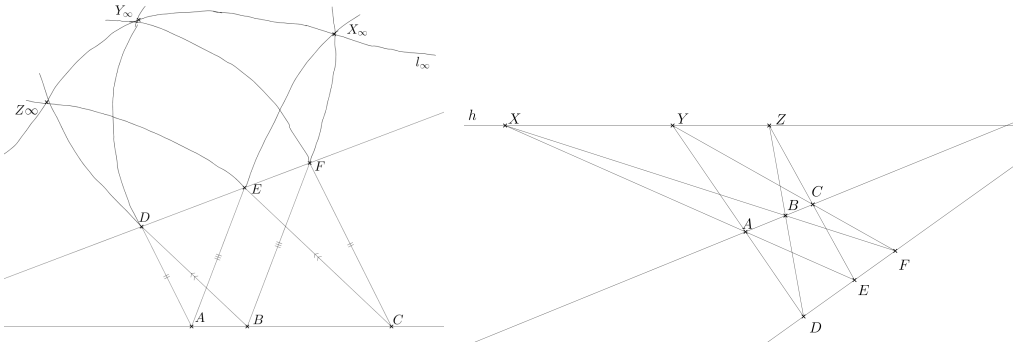

(a) Parallelism with the line at infinity

(b) Perspective point of view

Figure 1.2: Proof of the Pappus's hexagon theorem based on parallelism/perspective

There are several proofs of the Theorem 2. We will present one that uses collinearity, projectivity, and Steiner's definition. For clarity, we recall here this definition.

Definition 1 (Steiner's definition) *Let two pencils of lines at two points H, H' and a projective but not perspective mapping π from H to H' be given. For any line a in pencil H we have $\pi(a) = a'$ in pencil H'. The intersection points of corresponding lines $(a \cap a')$ form a non-degenerate projective conic section.*

Theorem 4 *In the projective plane, any projectivity between two different ranges h and h' of points can be created as the product of at most two perspectivities between ranges.*
A projetivity is a perspectivity if, and only if, the point $h \cap h'$ is mapped onto itself.

Using *Definition* 1 and *Theorem* 4, we can prove the Pappus–Pascal's theorem on the conic.

Proof of the Theorem 2. We prove the two implication separately.

1. There are 6 points on the conic $c = \{A, B, C, D, E, F\}$. According to Steiner's definition 1, we put $H = A$ and $H' = C$. The projectivity α from the pencil H to the pencil H' generates conic c. The straight line $h = \overline{DE}$ is in a perspectivity from the pencil H, and the straight line $h' = \overline{EF}$ is in a perspectivity from the pencil H'. According to the Theorem 4, h and h' are linked with a projectivity β, which is a perspectivity,

because $\alpha(E) = E$. The projectivity β sends $X = \overline{HB} \cap h$ to $Z = \overline{BH'} \cap h'$ because $\alpha(\overline{HB}) = \overline{BH'}$ [$\alpha(\overline{AB}) = \overline{BC}$]. Since β is pesrpective on X and $Z = \beta(X)$ is collinear with Y, which is the center of perspectivity β. Let $D' = \overline{H'D} \cap h'$ and $F' = \overline{HF} \cap h$. Using $\alpha(\overline{HD}) = \overline{H'D}$, we obtain $D = \beta(D')$ and $\beta(D') = D$. Similarly, it follows from $\alpha(\overline{HF}) = \overline{H'F}$ that $F = \beta(F')$ and $\beta(F') = F$. Therefore, the center of perspective is the point Y, found as $Y = \overline{DD'} \cap \overline{FF'}$ (Figure 1.3).

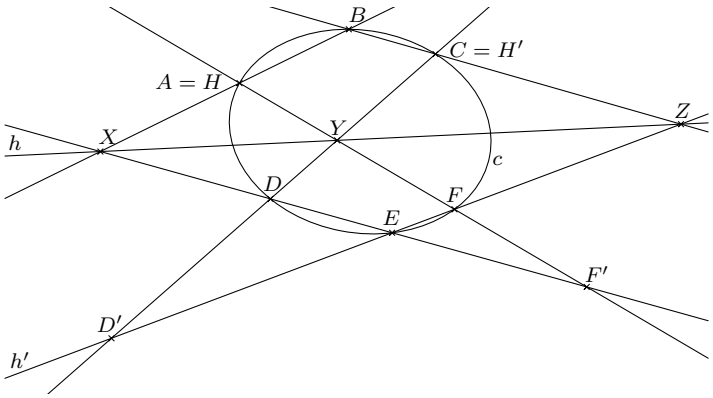

Figure 1.3: Geometric proof of collinearity of points X, Y, Z based on projectivities

2. Every conic is uniquely given by 5 points A, B, C, D, E. We need to prove that the point F lies on the same conic c. The chain β of perspectivities from pencil H to the line h and further to the line h' with the center in Y and then through the line h' to the pencil H' is a projectivity because it is a finite chain of perspectivities. Then β is well-defined and $\overline{HB} \to \overline{BH'}, \overline{HD} \to \overline{DH'}$ and $\overline{EB} \to \overline{EH'}$ for X, Y, Z are collinear. Therefore, the chain β is a factorization of the projectivity α and therefore $\overline{HF} \to \overline{FH'}$. Therefore, points A, B, C, D, E, F lie on the same conic c.

It is also worth mentioning that according to Steiner's definition 1, it does not matter which point is labelled as H and H'. □

Another geometric proof of Pappus–Pascal's theorem exists. For example, (Richter-Gebert [2011]) shows a proof based on double-ration and a proof via oriented triangle area, (Braun and Narboux [2017]) uses Tarski's geometry in proofs and (Roscoe [2021]) nicely reinterprets the proof of Pappus–Pascal's theorem using determinants.

Geometry is suitable not only for proofs but also for constructions. In differential geometry, an osculating circle exists at any point in an ellipse. The center of that osculating circle can be computed by curvature. In descriptive geometry, osculating circles are drawn only at the vertices of an ellipse. Usually, no general construction of an osculating circle is given. The following section describes the geometric construction of the center of the osculating circle.

1.3 Osculating circle of an ellipse

Description of osculating circles is often based on differential geometry:

"The osculating circle of a curve c at a given point P is the circle k that has the same tangent as c at point P as well as the same curvature. Just as the tangent is the line best approximating a curve at a point P, the osculating circle is the best circle that approximates the curve at P." (Gray [1997], pp. 111).

The set of all centers of the osculating circles forms an evolute (figure 1.4), where the cusps[1] are the centers of the osculating circles at the vertices of the ellipse. There are many constructions of osculating circles at the vertices of the ellipse. An ellipse is often drawn according to the plotted osculating circles in descriptive geometry. Let us begin constructing an osculating circle at any point of the ellipse.

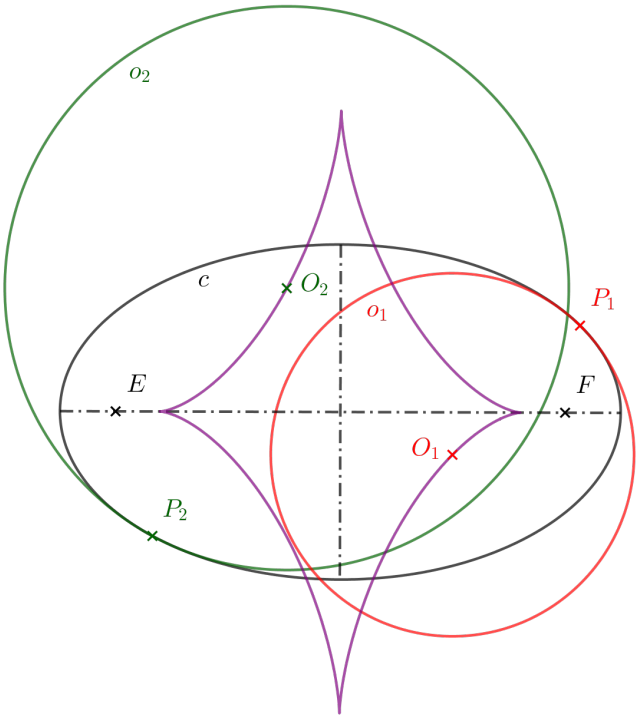

Figure 1.4: Evolute of an ellipse

Let c be a given ellipse, C a center and a, b the axes of this ellipse. Moreover, let P be an arbitrary point of the ellipse c, which is not equal to any of its vertices. We construct the tangent t to the conic c at the point P (see figure 1.5). We continue as follows:

1. We find a point P' and a tangent t' axisymmetric along one of the axes of the ellipse (WLOG a).

2. We draw a straight line r parallel to the tangent t' through the point P

3. The straight line r intersects conic c at points P and R. (Point R also lies on the osculating circle)

4. We find a line n_P normal to the tangent t at the point P (line n_P is perpendicular to the line t at the point P).

[1]Cusp is a point of a curve, where the moving point must reverse direction. It is a type of singular point of a curve.

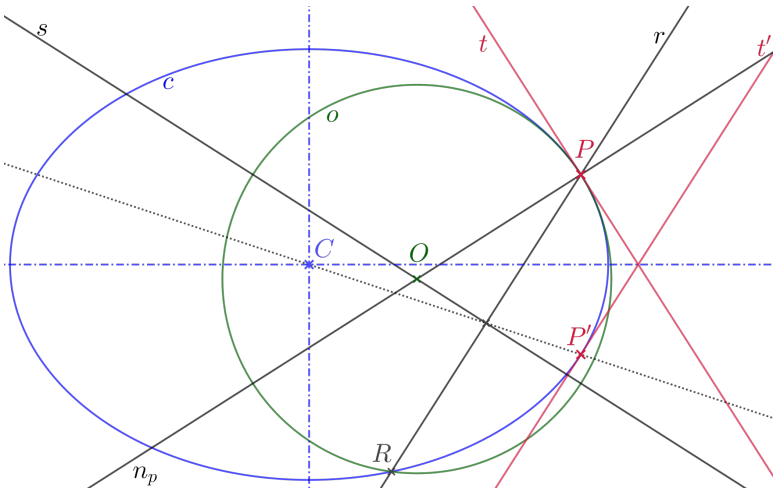

Figure 1.5: Construction of an osculating circle

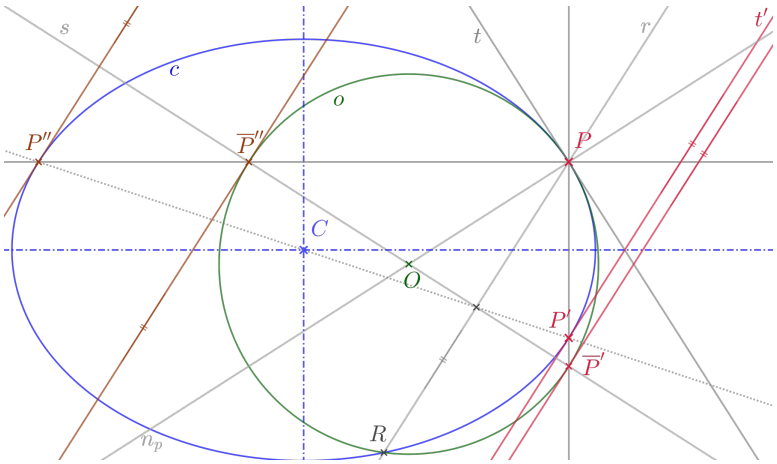

Figure 1.6: The Osculating circle o as collinear image of c

5. We draw a line s perpendicular to the line r at a point of intersection of lines $\overline{CP'}$ and r.

6. Then the lines s and n_P intersect at the center O of osculating circle o of the ellipse c at the point P.

The correctness of this construction could be verified using differential calculus. In this paper, we prefer a verification using projective geometry.

Firstly, we need to show that the center O of the osculating circle o lies on the normal line n_p. It follows from the basic knowledge of differential geometry.

Secondly, the osculating circle o and the ellipse c osculate each other at the common point P because perspective collineation exists with the center at P and the axis t. It follows from the fact that the straight line r of an elation passes through the point P. Finally, we need to prove that the tangents of the ellipse c parallel to the straight line r are mapped to parallel tangents of the circle o. Elation is a particular case of axial affinity, where the direction of the affinity is parallel to the axis of the elation. Therefore, we can conclude from figure 1.6 that tangents of the ellipse c parallel to straight line r are mapped to parallel tangents of the circle o. Therefore, we can say that o is the osculating circle of the ellipse

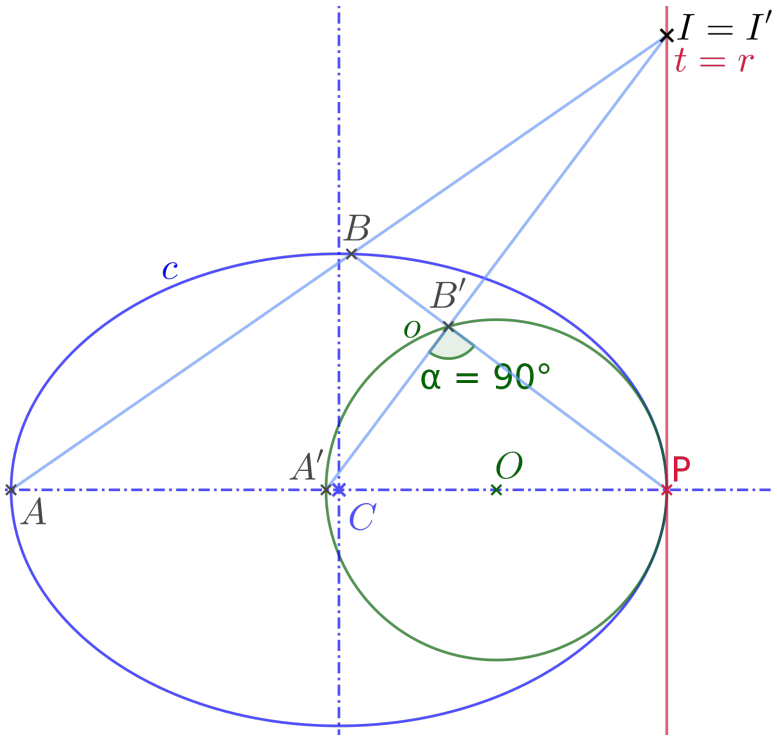

Figure 1.7: Hyperosculating circle

c at point the P.

We will now consider the previously omitted case of the osculating circle in the vertices. In the figure 1.7, there is the given ellipse c and the searched circle o. The tangent t through the vertex P is identical to the line r from the previous construction. Therefore, an invariant point on the tangent line t has to exist. For this reason, collinearity centred at the invariant point maps the ellipse c to the circle o.

Geometric constructions can also be used for various calculations. Instead of the sum of two natural numbers, we can connect two line segments. We can also compute the difference, ratio, product and more. With all of this, it is possible to compute the roots of quadratic equations with some limiting factors.

1.4 Solving a quadratic equation graphically

The quadratic equation is usually solved using the discriminant or product decomposition. In this section, we will show another method of finding the roots of a quadratic equation using a ruler and a compass (the so-called Euclidean construction).

Finding the roots of a quadratic equation classically

A general quadratic equation is given by $ax^2+bx+c=0$, where $a, b, c \in \mathbb{R}, a \neq 0$. One way how to solve quadratic equations is via discriminant, where the roots are

$$x_{1,2} = \frac{-b \pm \sqrt{b^2 - 4ac}}{2a}.$$

Another method used is product decomposition using Viète formulas. In this case, the equation is decomposed into the product

$$ax^2 + bx + c = a(x - x_1)(x - x_2),$$

where x_1 and x_2 are the roots of the quadratic equation since they satisfy $x_1 + x_2 = -\frac{b}{a}$ and $x_1 x_2 = \frac{c}{a}$. These two methods are described in detail in the textbook Equations and Inequalities (Charvát et al. [1999]). Now, we will describe an unconventional method of finding the roots of a quadratic equation by using the planimetric construction described by Descartes in his book *La Géométrie* (Descartes (translated by: J. Fiala), R. [2010]).

Finding the roots of a quadratic equation graphically

First, let the general quadratic equation be modified to the normalized form and express x^2

$$x^2 = px + q, \text{ where } p = \frac{-b}{a}, \ q = \frac{-c}{a}.$$

Construction of the roots for the case $q > 0$:

Let triangle MNO (figure 1.8a) be a right-angled triangle with right angle at vertex M with the sides of length $|MN| = \sqrt{q}$ and $|MO| = \left|\frac{1}{2}p\right|$. (The reader will recall that a right angle can be constructed using a compass and ruler). Then we construct a circle k centred at O with radius $|MO|$. Let us denote the points P and Q as intersections of the circle k with the extended side of the triangle ON. Then the lengths $|PN|$ and $|QN|$ are the roots of the quadratic equation except for the sign since the distance is always positive. We will determine the sign later.

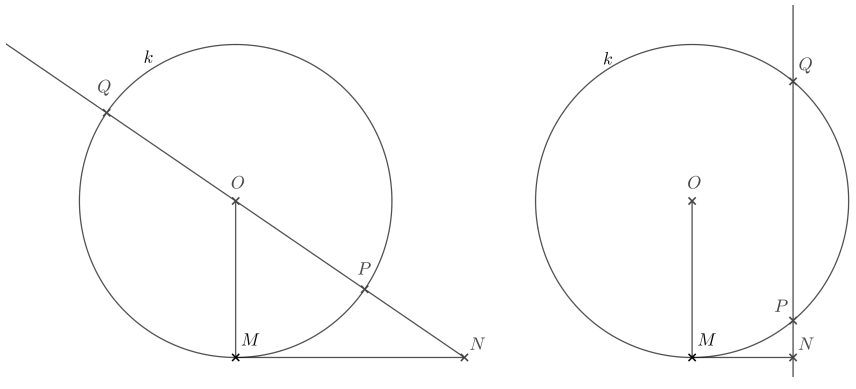

(a) Case $q > 0$ (b) Case $q < 0$

Figure 1.8: Roots of a quadratic equation $x^2 = px + q$ graphically.

Theorem 5 *Lengths $|PN|$ and $|QN|$ from construction above are the roots of quadratic equation $x^2 = px + q$, where $p = \frac{-b}{a}, q = \frac{-c}{a}$, except for signs.*

Proof. The roots of x_1, x_2 should be equal to the distances

$$x_1 = |PN| = |ON| - |OP| \text{ and } x_2 = |QN| = |ON| + |OQ|$$

except for the sign. Since $|OP| = |OQ| = |OM|$, we can simplify equations into

$$x_{1,2} = |ON| \pm |OM|.$$

According to the Pythagorean theorem, the length of the side $|ON|$ is

$$|ON| = \sqrt{\left(\frac{1}{2}p\right)^2 + (\sqrt{q})^2} = \sqrt{\frac{b^2}{4a^2} + \frac{-c}{a}} = \frac{\sqrt{b^2 - 4ac}}{2a}.$$

Thus, the solutions we are looking for is

$$x_{1,2} = |ON| \pm |OM| = \frac{\sqrt{b^2 - 4ac}}{2a} \pm \frac{b}{2a}.$$

It proves that the distances found are equal to our discriminant formula except for the sign because the distance cannot be negative. □

Construction of the roots for the case $q < 0$:

In this case, we start the same as the previous construction except that we put $|MN| = \sqrt{-q}$ (figure 1.8b). Thus, $|OM| = \left|\frac{1}{2}p\right|$ and $k(O, |OM|)$ remain the same. Then, we construct a parallel line with the line OM passing through the point N. (The reader will recall that we can construct a parallel line through a given point with a ruler and a compass). Let us denote the points P and Q as intersections of the circle k with the parallel line. The length of $|NP|$ and $|NQ|$ determine the sizes of the roots (again, except for the sign, which we will determine later).

The proof of this construction for the case $q < 0$ is analogous to proof ot the theorem 5.

Existence of solutions and constructability

The quadratic equation has no solution in $\mathbb{R}$ if the discriminant is negative. Similarly, constructions cannot be performed.

- If $a = 0$, the construction cannot be used. It is not a quadratic equation.
- If $b = 0$, the side of the triangle $|MO| = \frac{1}{2}p$ cannot be constructed. Construction is reduced to a line segment (figure 1.9a) of length $\sqrt{q}$. In this case, we get a purely quadratic equation. The equation has the same solution, again, except for the sign.
- If $c = 0$, the right triangle MNO is reduced to a line segment because the points M and N are identical(figure 1.9b). Then the roots are $x_1 = |ON| - |OM| = 0$ and $x_2 = |ON| + |OM| = 2|OM| = 2\left|\frac{1}{2}p\right| = \left|\frac{-b}{a}\right|$. It corresponds to an equation without the absolute term $0 = ax^2 + bx = x(ax + b)$, again, except for the sign.

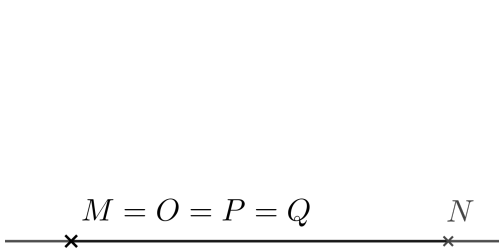

(a) A purely quadratic equation $ax^2 + c = 0$.

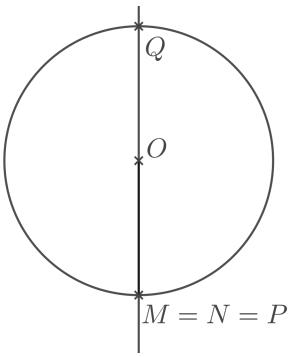

(b) Quadratic equation without absolute term $ax^2 + bx = 0$

Figure 1.9: Roots in special cases of quadratic equations

Determination of the sign

We conclude from an interactive version of the first construction in Geogebra (Řada [2022a]) that one root is always positive and the other negative. We justify it by using the fact that the product of the roots is equal to $\frac{c}{a}$. Since the sum of the roots is equal to $\frac{-b}{a}$ we get roots: for $p > 0$, $-|PN|,\ +|QN|$ and for $p < 0$, $+|PN|,\ -|QN|$.

The second construction (again, the interactive version of Řada [2022a]) says that both roots are positive or negative.
For $p > 0$, $+|PN|,\ +|QN|$ are roots,
for $p < 0$, $-|PN|,\ -|QN|$ are roots.

Auxiliary constructions

In the previous part, we used some mathematical operations to find the solution of the quadratic equation graphically; however, we would prefer to find the roots only with a ruler and a compass. Therefore we need to present a few necessary constructions (Pomykalová et al. [1993]).

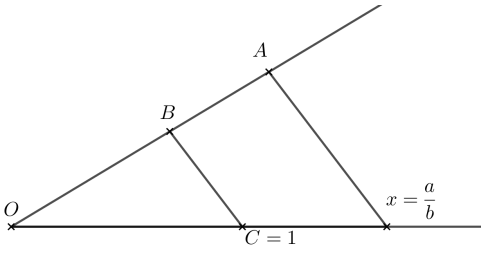

(a) Construction of the ratio of two numbers

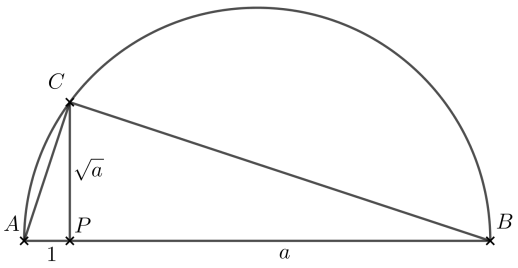

(b) Constructing of the square root of a positive number

Figure 1.10: Constructions instead of calculus

First, we need to introduce the construction of the fraction of two numbers $\frac{a}{b}$ (image 1.10a). This construction is based on the similarity of triangles. Let us

denote the unknown length by x. We modify $x = \frac{a}{b}$ to the form

$$\frac{x}{1} = \frac{a}{b} \quad (\text{or } x : 1 = a : b).$$

We choose any angle with vertex O. We construct segments of length $a = |OA|$ and $b = |OB|$ one arm, and we plot the length of the line segment $1 = |OC|$ on the other arm. Then, we draw a line through A parallel to the line joining BC and determine its intersection with the other arm. The distance between this intersection and the point O is the distance we are looking for.

Next, we need to know how to construct the square root of a (figure 1.10b). Therefore, we use Euclid's theorem. We construct a line segment AB of length $a+1$. We divide the line segment by the point P into two parts $|AP| = 1 \wedge |BP| = a$. Then, we construct a circular arc over the line segment AB. Next, we draw a perpendicular line to the line AB through the point P and mark the intersection point C of the perpendicular line with the circular arc. The distance $|CP|$ equals the distance $\sqrt{a}$.

1.5 Conclusion

In this chapter, which is composed of two conference papers, we have demonstrated the power of geometry. We showed two proofs of Pappus–Pascal's theorem that differed from the proof using homogeneous coordinates. Our proofs were based on perspectivity and projectivity. In the second part of this chapter, we showed the construction of an osculating circle of an ellipse, including geometric clarification, instead of using the standard method of computation via curvature. In the third part, we showed how it is possible to find the solution of a quadratic equation using only a compass and a ruler. We also showed the construction for particular forms of quadratic equations and discussed the cases where the solution does not exist using the ruler and compass. This method of finding the roots of a quadratic equation does not have the ambition to replace the standard solution. Moreover, it is susceptible to the accuracy of the plotting. It aims to broaden the reader's horizons and connect different parts of mathematics.

2. Across dimensions

This chapter describes the basics of multidimensional geometry (especially 4D). We will use analogies to describe the understanding of multidimensional space. We will use two approaches to describe multidimensional space (one using looking behind, the other using a cut). As the next chapter deals with 4D, this chapter will give a quick insight into 4D space.

2.1 Walking through a wall using 4D space

Introduction to n-D geometry using analogies

There are several basic ways of describing 4D geometry. From a geometric point of view, it is convenient to use analogies. In the following lines, we will show how to get n-D from 0D using two approaches. Both methods of describing multidimensional space are mentioned in (Abbott [2015]).

Look behind

In 0D geometry, there is only one point. We see the point, but something could be hiding right behind the point. To find out, we look at the point from the side. The side view shows we were wrong; the point was not a point but a straight line pointing directly at us (i.e., the line was displayed as a point in the projection). So we discover 2D geometry and see a straight line instead of a point (figure 2.1 - 0D $\rightarrow$ 1D).

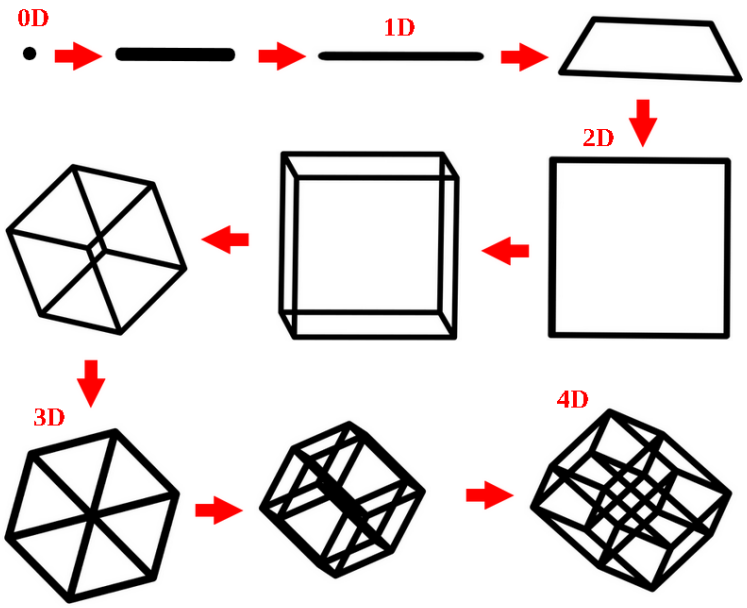

Figure 2.1: animation of looking behind

In 1D geometry, all geometry takes place in a straight line. In our case we narrow the straight line to a segment. If we look at the scene from above (in the

direction perpendicular to the axis x in 1D geometry), we see that we are not looking at a straight line but at a square from the side. This brings us to 2D geometry (figure 2.1 - 1D $\rightarrow$ 2D).

Similarly, we can look at a square in 2D geometry from a direction z perpendicular to the x and y axes. It shows that a cube is hidden behind the square (figure 2.1 - 2D $\rightarrow$ 3D). The square was its front face.

By analogy, if we look at a cube in 3D geometry from the direction w perpendicular to the x, y and z axes, a tesseract appears behind the cube. The cube was the front face of the tesseract. (figure 2.1 - 3D $\rightarrow$ 4D). Similarly, we can continue to n-dimensional space.

Using cut

Another way to introduce n-dimensional space is to use a cut.

In 3D space, there is a 3D sphere and a base plane $\pi : z = 0$. A 2D being living in the plane π only sees life in the ground plane π. Therefore, if the 3D sphere does not intersect the plane π, it is invisible to the 2D entity. If a 3D sphere decides to show itself to a 2D being, it must cross the plane π. When the sphere first touches the plane π, it appears as a point. As the sphere continues to pass through the plane π, it will appear as a set of increasingly larger circles until it becomes a circle with a radius equal to its diameter. Then, the sphere appears as a set of decreasing circles in the plane π, respectively. Finally, it appears as a point again until it disappears completely (figure 2.2a).

In this way, the 2D being gets a complete view of the 3D solid by using the 3D solid cuts. If a 2D creature can imagine a direction perpendicular to its space (the z-axis), it can imagine a 3D sphere from its cuts, like when you lay down a deck of cards (figure 2.2b).

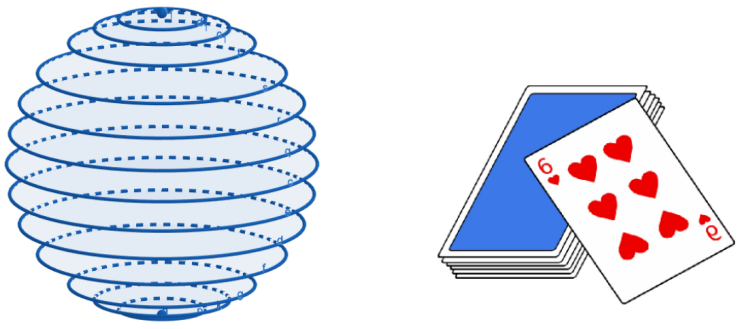

(a) sphere cuts (b) deck of cards

Figure 2.2: visualization of 3D-space by using cuts

Similarly, we cannot see the 4D sphere until it intersects our 3D world (axes x, y and z). If the 4D sphere decides to cross our (x, y, z)-space in the direction of the w-axes, the 4D sphere intersects our world first at a point, then as expanding spheres up to the size of its radius, then as shrinking spheres until it reaches a point again and finally the 4D sphere disappears completely (figure 2.3). Similarly, we get a set of cuts of a 4D sphere through the intersection plane $w = k$, $k \in \mathbb{R}$. If we can arrange the slices in a direction perpendicular to our world (the w-axis) like a deck of cards, we can imagine a 4D sphere.

Physicists use time t instead of the w axis. Instead of arranging the sections in a direction perpendicular to our world (the w-axis) like a deck of cards, they often use the unit of time (Bars et al. [2010], Lehrer [2010], Weinberg [2022]).

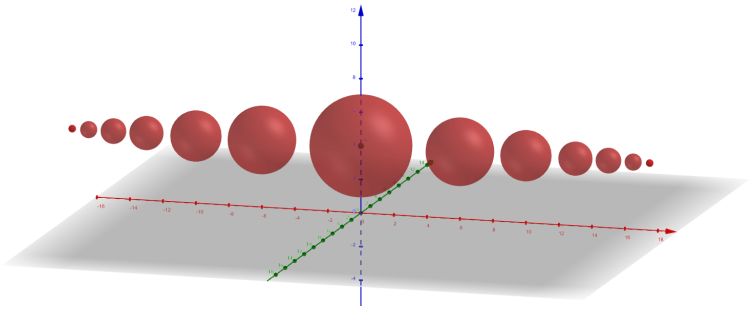

Figure 2.3: visualization of 4D-sphere by using cuts

This section is called how to walk through walls using 4D space. Let us clarify how this is possible.

Suppose there is a locked 4D being in a 3D prison (a cube with faces without a hole). The 4D being could escape from the prison by taking it across the w-axis. Let us describe this fact in less dimensional space in a plane. Let us start with a square drawn on a piece of paper (2D prison) and a pin placed inside the square. we can move the pin along the x and y axes, but we cannot move the pin out of the square (there are always edges of the square). However, if we lift the pin in the direction of the z axis (the direction perpendicular to 2D space), the pin will appear above the paper. Then it is possible to move the pin in any direction and put it back on the paper outside the square, the pin gets out of the prison without using any brute force. To the prison guard, the whole situation looks as if the pin is inside the prison, then the pin disappears for a while before reappearing outside the prison.

Both methods use a direction perpendicular to a given space. So we call the new axis w as the new direction perpendicular to x, y, z. This gives us a 4D space with axes (x, y, z, w). Now that we have a properly defined 4D space, it is time to introduce some ways to get 4D space on paper.

2.2 Various projections on paper

There are many different projections of 3D space on paper. (3D space to 2D space). A relatively well-known example is the Monge projection (Monge [1847]). It is the projection of 3D space onto two mutually perpendicular planes (π, ν). Then, one of these planes is rotated 90° around a common intersection line (the x-axis) to obtain a planar figure (figure 2.4a). Similarly, a 4D space is projected onto 2 mutually perpendicular 3-spaces (Ξ, Ω), where Ω (figure 2.4b Ω) is rotated 90° around a common ground plane $\pi(x, y)$ to obtain a 3D space figure. It is described in much more detail in the chapter 3.

The second most common method of representing 3D space on paper (2D space) is perspective (displaying space by seeing it with one eye). In principle, this is a central projection with a center O, where the 3D scene is projected

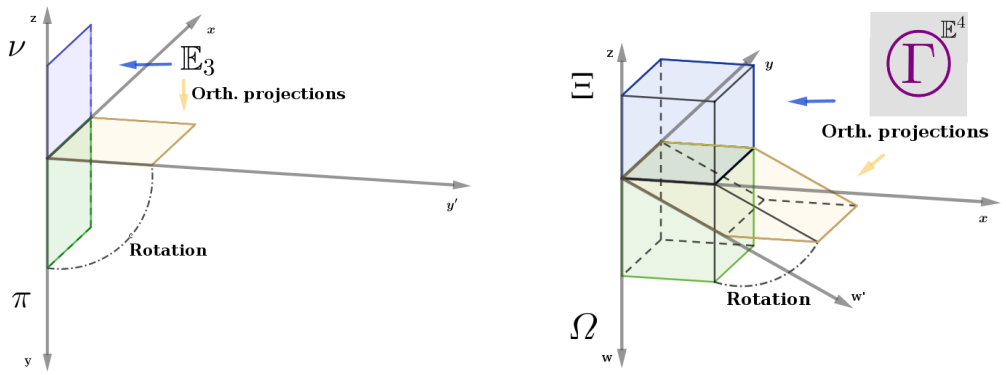

(a) 3D: Monge's projection (b) 4D: Double orthogonal projection

Figure 2.4: Visualization of double orthogonal projection

centrally onto a 2D drawing (Figure 2.5). Similarly, we can project 4D space in perspective onto 3D space. It is described in much more detail in the chapter 4.

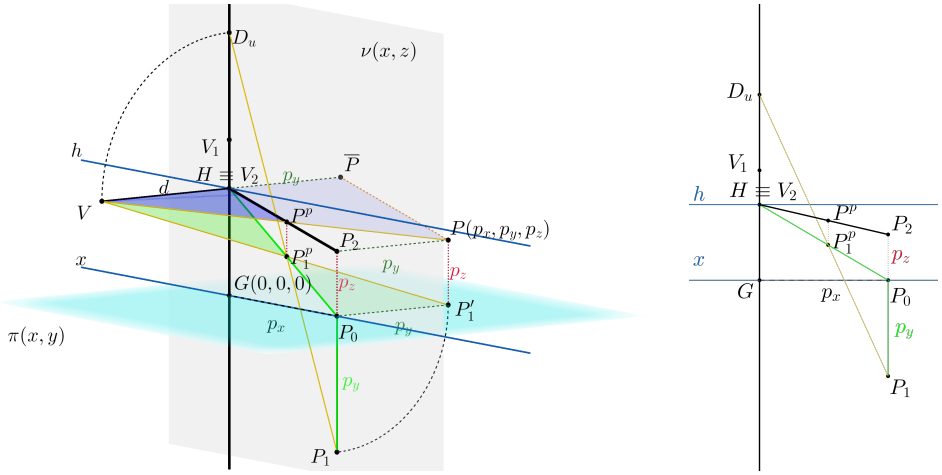

Figure 2.5: (Left) The principle of the 3-perspective construction of a point with associated Monge's projection. The 3D-image is projected in orthographic projection.(Right) The perspective image from the perspective center.

The projections described above have certain basic principles and constructions which are described in the following chapters. It is not necessary to draw the basic constructions. Drawing by hand is very difficult and clicking everything in any software (for example, Geogebra) is not much more accessible; fortunately, in Geogebra it is possible to create tools that can make the work easier. In the attachment B of this thesis we present how to create tools for creating smarter GeoGebra applets which are often used in this work. As mentioned above, we will describe the double orthogonal projection onto two mutually perpendicular 3-spaces in much more detail in the next chapter.

3. Double orthogonal projection

One way how to visualise 4D space is to project 4D space onto two mutually perpendicular 3-spaces (similar to the Monge projection used for 4D (section 2.2). This topic is covered in the publications (Bogdan and Serbanoiu [2021],Zamboj [2018b]). This section is inspired by the articles by Zamboj.

3.1 Double orthogonal projection of four-dimensional objects onto two perpendicular three-dimensional spaces

Projection of a point

The point $A[x_A, y_A, z_A, w_A]$ in 4D space is given by its two orthogonally projected points $A_3[x_A, y_A, z_A, 0]$ and $A_4[x_A, y_A, 0, w_A]$. The point A_3 is the orthogonal projection of point A onto $\Omega(x, y, z)$ and A_4 is the point of the orthogonal projection of point A onto $\Xi(x, y, w)$. $A_1[x_A, y_A, 0, 0]$ is the orthogonal projection of A_3 and A_4 onto reference plane $\pi(x, y)$ (figure 3.1).

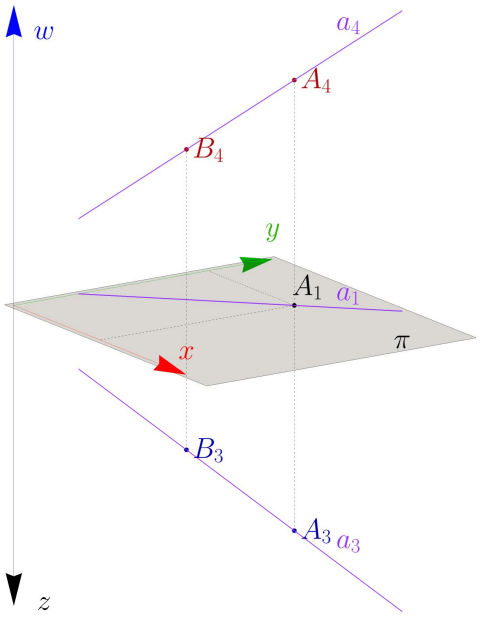

Figure 3.1: Projection of point $A = [x_A, y_A, z_A, w_A]$ and line $a = \overline{AB}$.

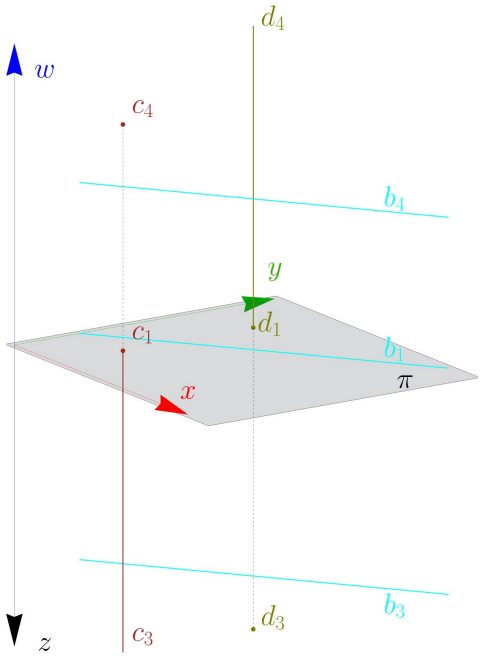

Figure 3.2: Lines in special positions.

Projection of a line

A line $a = \overline{AB}$ is represented by its conjugate images, which are orthogonal projected, $a_3 = \overline{A_3B_3}$ onto $\Xi(x, y, z)$ and $a_4 = \overline{A_4B_4}$ onto $\Omega(x, y, w)$. The orthogonal

projection of a_3 and a_4 onto reference plane $\pi(x, y)$ is marked with the label a_1 (figure 3.1). Let us describe some particular positions of lines.

- A line b parallel to the reference plane $\pi(x, y)$, represented by b_3 in $\Omega(x, y, w)$ and b_4 in $\Xi(x, y, z)$ as lines parallel to $\pi(x, y)$ (figure 3.2 cyan).
- A line perpendicular to the 3-space $\Xi(x, y, w)$ displays its c_3 image as line perpendicular to the reference plane $\pi(x, y)$ and c_4 image as a point (figure 3.2 brown).
- A line perpendicular to the 3-space $\Omega(x, y, w)$ displays its d_3 image as point and d_4 image as a line perpendicular to the reference plane $\pi(x, y)$ (figure 3.2 olive).

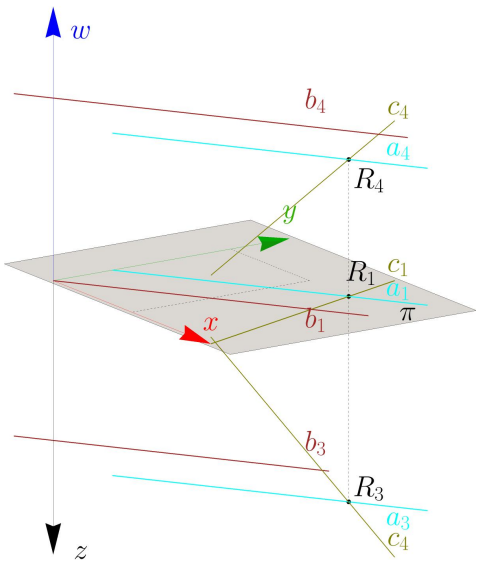

Figure 3.3: Relative position of lines a, b, c.

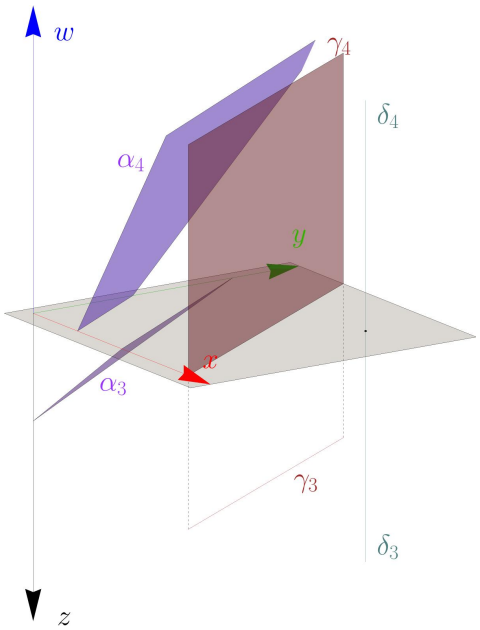

Figure 3.4: Plane α, γ, δ.

Relative position of two lines

Two lines are given by their orthogonal projections onto $\Omega(x, y, z)$ and $\Xi(x, y, w)$. Straight lines can be parallel, intersecting or skew (figure 3.3).

- The lines a, b (cyan, brown) are parallel if a_3 is parallel to b_3 and at the same time a_4 is parallel to b_4.
- The lines a, c (cyan, olive) intersect and the point R is an intersection point if $R_3/R_4/R_1$ are intersections of $a_3, c_3/a_4, c_4/a_1, c_1$, respectively and the points R_3, R_4 and R_1 lie on the ordinal line. (The ordinal line is perpendicular to the plane $\pi(x, y)$).
- The lines b, c (brown, olive) are skew if the intersection points R_3, R_4 and R_1 from the previous case do not lie on the ordinal line.

Planes

A plane α is represented by its orthogonal projection α_3 onto $\Omega(x, y, z)$ and α_4 onto $\Xi(x, y, w)$. The $\Omega(x, y, z)$ and $\Xi(x, y, w)$ images of the planes are

- planes (α figure in 3.4),
- plane and line (γ figure in 3.4),
- lines in special position (δ figure in 3.4).

Two planes λ, ω are given by their orthogonal projections λ_3, ω_3 onto $\Omega(x, y, z)$ and λ_4, ω_4 onto $\Xi(x, y, w)$. Planes λ, ω can be parallel in one direction (figure 3.6), parallel in two directions (figure 3.5), intersecting in a line (figure 3.7), intersecting in a point (figure 3.8) and skew (figure 3.9).

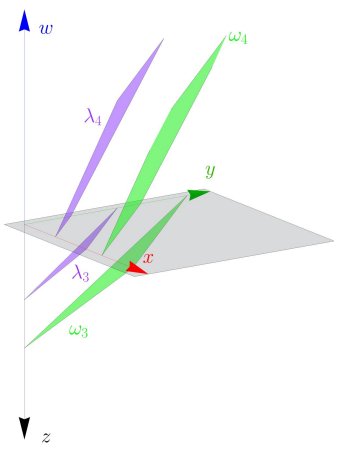

Figure 3.5: Planes λ, ω parallel in two direction.

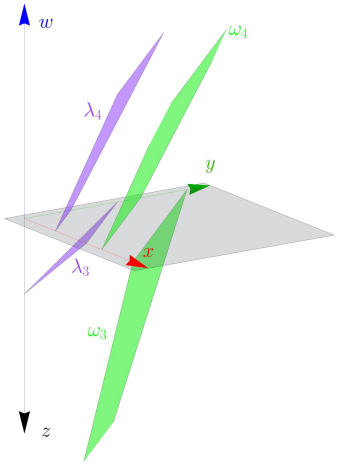

Figure 3.6: Planes λ, ω parallel in one direction.

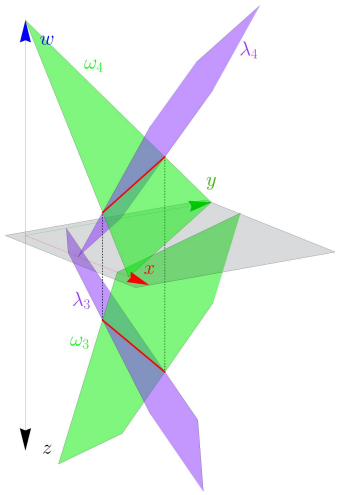

Figure 3.7: Planes λ, ω intersecting in a line.

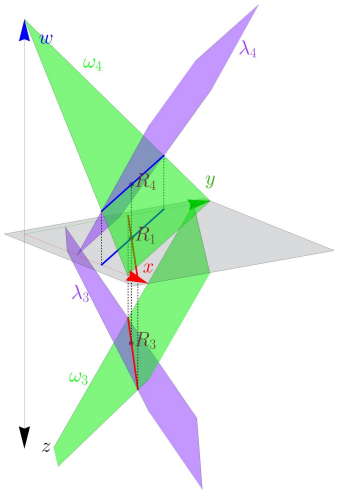

Figure 3.8: Planes λ, ω intersecting in a Point.

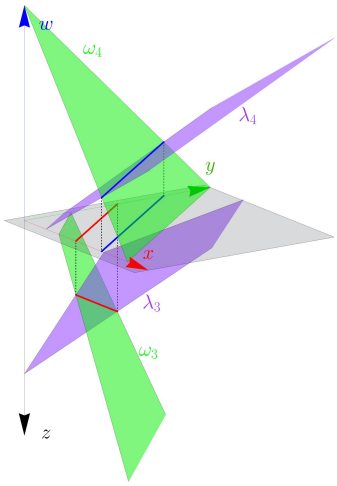

Figure 3.9: Planes λ, ω skew

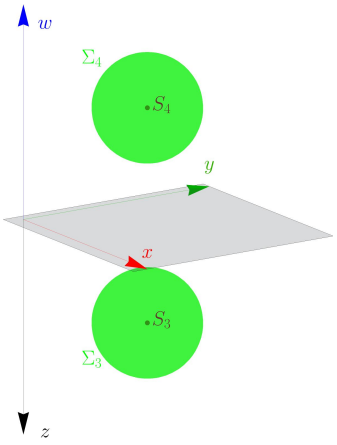

Figure 3.10: 3-Sphere Σ.

Shapes

Tesseract

The tesseract is a four-dimensional analogue of the cube. It consists of 16 vertices, 32 edges, 24 faces and 8 cells. Figure 3.11 shows the tesseract in a special position where all 8 different cells are coloured. The same tesseract was printed as a 3D model and published in the article *3D printed models of tesseract in double orthogonal projection and 4D perspective* (Řada and Zamboj [2020]). The figure shows all eight different cells in a 4D perspective, which we will discuss later.

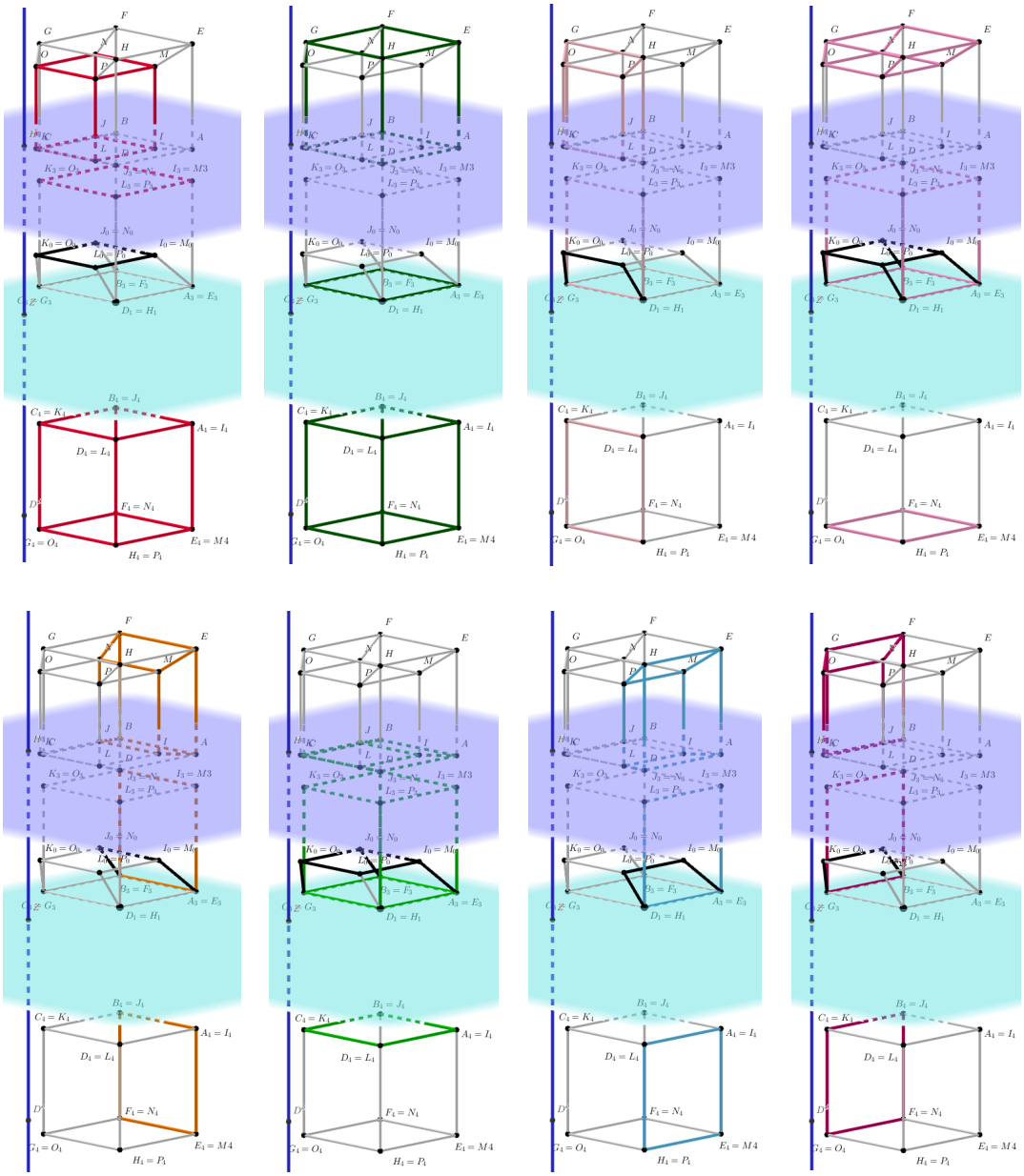

Figure 3.11: Cells of tesseract in double orthogonal projection and 4D perspective.

4-Sphere

The set of all points at a constant non-zero distance from a given point is a circle in a plane, a sphere in a 3-space, or analogically a 3-sphere in a 4-space.

Therefore orthogonal projections of the 3-sphere onto $\Omega(x, y, z)$ and $\Xi(x, y, w)$ are represented as a 2-sphere with the same radius and the centers S_3, S_4 on the ordinal line (figure 3.10). Sections of a 3-sphere are described in much more detail in the article *1-2-3-Sphere in the 4-Space* (Zamboj [2019]) or with visualisation in 4-perspective in the article *3-Shere in a 4-perspective* (Řada and Zamboj [2021]). This article is included in the chapter 4 of this thesis. Here, we have described the basic geometric shapes of 4D geometry.

Monge's projection is often used in linear perspective representation. There is a way to draw an object in Monge's projection and then visualise it in perspective. Therefore, we can similarly use double orthogonal projection onto two perpendicular three-dimensional spaces to display four-dimensional objects in a 4D perspective. For this reason, we have described the basics of the double orthogonal projection onto two perpendicular three-dimensional spaces here, and we will now look at the 4D perspective in the next chapter.

4. Perspective

The understanding of perspective space began to be represented in paintings in the first half of the 15th century (Šarounová [1995]). Over the years, it has been improved. The following lines describe some selected paintings from the perspective point of view. This part contains parts of the prepared, unpublished article on 4D perspective in the journal *"Rozhledy matematicko-fyzikální."*

4.1 Perspective in paintings

Introduction

Painting and geometry are based on seeing. That is why painting uses perspective to imitate human sight. In perspective, objects are projected from a center of projection (the eye) onto a plane (the retina). Photographs taken with a single-lens camera are the most familiar perspective paintings. An essential element of perspective is the size of the objects; the further the object is from the centre of projection (the eye), the smaller the object appears. Another vital element of perspective is the convergence of lines.

Main Principles of Perspective

Perspective is concerned with placing objects in space, including their relationships to each other. In the illustration 4.1, the left part of the image shows an avenue of trees running towards the horizon. The trees appear smaller and smaller as the trees move away from the point of view, but corresponding pixels of each tree always lie on a straight line converging on the horizon (illustration 4.1). The right part of the figure shows three views of the same-sized cube. The cube's position relative to the horizon indicates whether it is a top view, a front view or a bottom view of the cube. A more detailed description of the principles of perspective can be found on the website (ČVUT [2022]).

Reconstruction of the perspective formation

Perspective began to develop in the early 15th century in Florence, where Filippo Brunelleschi, Donatello and Masaccio began experimenting with the illusory possibilities of linear perspective.

Reconstructing how it all came about and how a coherent perspective method was developed is quite complex. The history of perspective development has mainly been reconstructed based on two different sources. On the one hand, researchers have analysed some works by Donatello and Masaccio from the beginning of the century and traced the gradual development of the perspective scheme. On the other hand, they have studied Brunelleschi's biography, written around 1480 by Antonio Manetti (Manetti et al. [1970]), which contains some valuable information about Brunelleschi's experiments with perspective. Let us describe some parts of the development of perspective.

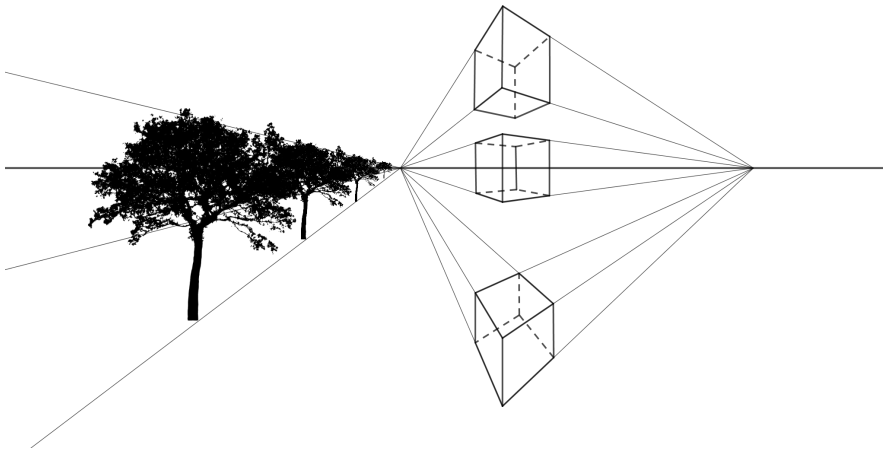

Figure 4.1: Perspective representation of objects.

The beginnings of perspective in paintings

In 1325, Giotto di Bondone recognised the need for converging lines to create depth in his painting *"The Apparition To Brother Augustin And The Bishop"* (figure 4.2a). In his painting, he uses the converging lines in the coffered ceiling. His perspective was not perfect yet, as the lines added by Kadeřávek (Kadeřávek [1922]) show. In his work, Kadeřávek shows how parallel lines converge into two different points that do not even lie on the horizon line.

(a) The Apparition To Brother Augustin And The Bishop Giotto di Bondone

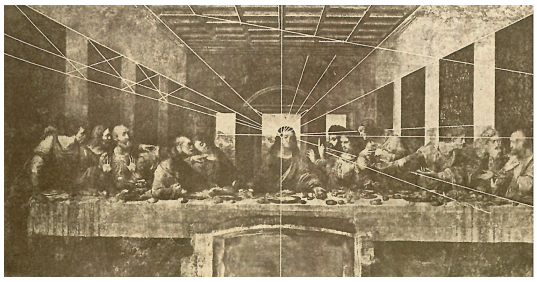

(b) The Last Supper Leonardo da Vinci

Figure 4.2: Kadeřávek's analysis of perspective in paintings, taken from the book (Kadeřávek [1922]).

Many years later, the painting of *"The Last Supper"* (figure 4.2b) by Leonardo da Vinci has its vanishing lines perfectly matched to the painting (Kadeřávek [1922]). In addition, Leonardo da Vinci skilfully uses and plays with his knowledge of perspective. It is not apparent in the paintings in the book. It is necessary to examine the original painting more closely, which is in the refectory of Santa Maria delle Grazie in Milan, Italy. In order to see the whole painting from one place with one eye, you need to stand one-third further away from the painting than the distance from where the painting was painted. To keep the proportions

correct, the artist enlarged the figures in the painting by a third of their actual size. (Kvasz [2020]) in his book describes this effect that Florensky found.

Paintings with multiple principal points

Many years later, Paul Cézanne rejected the classical perspective and did not recognise the classical position of objects in space. As a result, he painted objects (sometimes parts of objects) in space from different angles. Between 1888 and 1890, he painted The Kitchen Table (figure 4.3). In this painting, the directions from which the objects are seen are indicated by red arrows. In this painting, the various objects are painted from different angles. Some selected objects are painted from several angles at the same time.

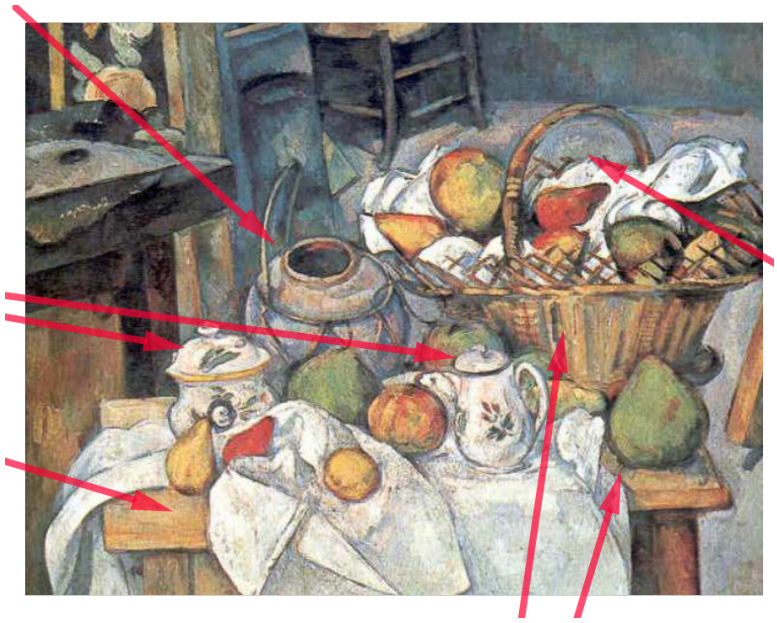

Figure 4.3: Kitchen Table - Paul Cézanne

The bottom of the basket is painted from the front, while the handle is painted from one side. The same is done with the table. To not show that the table breaks when the angle of view is changed, the artist has hidden the fracture under a white tablecloth.

Perspective in Cubist paintings

Cubist artists went even further. Not only did they look at objects from different angles, but they also broke down traditional vision into its elementary parts. Often, they would break down all sorts of surfaces into the simplest geometric shapes, most often triangles (image 4.4a), or show an object's most characteristic individual parts. For example, in image 4.4b, the violin is represented by its characteristic elements (the snail-shaped end, the sides and the f-shaped holes). At the same time, it should still be a matter of perspective. That is, seeing and understanding objects with one eye.

(a) Woman in an Armchair
Pablo Picasso

(b) Violin and Grapes
Pablo Picasso

Figure 4.4: Cubist paintings by Pablo Picasso

Perspective in paintings of icons

From a slightly different perspective, the perspective of icons is interesting. It is interesting to note that some perspective paintings of icons use reverse perspective. So, the convergence is not from us to the horizon but vice versa from the horizon to us. The painting gives us the feeling that we are not part of the scene (Florenskij [2001]). Luptáková explains that the artist often wants to depict everything from different perspectives. Since, in reverse perspective, everything comes towards us, we see, for example, the house painted from the front, including its side walls (Figure 4.5).

Conclusion

The text has outlined some of the problems of perspective that different painters have tried to deal with in different ways. This text does not aim to give a comprehensive view of perspective in paintings. Instead, it is intended to make the reader think about the paintings. The text would have to be many times longer to give a comprehensive view. For a deeper understanding of perspective in painting, the book *"Space between Geometry and Painting"* by (Kvasz [2020]) is recommended, which I used as an inspiration for this text or the English book *"The fourth dimension and non-Euclidean geometry in modern art"* by (Henderson [2013]), which describes literary texts rather than the paintings themselves. So far, we have seen the development of perspective; how it was imperfect in the beginning and how it was perfected until cubist works were created. Now, we are going to take perspective further and introduce a 4D perspective.

Figure 4.5: Reversed perspective in the under-construction Temple of St. Sava (Belgrade)

4.2 Four-dimensional perspective

Introduction

The rapid emergence of dynamic 3D geometry software tools has pushed the boundaries of geometric design accuracy beyond previous limits. Using a virtual 3D modelling environment, we can perform synthetic geometric constructions like those drafted on paper. As a result, classical descriptive geometry, which uses planimetric (2D) methods to visualise spatial (3D) objects, can be easily generalised to visualise 4-D objects in 3-space. The four-dimensional descriptive geometry method using double orthogonal projection of a 4-space onto two mutually perpendicular 3-spaces (4DDOP) was introduced in (Zamboj [2018b]), and the construction of shades and shadows in (Zamboj [2018a]).

While two images in orthogonal projections are often suitable for measurements, there are more interpretative ways of visualising in one representative image; leastwise, in 3-D to 2-D projections. The 4DDOP method is applied to construct a 3-dimensional perspective image and lighting of a 3-sphere embedded in a 4-space in this paper, where the 3-sphere is a 4-dimensional analogy of a classical (2-)sphere, i.e., a 3-sphere is the set of all points in the same distance from a fixed point in a 4-space. Projections and intersections of a 3-sphere with 3-spaces, planes, and lines in 4DDOP are described in (Zamboj [2019]).

Previously, central projections of four-dimensional hypercubes in computer graphics were discussed in the pioneering work by (Noll [1967]). Analytically treated description and visualisation of central and orthogonal images of various curves and surfaces are, for example, in (Banchoff [1990], Zachariáš and Velichov'a [2000]). Particularly animations and interactive methods of multidimensional visualization were used by (Black [2010], Bosch [2020], Chu et al. [2009], Hanson and Cross [1993], Matsumoto et al. [2019], Miwa et al. [2017], Zhang and Hanson [2007]).

4.2.1 Basics of four-dimensional perspective

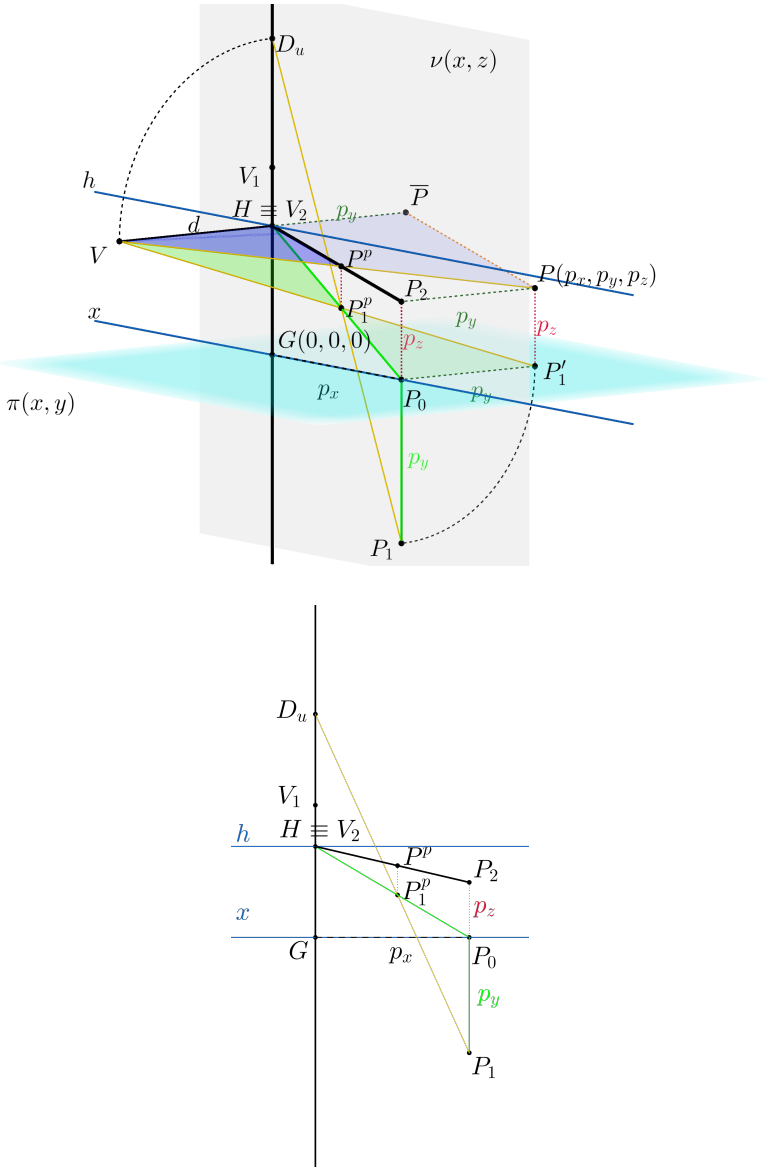

Figure 4.6: (Top) The principle of the 3-perspective construction of a point with associated Monge's projection. The 3D-image is projected in orthographic projection.(Bottom) The perspective image from the perspective center.

To start with, we describe the generalization of linear perspective in a four-dimensional setting.[1] The 3-perspective is a central projection, in which each point is projected from a fixed center (viewpoint, entrance pupil of an eye or camera) into a picture plane. The resulting intersection of the projecting ray and picture plane is called the perspective image of the point. Classical linear perspective should satisfy certain conditions appropriate for human vision (degree limit for vision cone, minimal distance of the viewpoint from picture plane). In the context of four-dimensional generalization, no human will (hopefully) argue if we do not take these conditions into account while keeping our figures illustrative.

[1]To simplify the language, we will refer to linear perspective in three dimensions as 3-perspective and its four-dimensional analogue as 4-perspective.

Furthermore, basic elements of 3-perspective are generalized in 4-perspective as follows (Figures 4.6 and 4.7). In the 4-perspective, a point is projected from a fixed perspective center into a modeling 3-space instead of a picture plane. In both cases, we label d the distance between the perspective center and the picture plane or modeling 3-space, i.e., the focal length. In both cases, the orthogonal projection of the perspective center into the picture plane or modeling 3-space is the principal (vanishing) point H. Assuming the surrounding 3-space in 3-perspective, the picture plane is in the vertical position, and we assume the ground (or base) plane in the horizontal position. The orthogonal projection of the principal point H into the ground plane (chosen not through H) is the ground point G. Let us rather use the Cartesian coordinate system (x, y, z, w) in the four-dimensional case. Instead of the ground plane assume ground 3-space $\Xi(x, y, z)$ and the modeling 3-space is $\Omega(x, y, w)$. The orthogonal projection of the principal point H into the ground 3-space is the ground point G. In 3-perspective, the intersection of the ground plane with the picture plane is the ground line. In 4-perspective, the intersection of the ground 3-space $\Xi(x, y, z)$ with modeling 3-space $\Omega(x, y, w)$ is the ground plane $\pi(x, y)$. In 3-perspective, the horizon plane is parallel to the ground plane through the perspective center, and its intersection with the picture plane is the horizon line, i.e., the line of vanishing points in horizontal planes. In the four-dimensional case, we have the horizon 3-space through the perspective center and totally parallel to the ground 3-space $\Xi(x, y, z)$. Its intersection with the modeling 3-space $\Omega(x, y, w)$ is the horizon plane η.

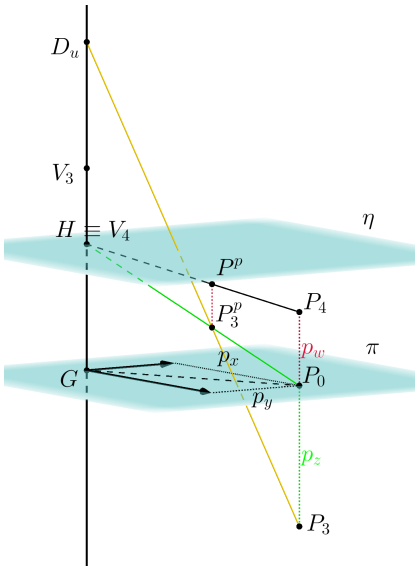

Figure 4.7: The principle of the 4-perspective construction of a point with associated 4DDOP in the modeling 3-space.

One way of constructing perspective images of points in 3-perspective is to use associated Monge's projection with the same picture plane, in which the ground plane (x, y) is rotated onto the picture plane (x, z) about the ground line (x-axis) (Figure 4.6). We will use similar construction in the 4-perspective associated with 4DDOP.[2] Consider the situation in the 4-space (x, y, z, w), the ground 3-space

[2]In 3-perspective (Figure 4.6), points P_1, P_2 play the same role as P_3, P_4 in the 4-perspective

$\Xi(x,y,z)$ is rotated around the ground plane $\pi(x,y)$ onto the modeling 3-space $\Omega(x,y,w)$ (Figure 4.7). The perspective image P^p of a point P is the intersection of the projecting line VP of the point P from the perspective center V with the modeling 3-space. Let P_3' and P_4 be the orthogonal projections of the point P into $\Xi(x,y,z)$ and $\Omega(x,y,w)$, respectively. Moreover, label P_3^p the perspective image of the point P_3' and P_3 the image of the point P_3' after the initial rotation of Ξ onto Ω. The orthogonal projection of P_3' into the modeling 3-space is labeled P_0. The lines P_0H and P_3P_0 are, respectively, the perspective image and the Ξ-image in 4DDOP of the line $P_3'P_0$ orthogonal to the modeling 3-space. Furthermore, let D^u (upper distance point) be the image of the viewpoint V rotated about the horizon plane η into $\Omega(x,y,w)$.[3] Note that the triangles VHP_3^p and $P_3'P_0P_3^p$ are homothetic with center P_3^p (from initial construction). Furthermore, the triangles VHP_3^p and $D_uHP_3^p$ are congruent (due to rotation). Also $P_3'P_0P_3^p$ and $P_3P_0P_3^p$ are congruent (due to rotation). Hence $D_uHP_3^p$ and $P_3P_0P_3^p$ are similar. Since $HP_3^pP_0$ are collinear, then also $D_uP_3^pP_3$ are also collinear. Consequently the triangles $D_uHP_3^p$ and $P_3P_0P_3^p$ are homothetic with the center P_3^p and coefficient $\frac{|VP|}{|P_3'P_0|} = \frac{|D_uP|}{P_3P_0} = \frac{d}{p_z}$, where d is the perspective distance and p_z is the z-coordinate of the point P. These are the key relations for synthetic construction between the perspective image and Ξ-image in 4DDOP images and vice versa. The Ω-image P_4 is the orthogonal projection of P into the modeling 3-space Ω, and so it lies on the perpendicular through P_0 to π and also on the line through P^p and the principal vanishing point H. The distance $|P_0P^p| = p_w$ is the w-coordinate of P. The triangles VP^pH and PP_4P^p are also homothetic with the center P^p and the same coefficient $\frac{d}{p_z}$. For further constructions note that the Ω-image of the viewpoint V is equal to the principal point, $V_4 \equiv H$, in the modeling 3-space, and the Ξ-image V_3 lies on the ray GH such that $|GV_3| = d$.

For analytic representation, it is convenient to translate the origin of the 4-space into the viewpoint $V(0,0,0,0)$ by vector $\overrightarrow{GV}$. In such case, the modeling 3-space has the equation $z = d$, where d is the perspective distance and a point P has newly acquired coordinates (p_x', p_y', p_z', p_w'). Let $\overline{P}$ be the orthogonal projection of the point P into the z-axis (similarly in the 3-perspective in Figure 4.6, where $\overline{P}$ is the projection into y-axis), then the triangles $VP\overline{P}$ and VP^pH are homothetic with the center V. Thus, the coordinates of the perspective image of the point P are given by the scaling factor $\frac{d}{p_z'}$, and so, omitting the z-coordinate in the modeling 3-space Ω, we have $P^p(\frac{d}{p_z'}p_x', \frac{d}{p_z'}p_y', \frac{d}{p_z'}p_w')$.

4.2.2 Projection of tesseract

A tesseract is a four-dimensional hypercube. It is an analogue of the cubic in 4D geometry. It contains 8 cells, 24 faces, 32 edges and 16 vertices.

A tesseract in a special position has the vertex A at the origin, and the edges through the point A lie on the axes (x,y,z,w). Therefore, the neighbouring points B, D, E, I lie on the axis at the same distance from the point A (distance in more detail in section 4.2.5). To set up all vertices of the tesseract with the length of the edge n, generating a list of all possible 4-tuples of zero and n is

(Figure 4.7), respectively. Similarly for other points with the same indexes.

[3] To shorten the construction, the rotation has the same orientation as the initial rotation of the ground 3-space Ξ onto the modeling 3-space Ω.

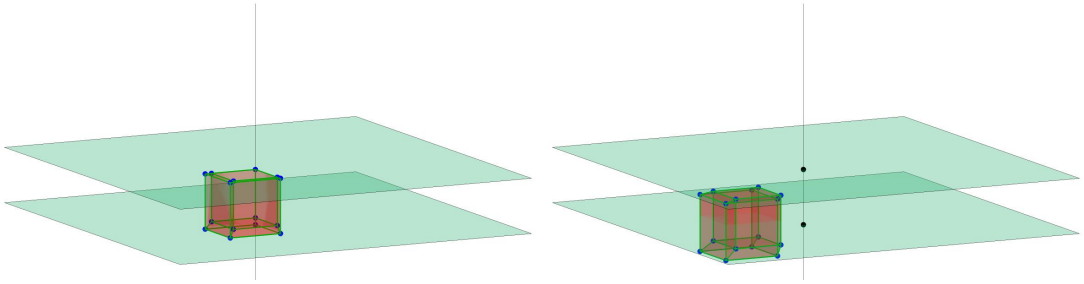

(a) Tesseract with the vertex in the origin. Edges are identical with the axis.

(b) Shifted tesseract from the origin. $\vec{v} = (1, -8, -1, -3)$

Figure 4.8: Tesseracts in 4D perspective

convenient. The tesseract with the vertex at the origin is shown in the figure 4.8a Left. Adding a shift to all points in 4-tuples gives us a tesseract at any position 4.8b Left. In figure 4.9, a tesseract is shifted in the axial direction.

4.2.3 Projection of four-dimensional hyperpyramid

Four-dimensional hyperpyramid is a generalisation of the normal pyramid to 4 dimensions. There are several ways of visualising 4-dimensional hyperpyramids. One starts with the vertex V and the center of the base C. There is a given line VC (axis of the hyperpyramid). The base of the hyperpyramid is in the subspace perpendicular to the given line VC. So, we must find all three orthogonal vectors to the axis VC. Now, we can construct the base of the hyperpyramid in the subspace given by the three orthogonal vectors. Adding a constant distance to all three orthogonal vectors gives us a hyperpyramid with an octahedral base (Figure 4.10a). We can also construct a hyperpyramid with a cubic base by constructing a cube in subspace (Figure 4.10b). In a given subspace, we can construct any 3-dimensional object as a base for the hyperpyramid.

4.2.4 Four-dimensional prism

Four-dimensional prism is a generalisation of the normal prism to 4 dimensions. We can visualise any four-dimensional prism in the same way as the hyperpyramid. An edge AB of the prism is given. As before, we can construct a subspace given by the three orthogonal vectors. These three vectors are directions of other edges. In other words, these three vectors with the given edge AB are four directions perpendicular to each other. These four directions determine the directions of the remaining vertices. If the lengths of the edges are different, we get a 4D prism; if the lengths of the edges are the same, we get a tesseract.

4.2.5 Measuring in 4D perspective

In each dimension, the measurement is the same using the Pythagorean Theorem. In 4D, to find the distance between two given points, AB is calculated as the

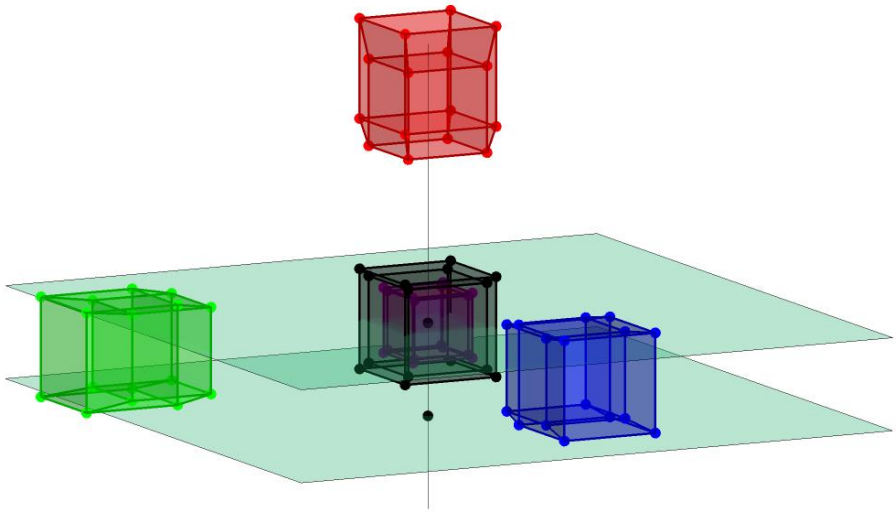

Figure 4.9: Black tesseract is centred to point H. Green tesseract is shifted in direction of the axes x. Blue tesseract is shifted in direction of the axes y. Red tesseract is shifted in direction of the axes z. Purple tesseract is shifted in direction of the axes w.

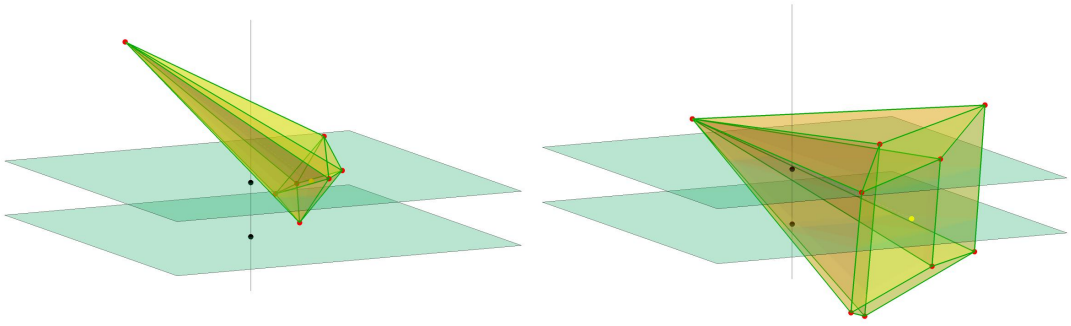

(a) 4-dimensional hyperpyramid with a octahedron base

(b) 4-dimensional hyperpyramid with a cube base

Figure 4.10: Four-dimensional hyperpyramid in 4D perspective

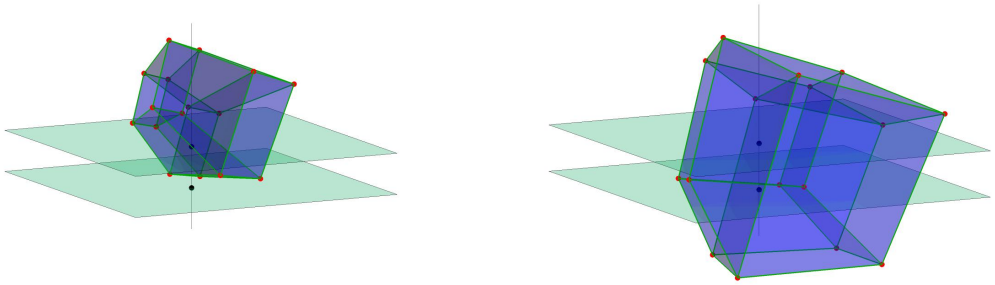

(a) 4-dimensional prism with with different length of edges

(b) 4-dimensional prism with the same length of edges - tesseract

Figure 4.11: Four-dimensional prism in 4D perspective

square root of the sum of the second power of the coordinates of the points

$$|AB| = \sqrt{(x_A - x_B)^2 + (y_A - y_B)^2 + (z_A - z_B)^2 + (w_A - w_B)^2}$$

.

4.2.6 3-sphere in a 4-perspective

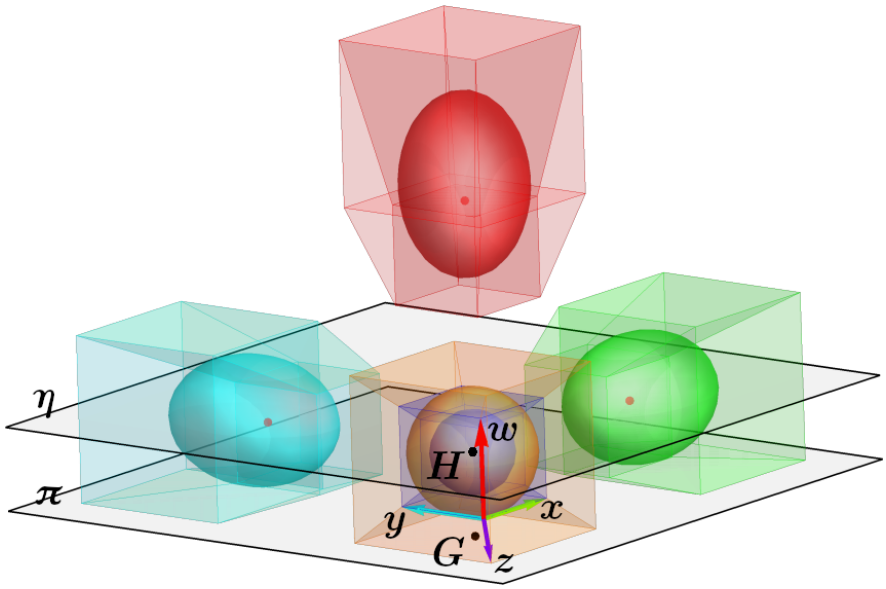

Figure 4.12: A perspective image of a system of 3-spheres inscribed into hypercubes in the modeling 3-space. Assuming the orange 3-sphere to be the center of an arbitrary reference system, the green, cyan, blue, and red 3-spheres are translated in x, y, z, and w-direction, respectively.

The apparent contour of the 3-sphere in the 4-perspective is the projection of its contour generator. The contour generator is the intersection of the 3-sphere and the polar 3-space of the viewpoint (pole) with respect to the 3-sphere. Therefore, the contour generator is a 2-sphere and its perspective image is an unruled regular quadric (assuming the center of the projection is not incident

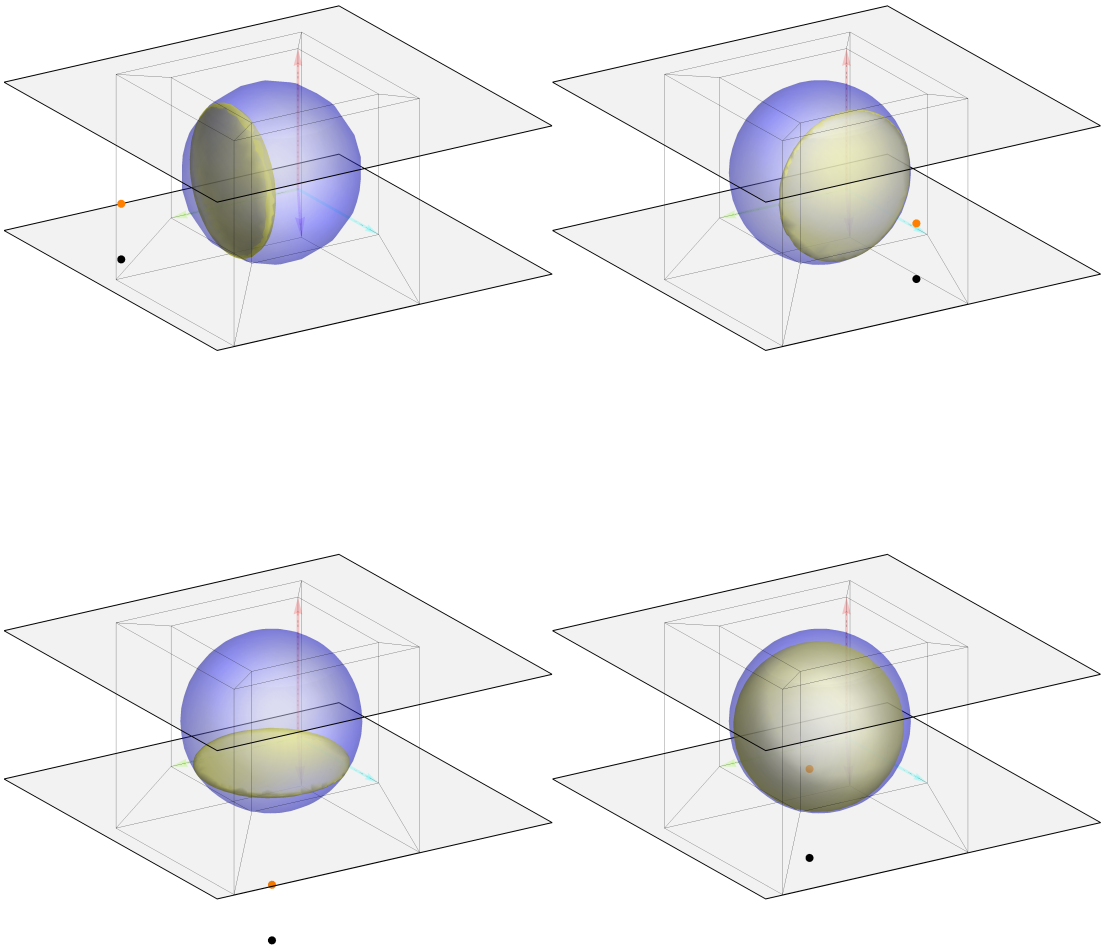

Figure 4.13: Perspective images of shades of a 3-sphere with respect to point light sources represented by orange points in various positions. Black points are the orthogonal projections of the light sources into the ground 3-space used to locate the sources in the 4-space.

with the 3-sphere). Figure 4.12 shows a 4-perspective image of a system of 3-spheres inscribed into hypercubes for better control. Figures 4.12 — 4.14 are created in *Wolfram Mathematica 11* with the use of analytic representation. In this case, we use homogeneous coordinates (with the homogenizing coordinate at the end) in the projective extension of the real space. Hence the viewpoint has coordinates $V(0,0,0,0,1)$, the equation of the modeling 3-space becomes

$$x_3 = dx_0.$$

A 3-sphere Σ with a radius r and proper center $S(s_1, s_2, s_3, s_4, 1)$ has the equation

$$(x_1 - s_1x_0)^2 + (x_2 - s_2x_0)^2 + (x_3 - s_3x_0)^2 + (x_4 - s_4x_0)^2 - r^2x_0^2 = 0.$$

The matrix of the quadratic form of the 3-sphere is

$$\mathbf{\Sigma} = \begin{pmatrix} 1 & 0 & 0 & 0 & -2s_1 \\ 0 & 1 & 0 & 0 & -2s_2 \\ 0 & 0 & 1 & 0 & -2s_3 \\ 0 & 0 & 0 & 1 & -2s_4 \\ -2s_1 & -2s_2 & -2s_3 & -2s_4 & s_1^2+s_2^2+s_3^2+s_4^2-r^2 \end{pmatrix}.$$

Therefore the polar 3-space Θ of the pole V with respect to Σ is (matrix multiplication on the left side)

$$\Theta : V^T\mathbf{\Sigma}(x_1,x_2,x_3,x_4,x_0) = s_1x_1+s_2x_2+s_3x_3+s_4x_4-(s_1^2-s_2^2-s_3^2-s_4^2+r^2)x_0 = 0$$

The intersection of the 3-sphere Σ and 3-space Θ is the contour generator — 3-sphere ϕ. Finally, to obtain the perspective image ϕ^p of the 3-sphere Σ, we apply the above-mentioned transformation of coordinates.[4]

Similarly, if we use arbitrary point P instead of the viewpoint, we can create the edge of the shade of the 3-sphere from either point (Figure 4.13) or directional (Figure 4.14) light source (proper or improper pole P in the projective extension). The shade is a 2-sphere — the intersection of the polar 3-space of the light source with respect to the 3-sphere and the 3-sphere. Its perspective image becomes, again, an unruled regular quadric.

Construction of a perspective image of a 3-sphere in 4-perspective

By analogy in the 4-space, the contour generator ϕ of the 3-sphere Σ is a 2-sphere, and its perspective image ϕ^p is an unruled quadric. Instead of the 5-point construction of a conic, we can use the 9-point construction of a quadric (see Korotkiy [2018], Blossier [2019]).

Let us have a 3-sphere Σ with center S in the 4-space given by its Ξ and Ω-images — 2-balls Σ_3 and Σ_4 in the associated 4DDOP (Figure 4.16). The 4-perspective is given with the horizon plane η with principal point H, ground plane $\pi(x,y)$ with ground point G and principal distance d with the upper distance point D_u. See also step-by-step construction in (Řada [2021a]).

1. Construct the 4DDOP conjugated images V_3, V_4 of the viewpoint V such that $V_3 \in \overrightarrow{GH}, |V_3G| = d = |D_uH|$ and $V_4 \equiv H$.

2. In 4DDOP, construct the trace planes ξ_3^Θ and ω_4^Θ (intersections with Ξ and Ω) of the polar 3-space Θ. The 3-space Θ is perpendicular to VS and contains the tangent points of the tangent cone to Σ with vertex V.

3. In 4DDOP, find the quadric ϕ of intersection of Σ and Θ. For example, with the use of the rotated image Σ_0 (see Zamboj [2019]). It is also sufficient to find 9 suitable points.

4. From the conjugated images in the 4DDOP, construct the perspective images of points on ϕ (Figure 4.7).

[4] Alternatively, we could construct the intersection of the modeling 3-space and the tangent hypercone with the base 2-sphere ϕ and vertex V, obtaining the same collinear mapping.

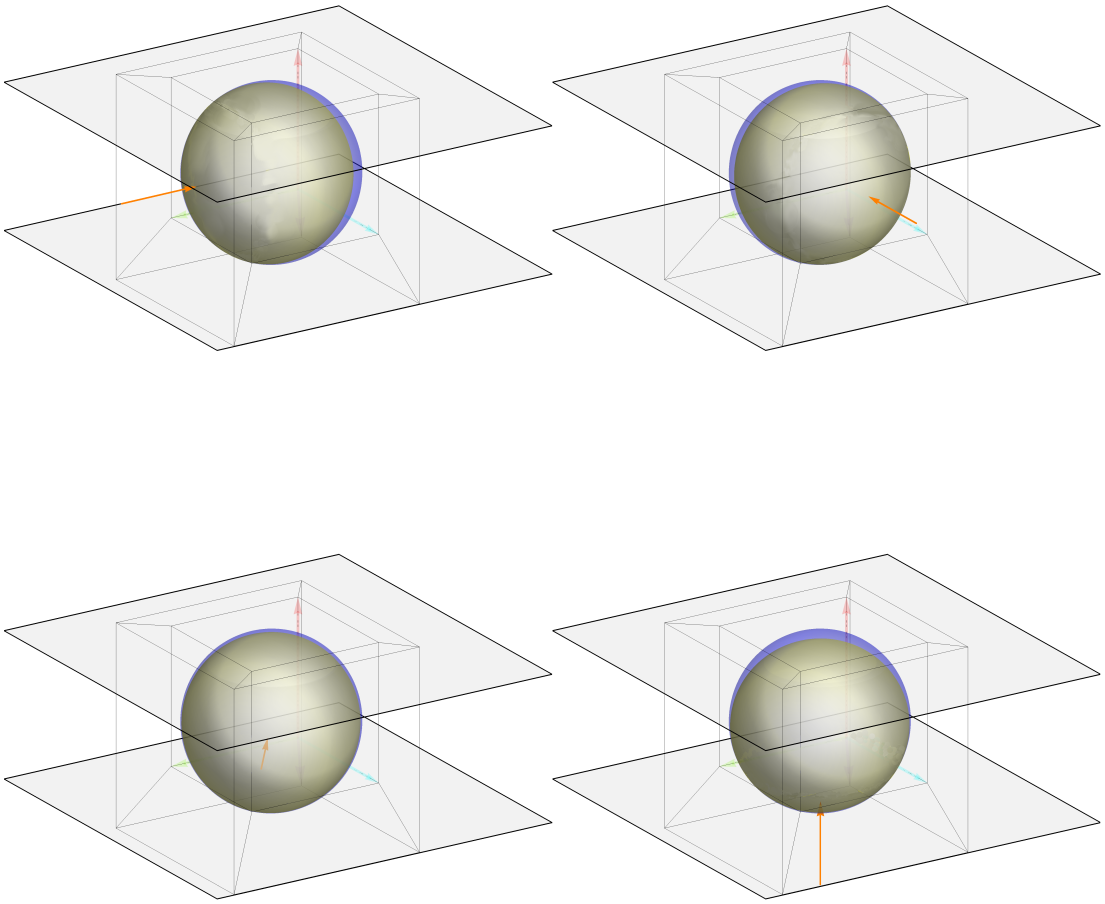

Figure 4.14: Perspective images of shades of a 3-sphere with respect to directional light sources represented by orange arrows in various positions. The sources are in the directions of the reference axes x, y, z, and w.

5. Use the 9-point construction to obtain the perspective image ϕ^p.

In addition, we have constructed a hypercube circumscribed around σ with its perspective image (see also Řada [2021a]).

Construction of a section of a 3-sphere with a 3-space in 4-perspective

Let us continue the previous construction with the construction of a section χ of the 3-sphere Σ with the polar 3-space Γ of an arbitrary point P given by its conjugated images P_3, P_4. The construction is similar to the construction of the perspective image ϕ^p of Σ. Instead of the polar 3-space Θ of the viewpoint V, the polar 3-space Γ of the pole P must be constructed. The intersection of Γ and Σ is the 2-sphere χ constructed first in the 4DDOP as χ_3, χ_4 and consecutively

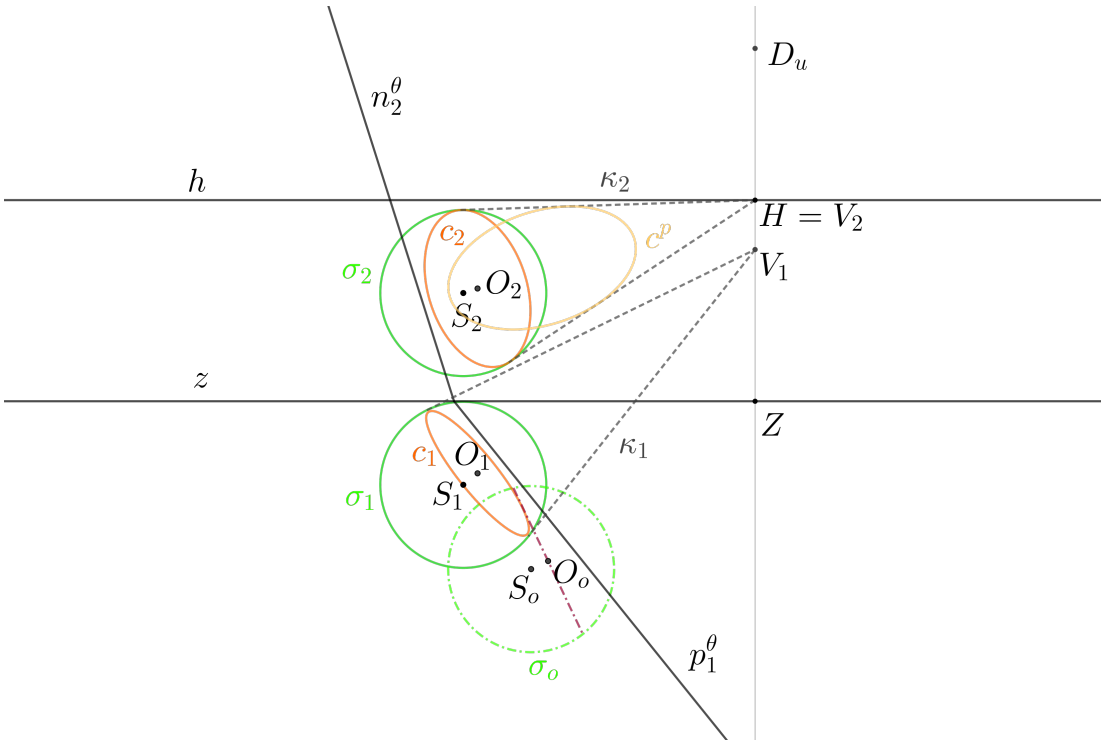

Figure 4.15: 3-perspective image c^p of a 2-sphere σ, with the construction in associated Monge's projection.

with the use of the 9-point construction in the 4-perspective as χ^p (Figure 4.17), which is again an unruled quadric.

Additionally, the section χ is also the shade of light from the source P. Assuming the position of the point P in the 4-perspective, we can choose P to be proper (not in η) or improper (in η), defining central or directional lighting, respectively.

Conclusion

We have described the synthetic construction of a perspective image of a 3-sphere in a generalized perspective projection of a 4-space to a three-dimensional modeling space. The construction is based on the associated double-orthogonal projection of the 4-space onto mutually perpendicular 3-spaces. Furthermore, we have provided a construction of a 2-sphere-section of 3-sphere with a 3-space, using polar properties of quadrics. The provided construction might also serve as a construction of a shade of a 3-sphere with respect to a point or directional source of light. Our interactive synthetic constructions in GeoGebra are available for readers online.

Throughout the work on this contribution, we have opened some further issues. By creating the models in Wolfram Mathematica based on the analytic representation, we have obtained a tool to visualize any set of points in the 4-perspective. Such 4-perspective mapping is opened for interactive elements (e.g., motion of the object or viewpoint, or manipulable parts of the object). Moreover, the problem of lighting of a 3-sphere might be easily generalized for any algebraic hypersurface.

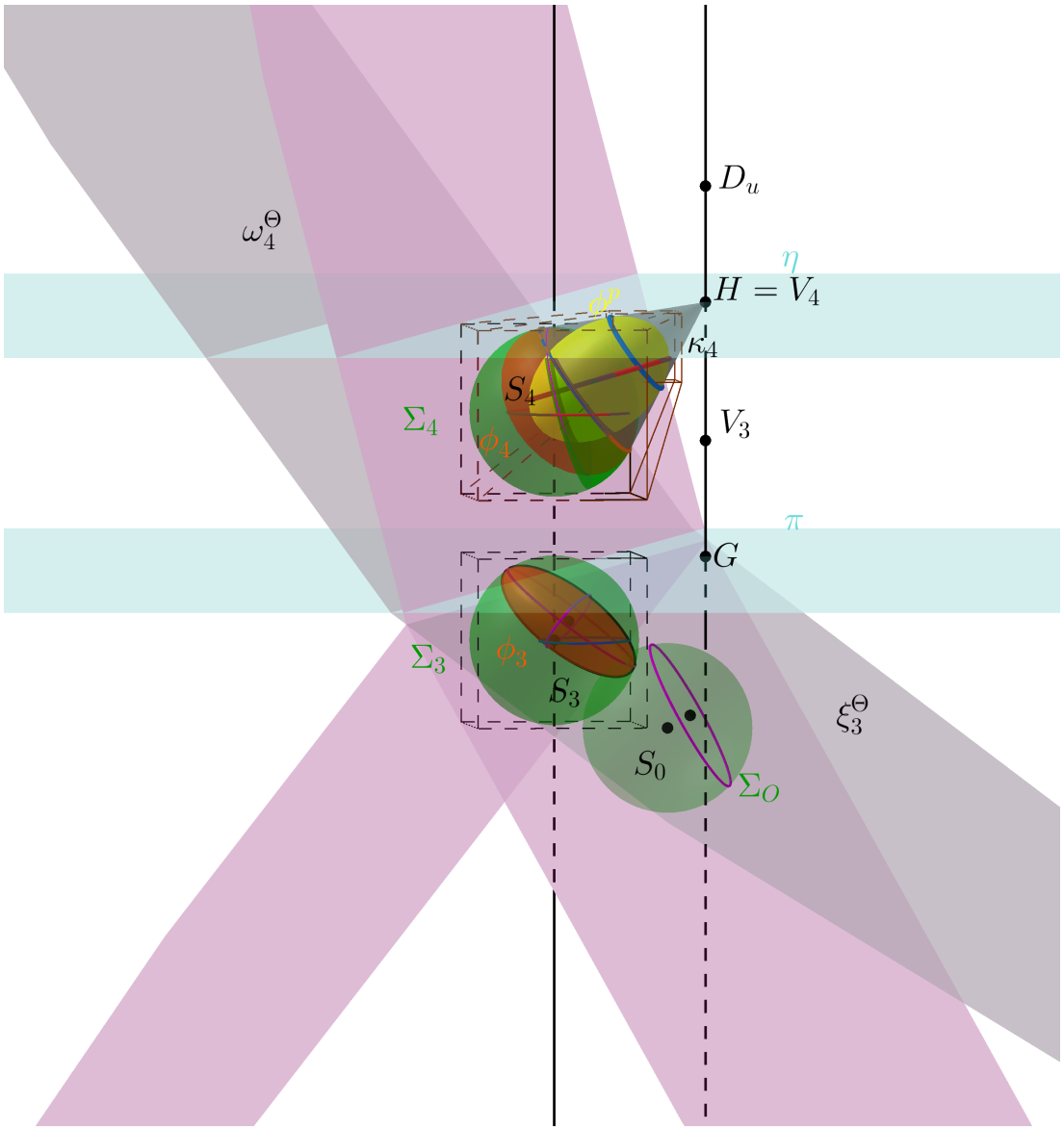

Figure 4.16: 4-perspective image ϕ^p of a 3-sphere Σ, with the construction in associated 4DDOP projection.

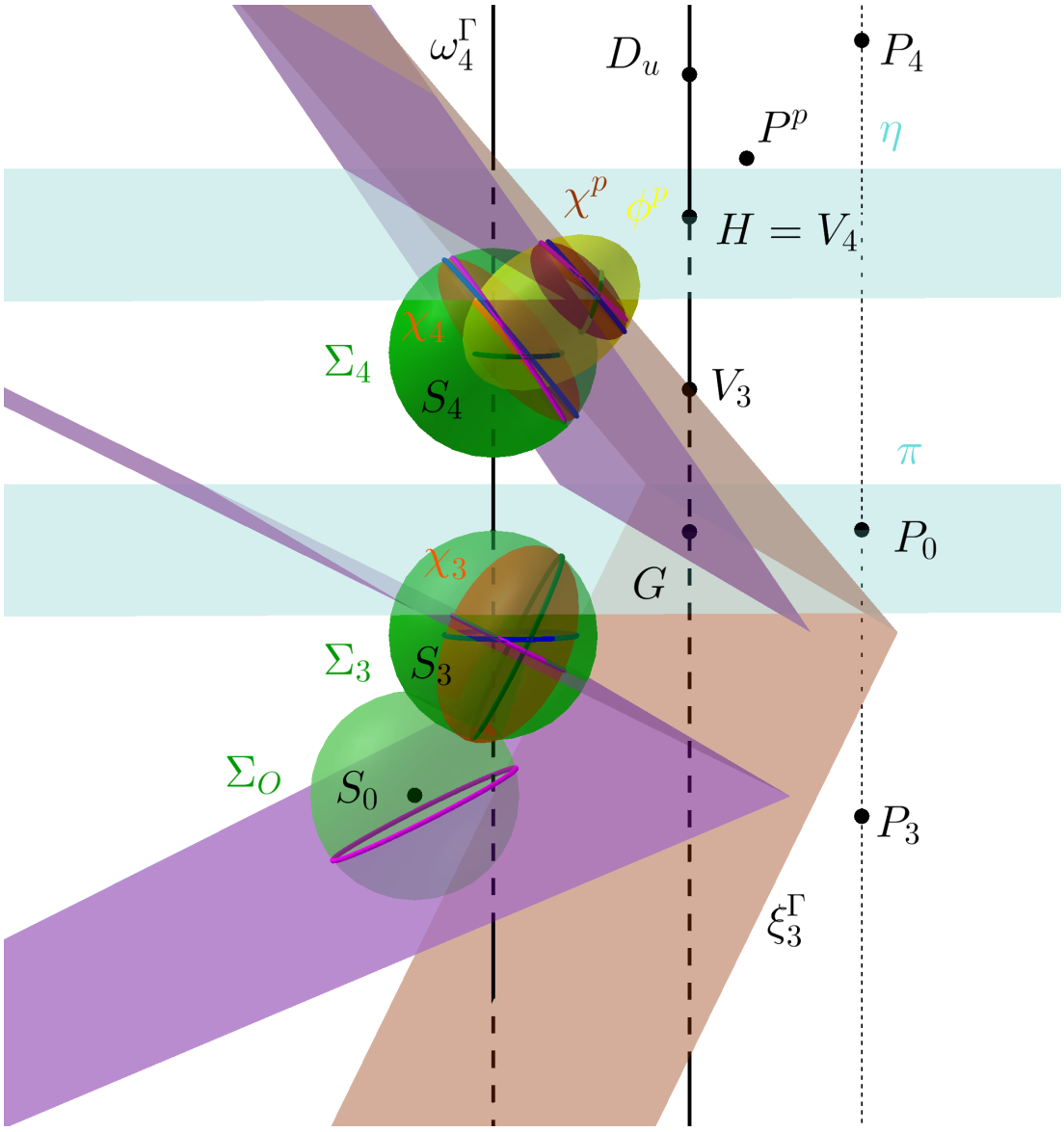

Figure 4.17: 4-perspective image χ^p of a section χ of a 3-sphere Σ with the polar 3-space Γ of a pole P with respect to Σ.

5. Use of 4D visualisation

In previous chapters, we discussed the visualisation of 4D objects. In this chapter, we will describe some practical applications of 4D visualisation. We cannot visualise and graphically solve any problem in the complex number plane[1] ($\mathbb{C}^2$) in the Euclidean plane. It is because an imaginary part is somewhere above and below the Euclidean plane. For this reason, it is more appropriate to visualise the complex number plane in a double orthogonal projection onto two mutually perpendicular three-spaces or in a four-dimensional perspective.

In the first part of this chapter, we will use 4DDOP and 4D perspective to visualise the complex number plane and show a way to solve some problems in the complex number plane.

The second part of this chapter is about shadows. We play with shadows every day. Shadows are all around us. For example, dear reader, we are sure you are trying not to cast a shadow on this text you are reading now. That is why it is essential to understand shadows in 4D. Therefore, the second part of this chapter is about 3D shadows of 4D algebraic hypersurfaces in 4D perspective.

The last part of this chapter contains a better understanding of 4D space. It is tough to understand 4D space and its visualisation. Therefore, the third part of this chapter is about 3D printed models of tesseract in double orthogonal projection and 4D perspective. This part shows how to understand 4D visualisation better because the printed model can be touched and rotated in the hands.

5.1 Complex number plane

Introduction

Let us consider a circle and a line in a real plane. The line intersects the circle in two real points, touches the circle in the point of tangency, or has no real but two complex conjugate points on the circle. This could be an elementary exercise in analytic geometry. However, the geometric construction or visualization of the last case is not as obvious. In this paper, our focus lies on the visualization of complex points.

The property of keeping the number of intersecting points of a line and a conic (or algebraic curve in general) and their geometric construction based on the polar properties of conics were described in Poncelet's early texts on the principle of continuity in the framework of projective geometry. Fig. 5.1, from the second edition of his comprehensive work — *Traité des propriétés projectives des figures* (Poncelet [1866]) shows a construction of a secant and non-secant line intersecting an ellipse. These ideas were thoroughly revisited and presented by Hatton around one hundred years later (see Hatton [1920]). In Chapter 6, Hatton described the process of "tracing of conics" along their conjugate diameters and created their planar graphs called Poncelet figures. We aim to lift this idea into a four-dimensional space to visualize the complex points of all branches at once.

[1] Not to be confused with the term "complex plane", which usually indicates the (Argand, Wessel, or also Gauss) plane with coordinate axes corresponding to real and imaginary elements of one complex variable.

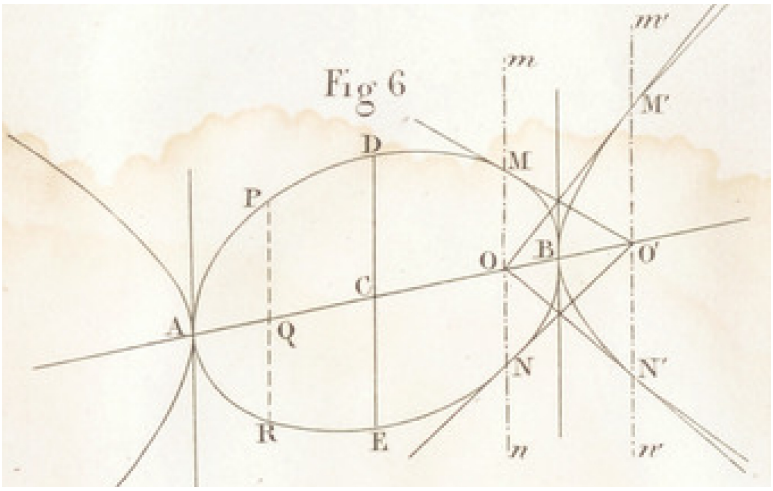

Figure 5.1: Poncelet's Fig. 6 (Poncelet [1866]). The points M, N are real points on the ellipse, while M', N' are complex points on the same ellipse. The points O and O' are poles of the polars $M'N'$ and MN with respect to the ellipse. (Source gallica.bnf.fr / Bibliothèque nationale de France).

In fact, the presently often used and popular visualizations of complex numbers founded by Argand and Wessel had appeared only two decades before Poncelet's *Traité* (see Scriba and Schreiber [2015] pp. 438–439 for historical details). To visualize two complex numbers as coordinates of the complex number plane $\mathbb{C}^2$ in a similar manner, one has to approach a four-dimensional real space. The advancement of computer graphics brought effective visualization tools in higher dimensions. Several authors displayed complex elements in separate 3-dimensional spaces (see Banchoff [2022], Avitzur [2022a]). A four-dimensional set of points is plotted in

$$(Re(x), Re(y), Im(x)),\ (Re(x), Re(y), Im(y)),$$

$$(Re(x), Im(x), Im(y)),\ \text{or}\ (Re(y), Im(x), Im(y)).$$

The author of (Avitzur [2022a]) has also created an iOS application (Avitzur [2022b]) that can display each of these graphs. Butler in (Butler [2022]) placed a perpendicular plane with axes $(Im(x), Im(y))$ at each point of the real plane $(Re(x), Re(y))$, then the perpendicular plane is rotated to the real plane such that the axes $Re(x)$ with $Im(x)$ and $Re(y)$ with $Im(y)$ are parallel at each point. Bozlee in (Bozlee and Amethyst [2022]) used 3D printing to create a 3D printed model with complex parts of elliptic curves using Amethyst's bertini_real software.

In this paper, we contribute to the topic by the visualization of complex points on a circle created in a double orthogonal projection into two mutually perpendicular 3-spaces (4DDOP, see Zamboj [2020]) and in a four-dimensional perspective (4D perspective, see Řada and Zamboj [2021]). Furthermore, we elaborate the visualization of a line through two points in $\mathbb{C}^2$. All the upcoming figures are created in *Wolfram Mathematica*.

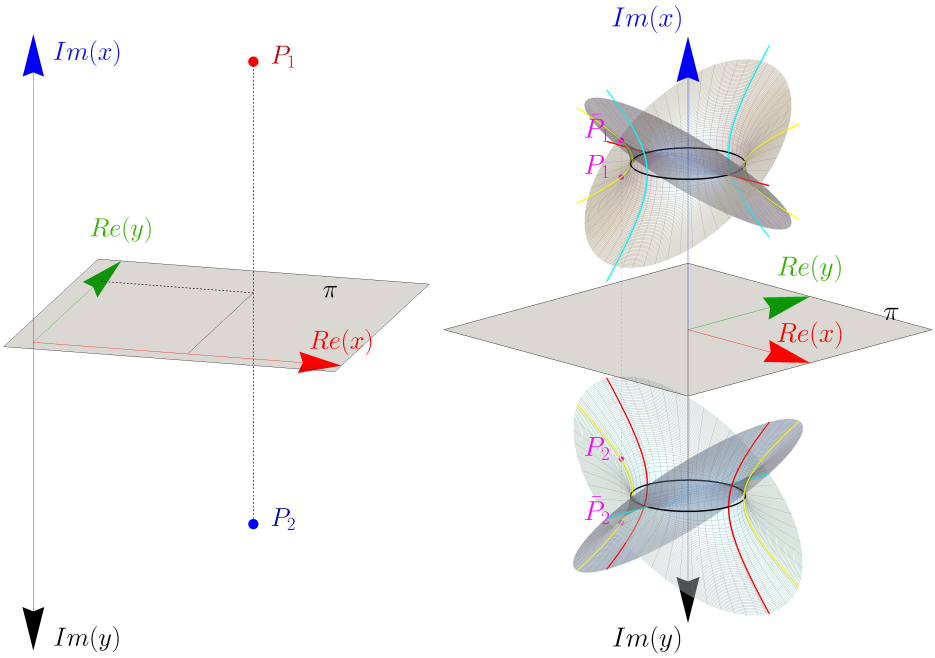

(a) (b)

Figure 5.2: (a) A point P with the coordinates $P[(Re(p_x), Im(p_x)); (Re(p_y), Im(p_y))]$ graphically represented in 4DDOP. $P_1[Re(p_x), Re(p_y), Im(p_x)]$ and $P_2[Re(p_x), Re(p_y), -Im(p_y)]$ are its Ξ- and Ω-images in one modeling 3-space.
(b) The intersections of a circle $c : x^2 + y^2 = 1$ traced by the lines $n : x\cos\varphi + y\sin\varphi = k$ for $k \in \mathbb{R}$ and $\varphi = 0$ (red), $\frac{\pi}{6}$ (yellow), $\frac{\pi}{2}$ (cyan). Points P and $\overline{P}$ are complex conjugate intersections on the line for $\varphi = \frac{\pi}{6}$.

Tracing a circle

Let us return to the circle – line problem. Suppose we have a real plane $\mathbb{R}^2$ with the coordinate system (x, y), the circle

$$c : x^2 + y^2 = 1,$$

and trace it with the line

$$l : x = k,$$

for $k \in \mathbb{R}$ parallel to y-axis. For $k \in (-\infty, -1) \cup (1, \infty)$, the roots of the corresponding quadratic equation in y are $\pm i\sqrt{k^2 - 1}$. The intersecting points $[k; i\sqrt{k^2 - 1}]$ and $[k; -i\sqrt{k^2 - 1}]$ are on c and l, but not in the plane $\mathbb{R}^2$. Let us extend the real plane with the imaginary components such that the real coordinates x and y will be denoted $Re(x)$ and $Re(y)$ and the imaginary parts $Im(x)$ and $Im(y)$. A point P in the complex number plane has coordinates $P[p_x, p_y]$ in $\mathbb{C}^2$ and $P[(Re(p_x), Im(p_x)); (Re(p_y), Im(p_y))]$ in $\mathbb{R}^4$, for $p_x = (Re(p_x), Im(p_x))$ and $p_y = (Re(p_y), Im(p_y))$. Consequently, we identify the complex number plane $\mathbb{C}^2$ with $\mathbb{R}^4$ with the orthogonal system of axes $(Re(x), Im(x), Re(y), Im(y))$. For example, the above-mentioned complex intersecting points of l and c have coordinates $[(k, 0); (0, \sqrt{k^2 - 1})]$ and $[(k, 0); (0, -\sqrt{k^2 - 1})]$ in $\mathbb{R}^4$ (while the purely real points for $k \in \langle -1, 1\rangle$ are $[(k, 0); (\sqrt{1 - k^2}, 0)]$ and $[(k, 0); (-\sqrt{1 - k^2}, 0)]$).

For visualization, we use the 4DDOP method. Each point

$$P[(Re(p_x), Im(p_x)); (Re(p_y), Im(p_y))]$$

is orthogonally projected into the reference 3-spaces $\Xi(Re(x), Im(x), Re(y))$ and $\Omega(Re(x), Re(y), Im(y))$ with the common plane $\pi(Re(x), Re(y))$ (Fig. 5.2a). Both 3-spaces Ξ and Ω are represented in one modeling 3-space such that a perpendicular line to the plane $\pi(Re(x), Re(y))$ creates axes $Im(x)$ and $Im(y)$ with the opposite orientations ($Im(x)$ upwards, $Im(y)$ downwards).

Let us have a closer look at the example above. Observe the locus of intersecting points of c and l, in 4DDOP (Fig. 5.2b). For $k \in \langle -1, 1\rangle$, $Im(x)$ and $Im(y)$-coordinates are zero, the real parts are obviously related by the equation

$$Re(x)^2 + Re(y)^2 = 1,$$

representing the circle in the plane $(Re(x), Re(y))$. However, for $k \in (-\infty, -1) \cup (1, \infty)$, equations

$$Im(x) = 0;\ Re(y) = 0;\ Re(x)^2 - Im(y)^2 = 1$$

represent a hyperbola in the plane $(Re(x), Im(y))$ and hence also in the 3-space $\Omega(Re(x), Re(y), Im(y))$. Both branches of this hyperbola are projected into two rays in the 3-space $\Xi(Re(x), Re(y), Im(x))$.

Tracing the circle c with a line

$$m : y = k,$$

for $k \in \mathbb{R}$, parallel with the x-axis (back in $\pi(Re(x), Re(y))$), we obtain the points of intersection $[(0, \pm\sqrt{k^2 - 1}); (k, 0)]$ for $k \in (-\infty, -1) \cup (1, \infty)$ and $[(\pm\sqrt{1 - k^2}, 0); (k, 0)]$ for $k \in \langle -1, 1\rangle$ in $\mathbb{C}^2$. Apart from the same circle in the plane $\pi(Re(x), Re(y))$, the complex points lie on a hyperbola in the plane $(Im(x), Re(y))$ and so in $\Xi(Re(x), Im(x), Re(y))$. The Ω-image of the hyperbola consists of two rays in $(Re(x), Re(y), Im(y))$.

For a general case, assume a line n given by the following equation

$$n : x\cos\varphi + y\sin\varphi = k \text{ for } \varphi \in \langle 0, 2\pi), k \in \mathbb{R}.$$

Its intersection points with c are

$$[k\cos\varphi - \sqrt{(1 - k^2)\sin^2\varphi};\ k\cos\varphi + \cot\varphi\sqrt{(1 - k^2)\sin^2\varphi}],$$
$$[k\cos\varphi + \sqrt{(1 - k^2)\sin^2\varphi};\ k\cos\varphi - \cot\varphi\sqrt{(1 - k^2)\sin^2\varphi}].$$

For $k \in \langle -1, 1\rangle$ the points must lie on the circle in $\pi(Re(x), Re(y))$. For $k \in (-\infty, -1) \cup (1, \infty)$ the values of coordinates always contain an imaginary element, and they represent a hyperbola rotated along the circle and twisted in $\mathbb{C}^2$. Orthogonal images of the surface generated in Fig. 5.3 are created by the extraction of the real and imaginary parts of the intersection points. At last, the image in 4D perspective is in Fig 5.4.

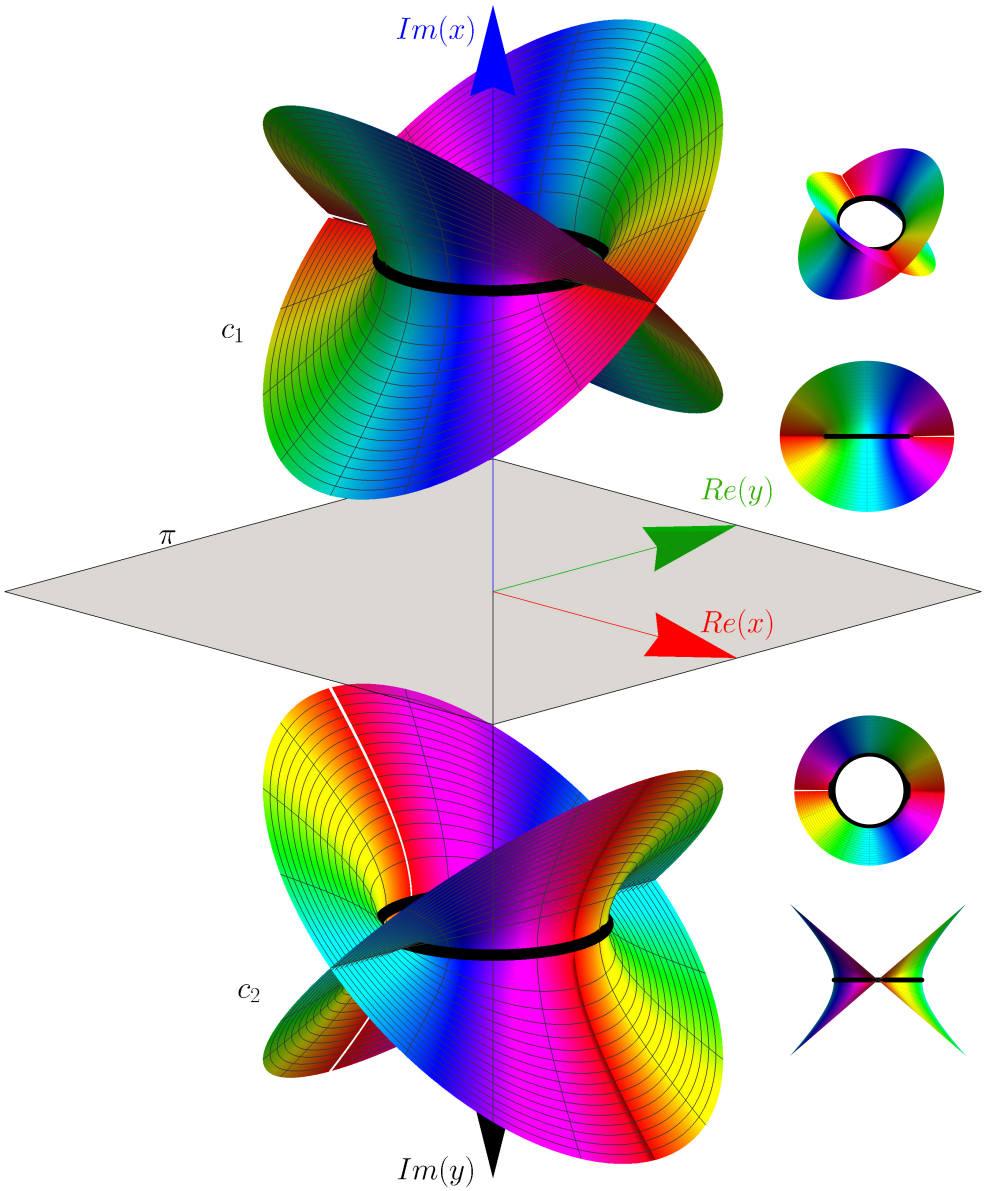

Figure 5.3: The surface of a real circle c generated by its complex points visualized in 4DDOP. Views in special positions are on the right side. The circle is shifted in the directions $Im(x)$ and $Im(y)$ so that images in the 3-spaces $(Re(x), Im(x), Re(y))$ and $(Re(x), Re(y), Im(y))$ do not overlap in the figure.

Further issues

The method used in the previous section is theoretically applicable for any algebraic curve over $\mathbb{R}$. At first, the curve is traced by all real lines in the real plane to obtain complex intersections. Next, we extract the real and imaginary parts of the complex points of intersection and plot the final image embedded in $\mathbb{R}^4$. The surfaces corresponding to some other conics: a hyperbola, parabola, imaginary regular conic; and a cubic are depicted in Figs. 5.5a–5.5d. However, raising the order of the curve, the computational complexity (equation solving, plotting) increases rapidly.

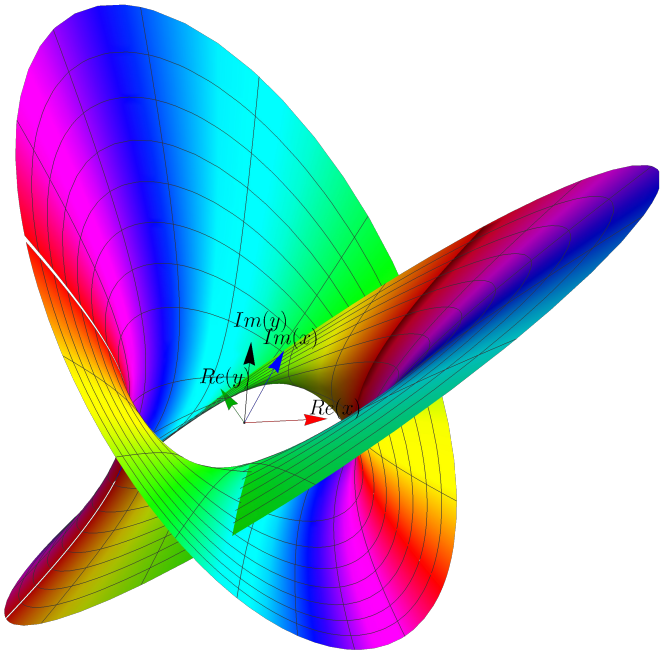

Figure 5.4: The surface of a real circle c generated by its complex points visualized in 4D perspective.

Lines in $\mathbb{CP}^2$

We have been constructing complex points of real curves and lines until now. On top of that, we can construct any point with coordinates in $\mathbb{C}^2$. In this section, we will move a little further and explore the construction of an arbitrary line in $\mathbb{C}^2$. Since our visualizations are created in the four-dimensional real space, we should be aware that images of lines in $\mathbb{C}^2$ will behave differently from the real lines. For example, one linear equation represents a hyperspace in $\mathbb{R}^n$. While this holds well for lines in $\mathbb{R}^2$, one equation in $\mathbb{R}^4$ represents a 3-space. Therefore, each line in $\mathbb{C}^2$ will generate a 3-space in $\mathbb{R}^4$. Furthermore, the lines $Re(x) = 0$ and $Im(x) = 0$ are equivalent in $\mathbb{C}^2$, due to multiplication by a constant i, but they seem distinct in $\mathbb{R}^4$. To avoid such confusion, we approach lines through the projective extension $\mathbb{CP}^2$.

A point P in $\mathbb{CP}^2$ has homogeneous coordinates $P(p_1; p_2; p_0) \neq (0; 0; 0)$ for $p_1; p_2; p_0 \in \mathbb{C}$ such that $(p_1; p_2; p_0) \sim (\lambda p_1; \lambda p_2; \lambda p_0)$ for $\lambda \in \mathbb{C}\backslash\{0\}$. Expanding real and imaginary parts of the point P, the coordinates will be in the form $P((Re(p_1), Im(p_1)); (Re(p_2), Im(p_2)); (Re(p_0), Im(p_0)))$. For the sake of visual representation, we always factorize the coordinates by the last nonzero coordinate. Therefore, proper points in $\mathbb{C}^2$ will be represented by points with coordinates $((Re(p_x), Im(p_x)); (Re(p_y), Im(p_y)); (1, 0))$ and directions or improper points as $((Re(p_x), Im(p_x)); (1, 0); (0, 0))$ or $((1, 0); (0, 0); (0, 0))$. Conveniently using the duality in projective spaces, the same holds for the coordinates of lines. Let $((Re(l_x), Im(l_x)); (Re(l_y), Im(l_y)); (1, 0))$ be (factorized) coordinates of a line l,

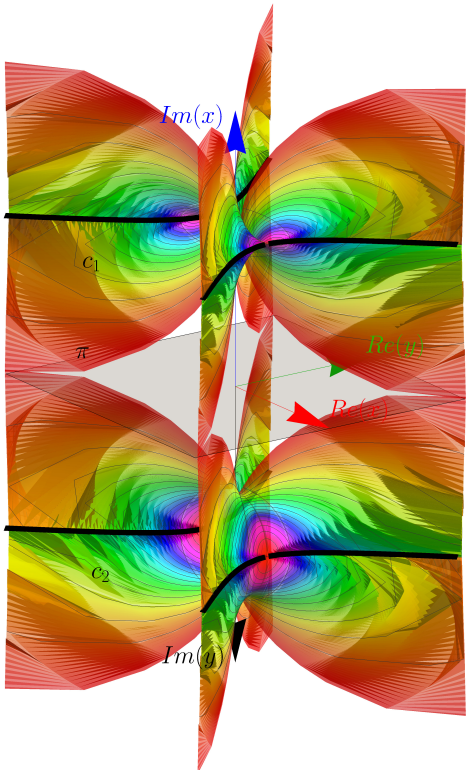

(a) Hyperbola: $x^2 - y^2 = 1$

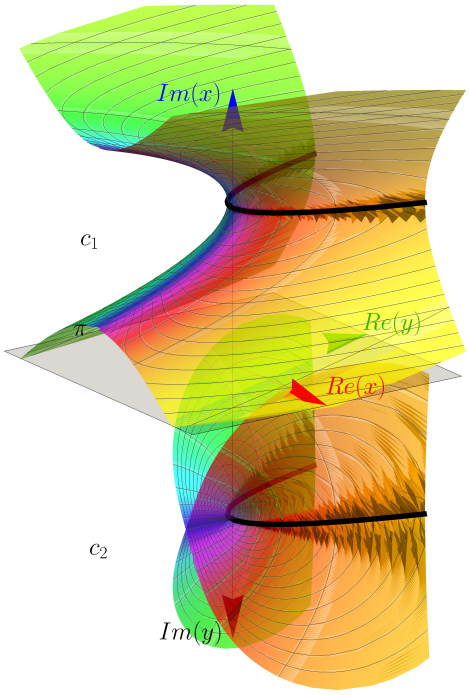

(b) Parabola: $y = x^2$

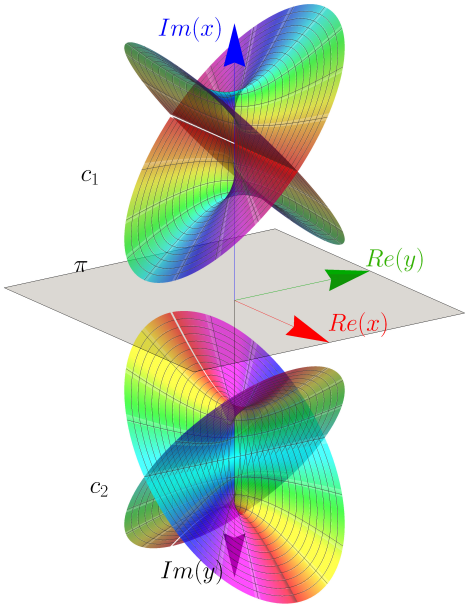

(c) Imaginary regular conic: $x^2+y^2 = -1$

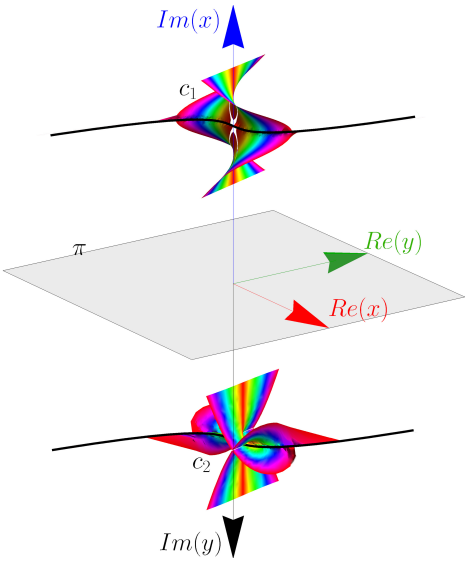

(d) Cubic: $y = x^3$

Figure 5.5: Surfaces of curves generated by their complex points visualized in 4DDOP. All the surfaces are shifted in $Im(x)$ and $Im(y)$ directions so that they do not overlap.

then its equation in the expanded form in $\mathbb{R}^4$ is

$$Re(l_x)Re(x) + Im(l_x)Im(x) + Re(l_y)Re(y) + Im(l_y)Im(y) + 1 = 0.$$

Similarly for lines with coordinates $((Re(l_x), Im(l_x)); (1, 0); (0, 0))$

$$Re(l_x)Re(x) + Im(l_x)Im(x) + Re(y) = 0$$

or for $((1,0);(0,0);(0,0))$

$$Re(x) = 0.$$

Such equations represent 3-spaces in $\mathbb{R}^4$. To visualize 3-space in orthogonal projection, we construct its *traces*, i.e., intersecting planes with the 3-spaces $\Xi(Re(x), Im(x), Re(y))$ and $\Omega(Re(x), Re(y), Im(y))$. Substituting $Im(y) = 0$ and $Im(x) = 0$ into the equation of the line, we obtain the respective Ξ- and Ω-traces (see also Zamboj [2018b] for synthetic constructions of traces of 3-spaces). As a consequence, the real part of the line is its intersection with the plane $\pi(Re(x), Re(y))$ obtained by vanishing the terms with $Im(x)$ and $Im(y)$.

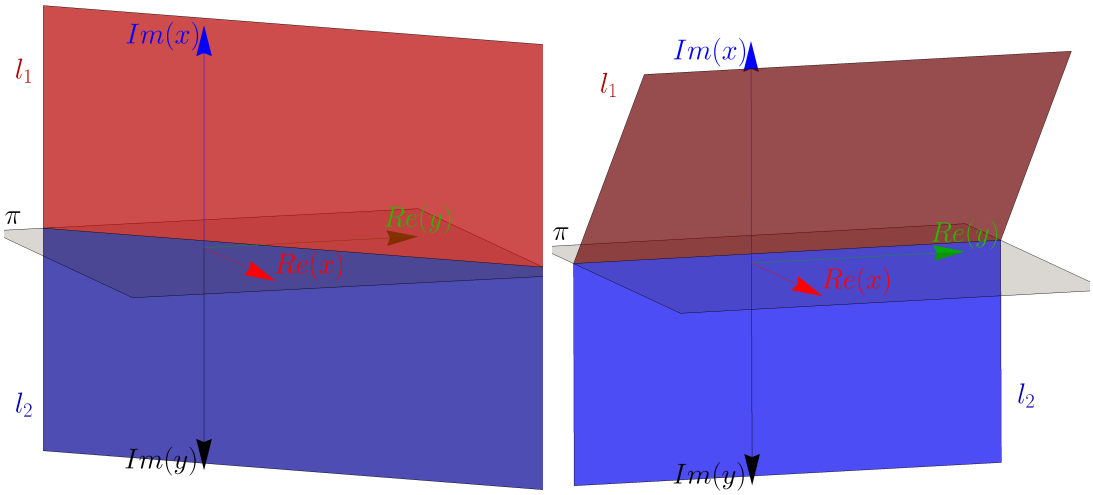

(a) $l((1,0);(-1,0);(1,0))$
$Re(x) - Re(y) + 1 = 0$

(b) $l((1,-1);(0,0);(1,0))$
$Re(x) - Im(x) + 1 = 0$

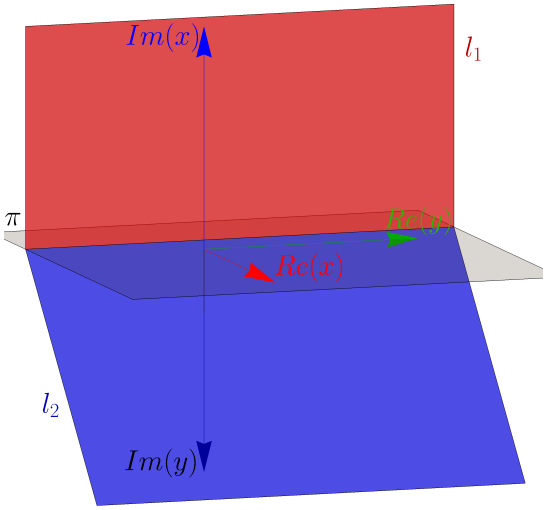

(c) $l((1,0);(0,-1);(1,0))$
$Re(x) - Im(y) + 1 = 0$

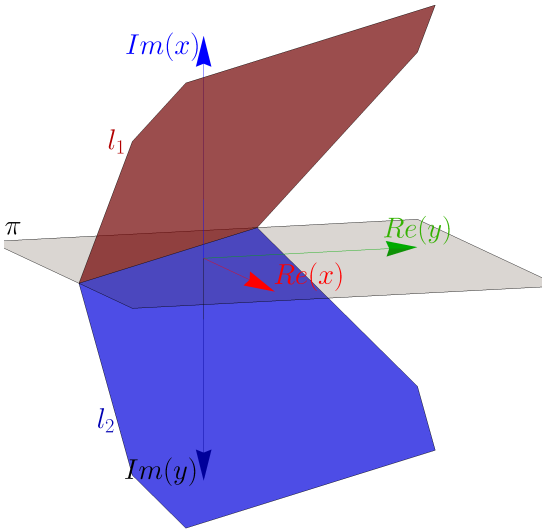

(d) $l((1,-1);(1,-1);(1,0))$
$Re(x) - Im(x) + Re(y) - Im(y) + 1 = 0$

Figure 5.6: Lines in $\mathbb{CP}^2$ represented as 3-spaces in $\mathbb{R}^4$ in 4DDOP. The 3-spaces are given by their intersections with reference 3-spaces $\Xi(Re(x), Im(x), Re(y))$ (red) and $\Omega(Re(x), Re(y), Im(y))$ (blue).

Let us examine the visual representations of lines with several examples in

Fig. 5.6.

1. A line l with coordinates $((1,0);(-1,0);(1,0))$ and the equation

$$Re(x) - Re(y) + 1 = 0$$

is depicted in Fig. 5.6a. Observe, that the intersection of l with the plane $\pi(Re(x), Re(y))$ does not change the equation. Furthermore, it is arbitrary in $Im(x)$ and $Im(y)$. The extension of the line in the directions $Im(x)$ in the 3-space $\Xi(Re(x), Im(x), Re(y))$ and in $Im(y)$ in $\Omega(Re(x), Re(y), Im(y))$ generates the trace planes of the 3-space of l. Therefore, the trace planes are perpendicular to π in the modeling 3-space. Additionally, we should remind the reader that, due to equivalence, the same representation will have all lines multiplied by a nonzero complex scalar, e.g.:

$$Im(x) - Im(y) + i = 0 \sim$$

$$Re(x) - Im(x) - Re(y) + Im(y) + 1 - i = 0 \ldots.$$

2. See Fig. 5.6b for $l((1,-1);(0,0);(1,0))$ with the equation

$$Re(x) - Im(x) + 1 = 0.$$

Apparently, the line $Re(x) + 1 = 0$ is the intersection with π. The Ξ-image could be reconstructed from the image in the plane $(Re(x), Im(x))$, and the Ω-image is, again, perpendicular to π in the modeling 3-space.

3. See Fig. 5.6c for $l((1,0);(0,-1);(1,0))$ with the equation

$$Re(x) - Im(y) + 1 = 0.$$

The situation is similar to the previous case. Now, the Ξ-image is perpendicular to π.

4. See Fig. 5.6d for $l((1,-1);(1,-1);(1,0))$ with the equation

$$Re(x) - Im(x) + Re(y) - Im(y) + 1 = 0.$$

In this case, none of the trace planes are perpendicular to π. The traces could be generated separately by setting the imaginary components to 0 in the respective 3-spaces.

Joins and intersections

In complex homogeneous coordinates in $\mathbb{CP}^2$, a point $P(p_1; p_2; p_0)$ lies on a line $l(l_1; l_2; l_0)$ if

$$p_1 l_1 + p_2 l_2 + p_0 l_0 = 0.$$

Using the dot product

$$P \cdot l = 0.$$

Another point Q lies on l if

$$Q \cdot l = 0.$$

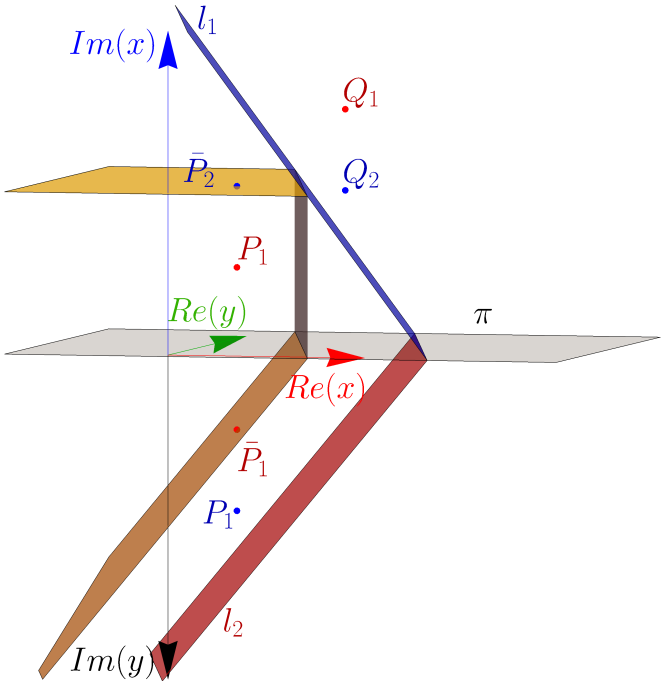

Figure 5.7: A line l in $\mathbb{CP}^2$ passing through points P, Q represented as a 3-space in $\mathbb{R}^4$. The complex conjugates $\bar{P}, \bar{Q}$ of P, Q lie on the 3-space, which is given by its planar intersections with $\Xi(Re(x), Im(x), Re(y))$ and $\Omega(Re(x), Re(y), Im(y))$ in $\mathbb{R}^4$ using the 4DDOP method.

Hence

$$l = P \times Q.$$

Dually, a point P is the intersection of distinct lines p and q, only if

$$P = p \times q$$

(see Richter-Gebert [2011], Chapter 3 for details).

Graphical representation in $\mathbb{R}^4$ of lines and points in $\mathbb{C}^2$ will work slightly differently, too. This is because the multiplication of imaginary components changes sign. For example, the dot product of a point $P(p_1; p_2; p_0)$ and a line $l(l_1; l_2; l_0) \in \mathbb{CP}^2$ is

$$p_1 l_1 + p_2 l_2 + p_0 l_0.$$

However, after the expansion into real and imaginary components, we have

$$\begin{aligned} P((Re(p_1), Im(p_1)); (Re(p_2), Im(p_2)); (Re(p_0), Im(p_0))) \cdot \\ l((Re(l_1), Im(l_1)); (Re(l_2), Im(l_2)); (Re(l_0), Im(l_0))) = \\ Re(p_1)Re(l_1) - Im(p_1)Im(l_1) + Re(p_2)Re(l_2) - Im(p_2)Im(l_2) + \\ Re(p_0)Re(l_0) - Im(p_0)Im(l_0). \end{aligned}$$

Therefore, in the visualizations in $\mathbb{R}^4$ the point P will not lie in the 3-space representing line l. On the other hand, the complex conjugate

$$\bar{P}((Re(p_1), -Im(p_1)); (Re(p_2), -Im(p_2)); (Re(p_0), -Im(p_0))$$

of the point P lies on the 3-space of the line l through P. And oppositely, the point P lies in the 3-space representing the complex conjugate $\bar{l}$ of the line l in $\mathbb{R}^4$. In Fig 5.7 the line l has coordinates

$$l = P \times Q,$$

but the complex conjugate points $\bar{P}$ of P and $\bar{Q}$ of Q lie on the 3-space of the line l. This is also verified in the figure by the construction of the plane in the 3-space of l through $\overline{P}$ parallel to $\Omega(Re(x), Re(y), Im(y))$.

Conclusion

We have revisited the method of finding complex points on a circle by tracing the circle with a line. Intersecting points generate a surface in the 4-dimensional space $(Re(x), Im(x), Re(y), Im(y))$. The final visualization of the images was plotted in a double orthogonal projection into 3-spaces $(Re(x), Im(x), Re(y))$ and $(Re(x), Re(y), Im(y))$ and in four-dimensional perspective projection. The method was applied to visualize complex points of other conics and a cubic curve. Moreover, it can be used for many other real curves; however, it is very limited by computational complexity. A further possibility of application is, for instance, in finding graphical solutions of complex intersections of real curves.

Furthermore, through a projective extension, we have described how to visualize a complex straight line as a three-dimensional subspace of a four-dimensional real space. We have also discussed how to verify the incidence of a point and a line and how to visualize the join of two points. These concepts are easily extendable and applicable for further research in visualizing a complex number plane identified with a four-dimensional real space.

To visualise the complex plane, we need to be able to represent 4D space. We teach architecture students to visualise shadows to improve clarity and depth. In the next section, we describe shadows in 4D space. We leave it to the reader to consider whether shadows improve visual understanding in higher dimensions.

5.2 3D shadows of 4D algebraic hypersurfaces in a 4D perspective

The part is focused on the four-dimensional visualization of hypersurfaces represented by implicit equations without their parametrization. We describe a general method to find shadow boundaries in an arbitrary dimension and apply it in a three- and four-dimensional space. Furthermore, we design a system of polynomial equations to construct occluding contours of algebraic surfaces in a 4-D perspective. The method is presented on a composed 3-D scene and three 4-D cases with gradual complexity. In general, our goal is to improve the understanding of spatial properties in a four-dimensional space.

Introduction

Visualizing shapes embedded in more-dimensional spaces faces several challenges. In many cases, mere projections into three- or less-dimensional spaces contain

overlapping parts, making them difficult to understand. One technique that enhances intuition about the properties of shapes and their mutual relations is to visualize shadows cast on themselves and on other objects. Apart from the general case, choosing algebraic hypersurfaces defined by polynomials is often convenient. These are good candidates for visualization using computational methods of algebraic geometry and elimination theory. In this sense, instead of sets of many points and operating with meshes, we can work with implicitly represented hypersurfaces, their projections, contours, intersections, etc. Since algebraic methods preserve many properties of the visualized shapes, they are suitable for precise mathematical visualization. The disadvantage of implicit representation is the computational speed when processing polynomials of higher degrees or adding more variables.

This paper aims to improve understanding spatial properties in a four-dimensional scene containing algebraic hypersurfaces. To do so, we join theoretical geometric construction and algebraic computational methods and provide concrete examples of visualizations of four-dimensional hypersurfaces and their shadows based on implicit representations.

In particular, we show visualizations of four-dimensional algebraic hypersurfaces (3-surfaces), their contours (2-surfaces), terminators, and 3-D shadows cast on other 3-surfaces with respect to a point light source. The process consists of two main parts – central projection of the scene into a 3-D modeling space (usually a virtual 3-D environment in some software, AR, VR, or even a real 3-D model) and construction of shadows from an arbitrary point light source. First, to construct a 4-D perspective image, a 3-surface given by a polynomial is intersected by its first polar (3-surface) with respect to the center of projection, and its (2-surface) contour generator is centrally projected into a modeling 3-space. The second phase is finding the terminator with respect to an arbitrary point light source and its projection to the 3-surface on which the shadow is cast. While geometrically, we describe intersections of surfaces,, algebraically, we need to find a polynomial that solves systems of polynomial equations with several variables (7 to 9 in the 4-D case). This leads to the use of standard computational methods such as finding a Gröbner basis or Dixon resultant. Finally, to complete the shadow, especially for 3-surfaces of degrees higher than 2, we need to find the regions in their own shade. Such regions are not algebraically omitted in the elimination procedure; hence, we need to carry out further selection.

Related Work

The algebraic concepts, in particular, the use of Gröbner basis and Dixon resultant for finding solutions of polynomial systems, are described in detail in (Kapur and Lakshman [1992]). A similar technique to find the implicit representation of an occluding contour in 3-D through the Dixon resultant was applied in (Khan [2007], Khan et al. [2014]). In our experiments, we used *Wolfram Mathematica 13* implementations of algorithms for finding Gröbner basis — (WM-GB Research [1991]) and the Dixon resultant — (WM-Dix Lichtblau [2023]), and also Dixon resultant — Fer-Dix-KSY or improved Fer-Dix-EDF (Lewis [2008a]) implemented in software *Fermat 6.5* (Lewis [2008b]) by Lewis, see (Lewis [2008c, 2018]).

In addition to our approach, where we start with surfaces given implicitly, a considerable part of previous research on computational aspects of surfaces deals with implicitization from parametric representation (e.g., Sederberg et al. [1984], Buse et al. [2003], Li et al. [2004], Lewis [2018]). The algebraic derivation of perspective images of surfaces and reconstruction with respect to further applications is shown in (Liu [2002]).

Four-dimensional projections through parameterization or point coordinates are described in (Noll [1967], Zachariáš and Velichov'a [2000], Miwa et al. [2013]). A 4-D perspective projection was also used to visualize implicitly given surfaces that arise in a complex number plane (Řada and Zamboj [2023]). A descriptive geometry approach for constructing 4-D perspective images of a 3-sphere in 3-D from orthogonal projections is discussed in (Řada and Zamboj [2021]). Visualizations of the 4-space, including hypersurfaces, are treated comprehensively in (Banchoff [1990]). In (Zhou [1991], Hoffmann and Zhou [1991]), the authors created projections of several examples of surfaces in 4-space, examined their properties geometrically and algebraically, and showed various applications. Four-dimensional lighting was used to study the shades of some mathematically interesting 3-surfaces in (Hanson and Heng [1991]). Interactive manipulation with four-dimensional objects based on their projections or shadows in a hyperplane is elaborated in (Banks [1992], Zhang and Hanson [2007]) and through a tetrahedral mesh construction in (Chu et al. [2009], Cavallo [2021]).

Contribution

Our approach emphasizes algebraic methods in four-dimensional visualization. Throughout the paper, we work purely with implicit representations of surfaces without the necessity of their parametrization. Visualizing shadows between 3-surfaces, we discuss their mutual relations in the 4-space. In this way, compared to previous attempts, we offer a more comprehensive perception of complex 4-D scenes projected into 3-D space. We also provide a direct method for visualization of 3-surfaces in a 4-D perspective. After all, the designs of polynomial systems for constructing tangent cones and shadow boundaries as intersections are general for any dimension.

Paper organization

The rest of the article is organized as follows: we start with a 3-D example to describe the algorithm to find the terminator of a 2-surface and its shadow cast on another 2-surface in Section 2. Next, we generalize it into 4D and describe the 4-D perspective from a 4-space into the modeling 3-space. Section 3 is focused on concrete examples. The 3-D scene from the previous explanation is supplemented with technical details. Next, we consecutively examine three 4-D scenes with respect to their geometric and computational complexity. In Section 4, we discuss the critical points of our method and propose further research directions. Section 5 summarizes the results of this paper. Computation times, and videos are attached in Appendices A.

5.2.1 Method

Constructing shadow of an algebraic hypersurface

In the first part, we examine the process of computing a shadow in an arbitrary dimension but visualized in a 3-D case[2].

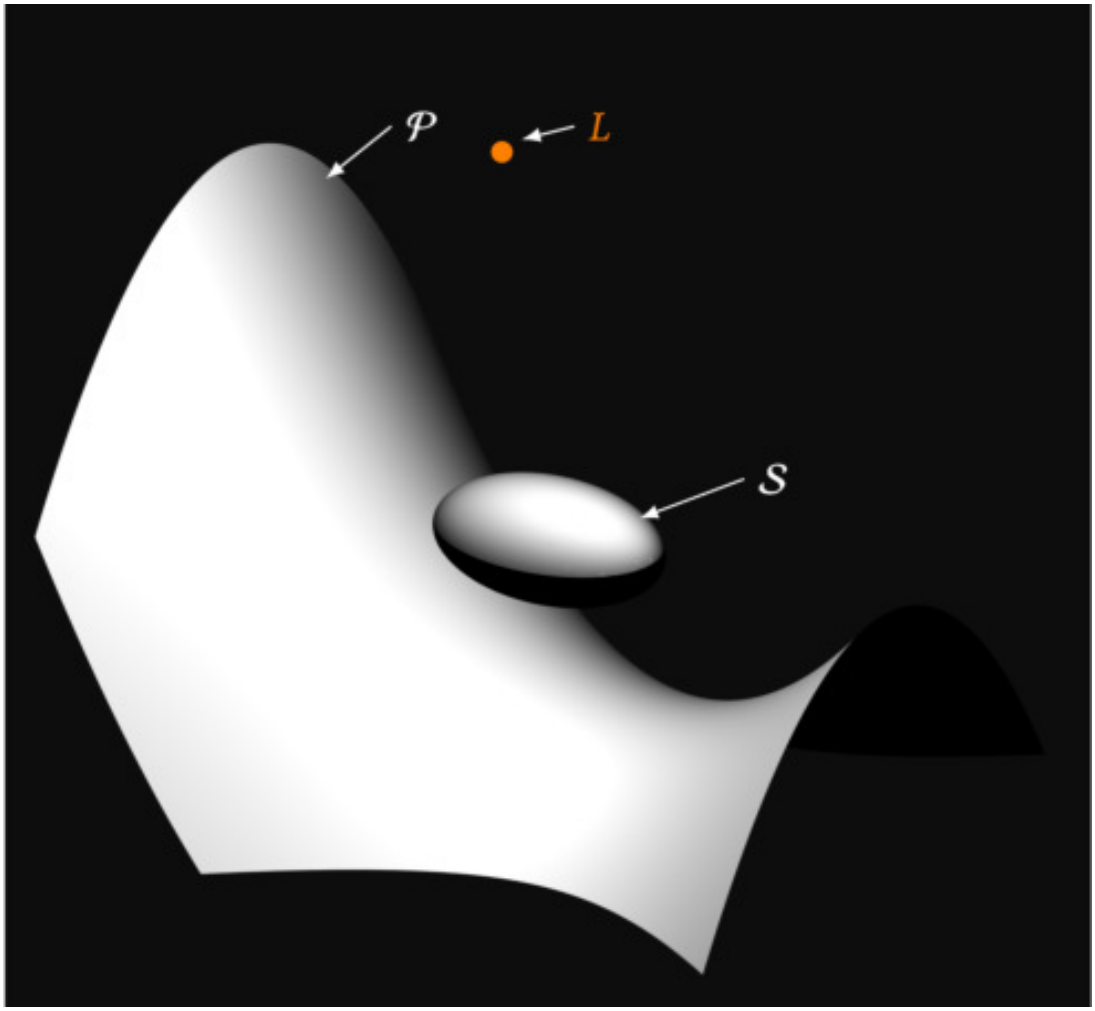

Figure 5.8: Initial setting of hypersurfaces $\mathcal{S}, \mathcal{P}$, and a point light source L.

Preliminaries

Let us have a hypersurface $\mathcal{S}$ (Figure 5.8), i.e., an $(n-1)$-surface embedded in a real n-space ($n \geq 1$) given by a polynomial equation in n variables

$$\mathcal{S} : \sigma = 0. \tag{5.1}$$

To find polar hypersurfaces, it will be convenient to work with homogeneous coordinates in the projectively extended real space.

[2]The upcoming 3-D visualizations are created in *Wolfram Mathematica 13* from outputs based on implicit equations (or inequalities) formulated in variables x, y, z. Therefore, they are also usable as 3-D graphics in an interactive environment.

Let us have $(x'_1, x'_2, \ldots, x'_n, x'_0), (y'_1, y'_2, \ldots, y'_n, y'_0) \in \mathbb{R}^{n+1} \setminus \{(0, 0, \ldots, 0)\}$. We define the equivalence $(x'_1, x'_2, \ldots, x'_n, x'_0) \sim (y'_1, y'_2, \ldots, y'_n, y'_0)$, if there exists $\lambda \in \mathbb{R} \setminus \{0\}$ such that $(x'_1, x'_2, \ldots, x'_n, x'_0) = (\lambda y'_1, \lambda y'_2, \ldots, \lambda y'_n, \lambda y'_0)$. The projective n-space is defined as equivalance classes of $\mathbb{R}^{n+1} \setminus \{(0, 0, \ldots, 0)\}$. A point $\overline{P}(p'_1, p'_2, \ldots, p'_n, p'_0)$ of the projective space has homogeneous projective coordinates $(p'_1, p'_2, \ldots, p'_n, p'_0)$. Additionally, for $p'_0 \neq 0$, we can obtain the Cartesian coordinates of $P(p_1, p_2, \ldots, p_n)$ by substituting $p_1 = \frac{p'_1}{p'_0}, p_2 = \frac{p'_2}{p'_0}, \ldots, p_n = \frac{p'_n}{p'_0}]$, or vice versa. In case $p'_0 = 0$, the point $\overline{P}$ represents a point at infinity. Throughout the text, $\overline{\sigma}, \overline{P}, \ldots$ denote representations of $\sigma, P, \ldots$ in homogeneous coordinates.

Let $\overline{P}$ be a regular point of $\mathcal{S}$ and assume a polynomial $\overline{\sigma_P} = \overline{P}^T \nabla \overline{\sigma}$. A polar hypersurface $\mathcal{S}_P : \overline{\sigma_P} = 0$ is called the first polar of the point $\overline{P}$ with respect to the hypersurface $\mathcal{S}$.

Terminator

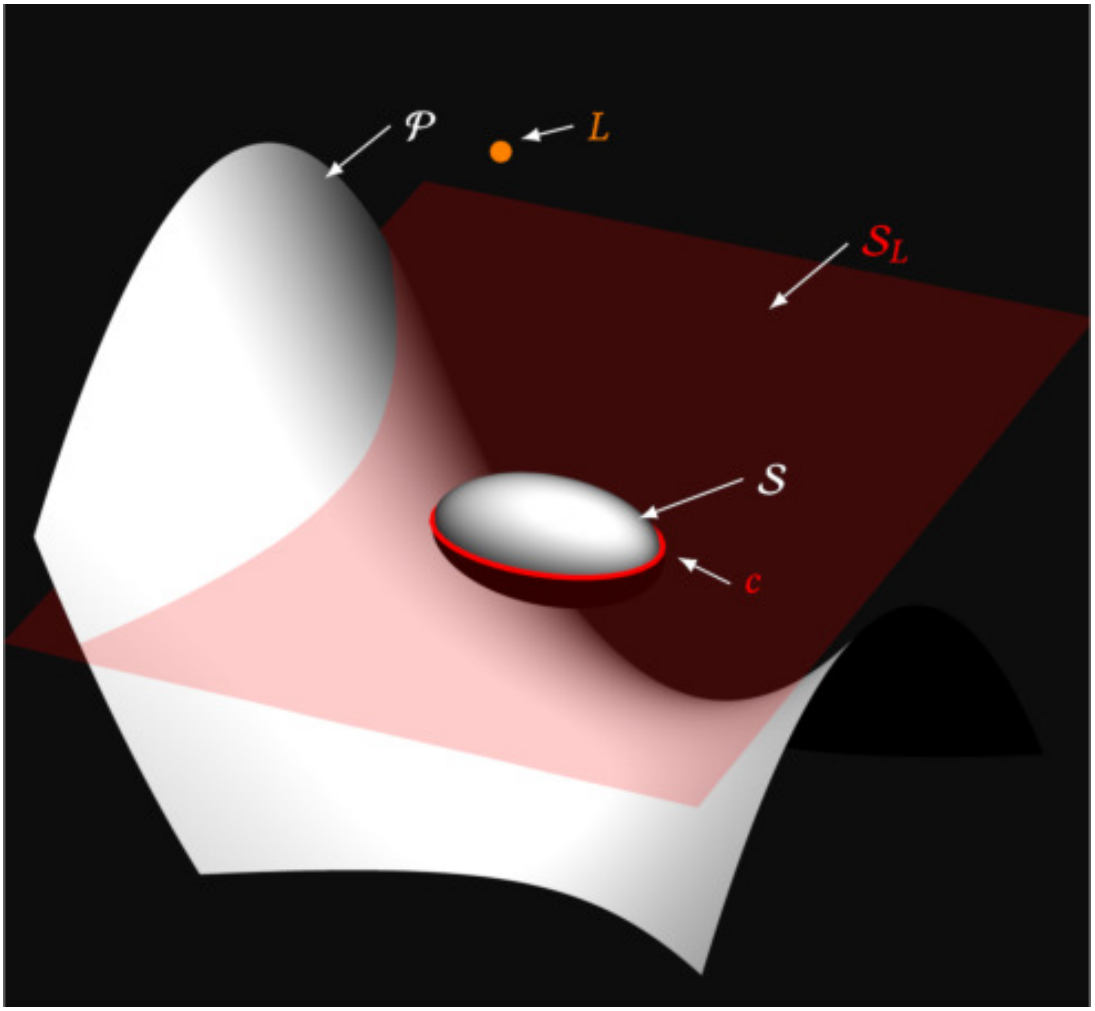

Figure 5.9: The polar hypersurface $\mathcal{S}_L$ of a hypersurface $\mathcal{S}$ with respect to a point light source L and its terminator c.

Let us have a point light source $L[l_1, \ldots, l_n]$ with homogeneous coordinates $\overline{L}(\overline{l_1}, \ldots, \overline{l_n}, \overline{l_0})$. The terminator c of the hypersurface $\mathcal{S}$ with respect to L is the

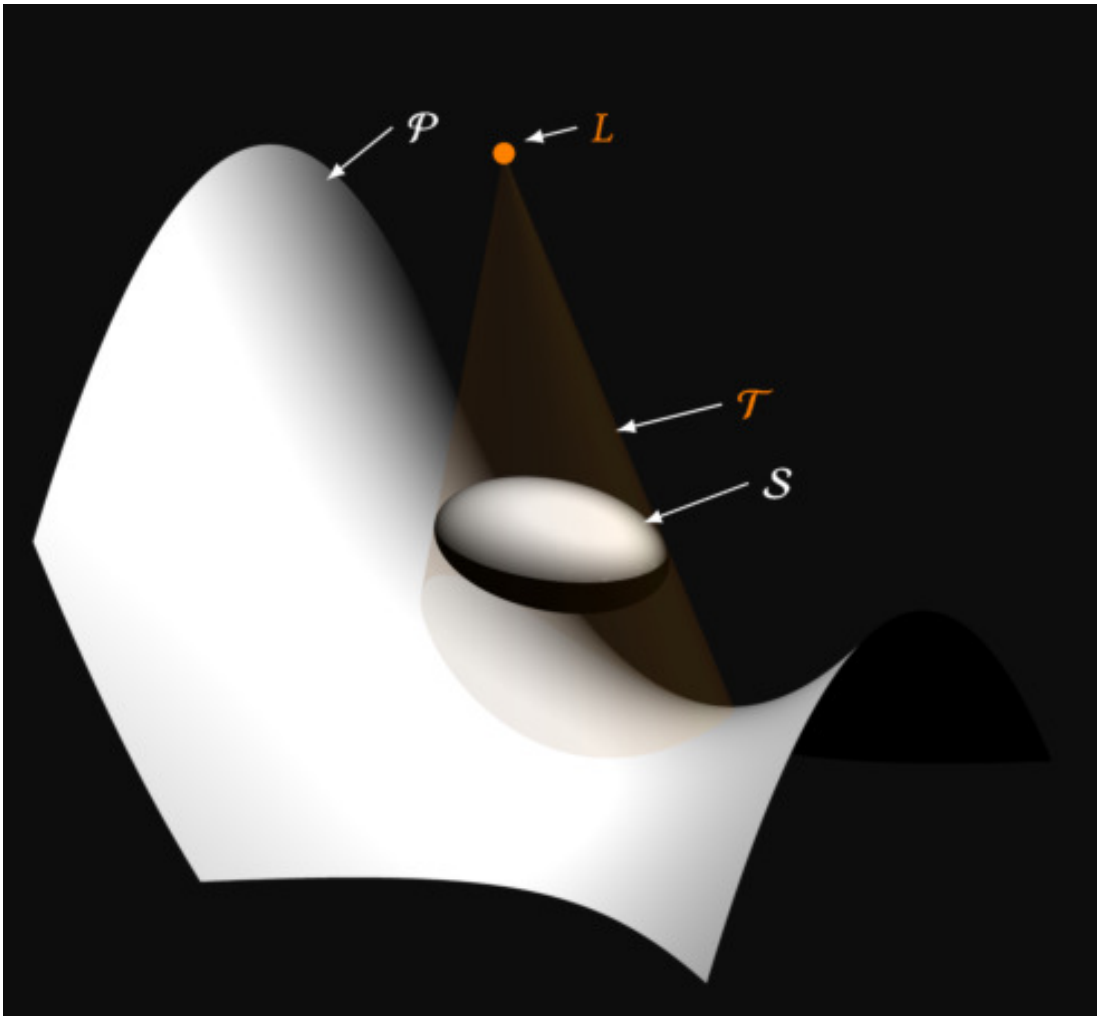

Figure 5.10: The tangent hypercone $\mathcal{T}$ to a hypersurface $\mathcal{S}$ through a light source L and the shadow cast on $\mathcal{P}$.

intersection of the first polar

$$\mathcal{S}_L : \overline{\sigma_L} = \overline{L}^T \nabla \overline{\sigma} = 0 \tag{5.2}$$

of the hypersurface $\mathcal{S}$ with the hypersurface $\mathcal{S}$:

$$c : \sigma = 0 \wedge \sigma_L = 0, \tag{5.3}$$

where σ_L is the dehomogenized polynomial $\overline{\sigma_L}$ (Figure 5.9).

Tangent hypercones

The next step is to find an implicit representation of the tangent hypercones[3] from the light source L. These are the hypercones through the terminator c. Thus, let $Q(q_1, \ldots, q_n)$ be a point on c. The tangent cone $\mathcal{T}$ is the set of lines LQ for all points Q. The line LQ can be (parametrically) represented in a general

[3]For the sake of readability, we use terms cones and hypercones instead of more proper terms conical surfaces, conical hypersurfaces, ..., over the paper.

dimension with the parameter $a \in \mathbb{R}$ as the set of points $X(x_1, \ldots, x_n)$ satisfying the following n equations (one equation for each coordinate):

$$aL + (1 - a)Q = X. \tag{5.4}$$

Thus, the implicit equation of $\mathcal{T}$ is the solution of the system:

$$\mathcal{T} : \sigma(Q) = 0 \wedge \sigma_L(Q) = 0 \wedge aL + (1 - a)Q - X = 0, \tag{5.5}$$

where $\sigma(Q)$ and $\sigma_L(Q)$ denote polynomials σ and σ_L in variables Q. By computing the Gröbner basis or Dixon resultant of the system

$$\{\sigma(Q), \sigma_L(Q), aL + (1 - a)Q - X\}$$

and eliminating variables $a, q_1, \ldots, q_n$, we obtain the polynomial θ in variables $x_1, \ldots, x_n$ representing the tangent hypercone

$$\mathcal{T} : \theta = 0 \text{ (Figure 5.10).} \tag{5.6}$$

Shadow cast on an algebraic hypersurface

Now, we find the shadow cast by $\mathcal{S}$ on itself and on another algebraic hypersurface $\mathcal{P}$ given by a polynomial equation

$$\mathcal{P} : \pi = 0. \tag{5.7}$$

The boundary of the shadow cast by $\mathcal{S}$ on itself — terminator, is the intersection of $\mathcal{T}$ with $\mathcal{S}$. The selection of illuminated parts is carried out in the following steps:

1. The n-space is divided by the first polar to two subspaces ($\sigma_L > 0$ or < 0), and the illuminated part is in the same subspace as the source of light L. The second part is in the shade.[4]

Since we cannot always divide the inner and outer parts, the selection fails with non-orientable or self-crossing surfaces (e.g., see Figure 5.11). Hence, for simplicity, we assume non self-crossing orientable finite hypersurfaces (or at least their terminators are finite).

For polynomials of degrees higher than 2, some regions of the hypersurface $\mathcal{S}$ can still be in their own shade (the tangent hypercone intersects itself), and we have to omit them from the final selection of the illuminated parts (Figures 5.12,5.13).

2. Decompose the tangent hypercone into conical subregions (subcones) divided by the terminator.[5] Eliminate empty subcones.

[4]The method is implemented in 4-D scenes up to this point. The upcoming decomposition to subcones seems, in most cases, computationally unbearable.

[5]We use cylindrical algebraic decomposition. The results of the decomposition are distinct subregions represented by polynomial equations and inequalities (see Strzebonski [2023] for details and implementation).

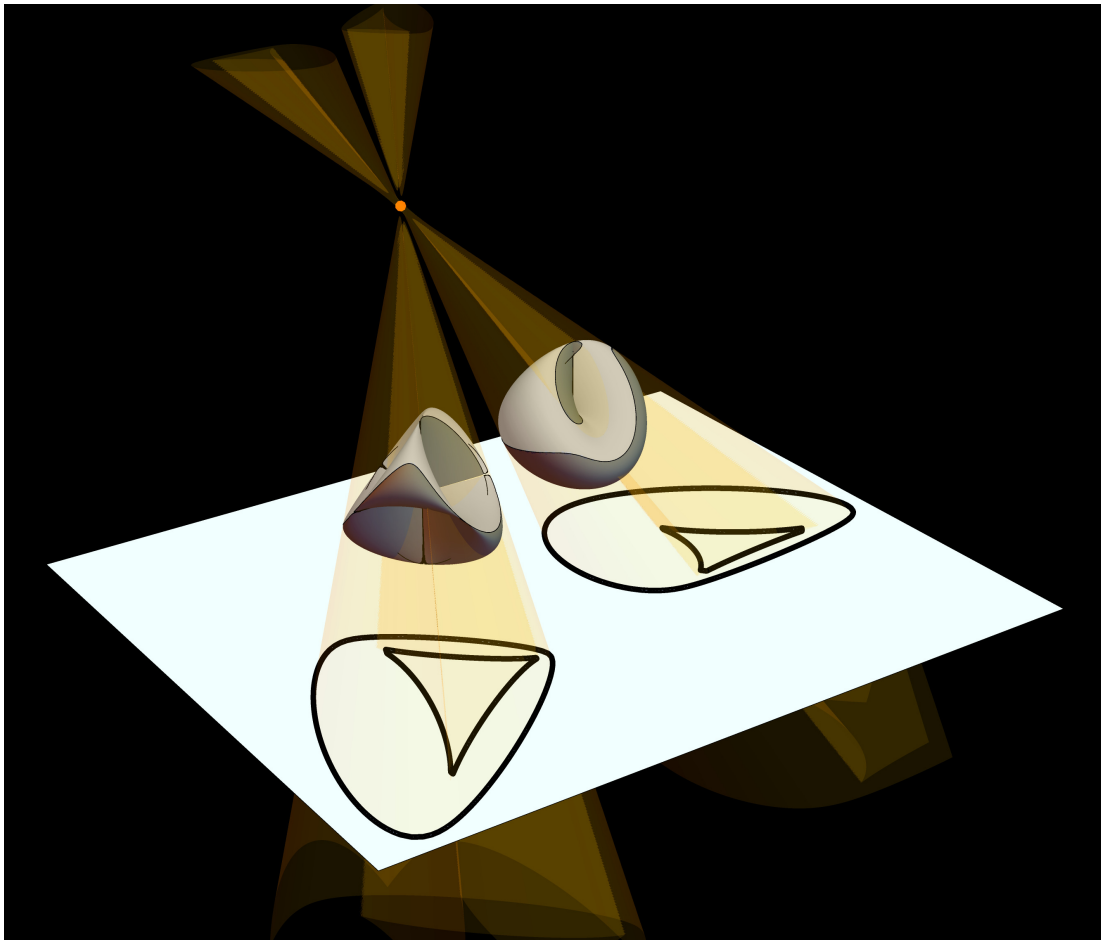

Figure 5.11: (left) Roman surface: $-2(x-2)(y-1)z+(x-2)^2(y-1)^2+(x-2)^2z^2+(y-1)^2z^2=0$ and (right) Cross-cap: $((x+1)^2+y^2)\,((x+1)^2+z^2)+(x+1)^2+\frac{y^4}{4}+y^2z=0$, their parts separated by the first polars, and polar boundaries projected to a plane $z+2=0$. Without omission of the self-shaded parts.

3. Select the parts of the hypersurface closest to the light source in non-empty subcones. This is carried out by constructing rays from the light source in each subcone and finding the region with the intersection nearest to the source. The selected nearest parts are illuminated, and the rest is in shade.

The boundary of the shadow cast by $\mathcal{S}$ on $\mathcal{P}$ is the intersection of its tangent hypercone $\mathcal{T}$ with $\mathcal{P}$. The final shadow contains inner points in the shade, i.e., inside the subcones containing previously selected regions.

If a scene contains more hypersurfaces, some of them might intersect, so we would not be able to distinguish their order with respect to the light source. In such cases, the selection algorithm can be further generalized for a hypersurface $\mathcal{Z}$ as a composition of hypersurfaces $\mathcal{S}_1,\ldots,\mathcal{S}_k, k\geq 1$:

$$\mathcal{Z}:\sigma_1\ldots\sigma_k=0. \tag{5.8}$$

However, this generally works when the light source is outside all composed hypersurfaces. Otherwise, the selection of the illuminated subspaces divided by the first polars must be carried out for some factors separately. For example, in Figure 5.14, we can define a surface $\mathcal{Z}$ as the composition of a sphere, ellipsoid, and torus. The (infinite) hyperbolic paraboloid would be treated separately.

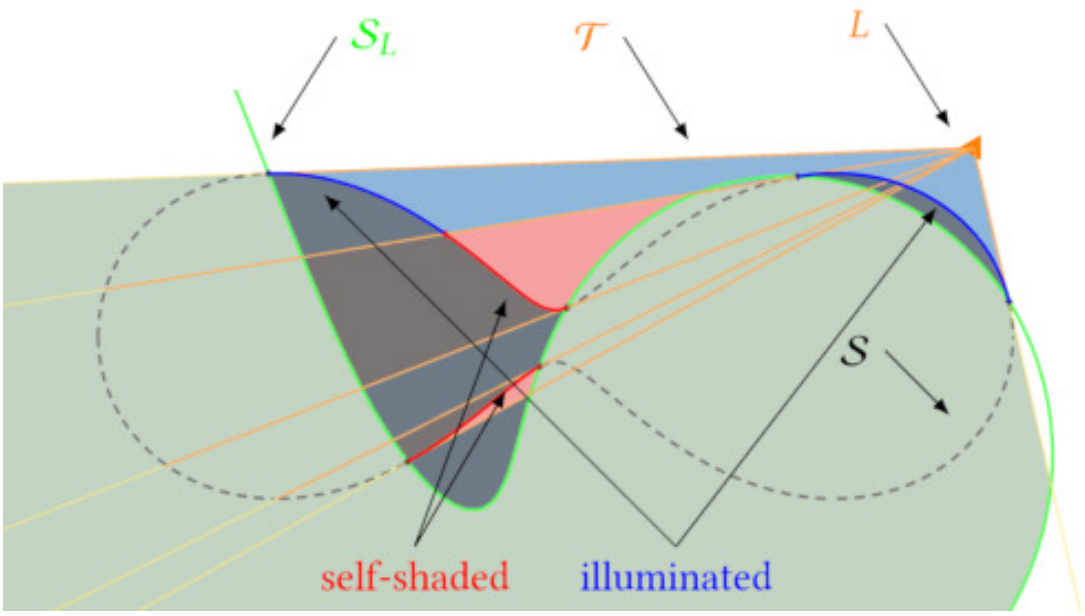

Figure 5.12: A 2-D situation of a Cassini oval (degree 4) and its self-shading from the point light source. The green curve is the first polar, dividing the plane into two areas. The area that does not contain the light source is excluded. The subcones in 2-D case are plane angles bounded by the rays from the light source. The blue arcs represent illuminated parts, and the red arcs are in the self-shade.

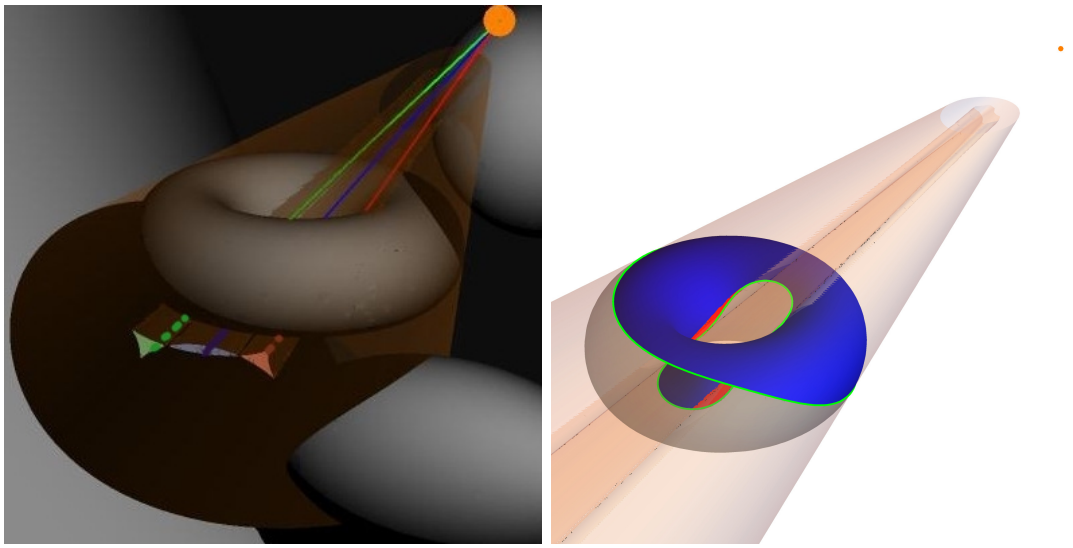

Figure 5.13: (left) A shadow of the torus cast on a surface without the self-shaded parts omitted. (right) Decomposition of a torus. The green curve is the terminator. The blue region is illuminated. The red regions are in the accepted subregion divided by the first polar but in the shade of the blue region.

5.2.2 The principle of a 4-D perspective

Figure 5.15 shows a 2-D view of the correspondence between the coordinates of a real point $P(p_x, p_y, p_z, p_w)$ and its centrally projected image $P^\nu(p_x^\nu, p_y^\nu, p_w^\nu)$ into the modeling 3-space $\nu(x, y, w)$ (an analogy to a picture plane in a 3-D perspective). Assume an orthogonal coordinate system (x, y, z, w) placed in the point O in ν,

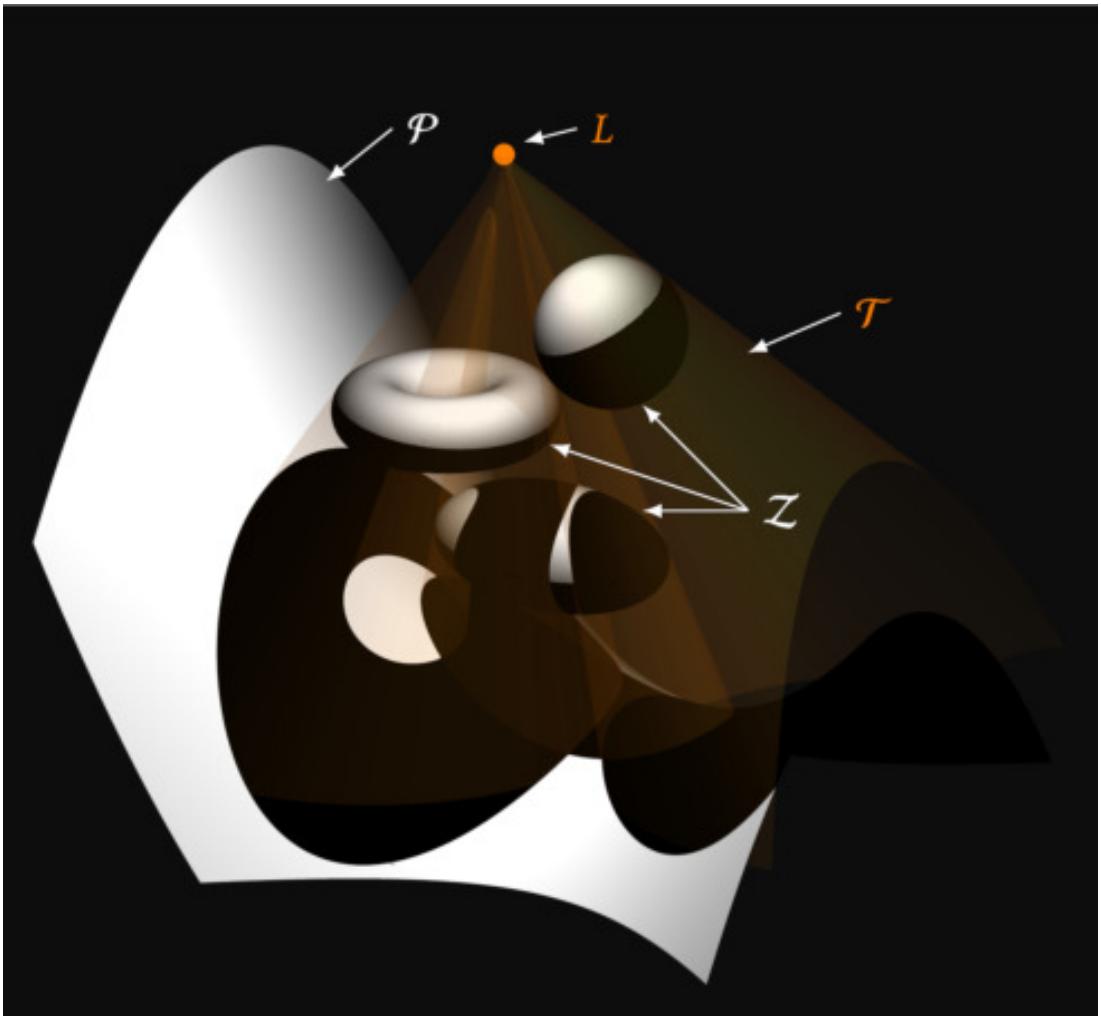

Figure 5.14: The final visualization of a scene with a sphere, torus, and ellipsoid casting shadows on themselves and on a hyperbolic paraboloid.

with the z-axis perpendicular to ν and the center of projection C in the oriented perspective distance d from ν such that $CO \perp \nu$. Observing the homothety, the coordinates of the 4-D perspective image P^ν of $P \neq C$ are

$$(p_x^\nu, p_y^\nu, p_w^\nu) = (d\frac{p_x}{d-p_z}, d\frac{p_y}{d-p_z}, d\frac{p_w}{d-p_z}) \tag{5.9}$$

(in the case of $p_z = 0$ the coordinates do not change; if $p_z = d$ the image is improper).

To find the implicit representation of the 4-D perspective image (3-D occluding contour) of an algebraic surface

$$\mathcal{S} : \sigma = 0 \tag{5.10}$$

(in variables x, y, z, w), we use a similar idea as in constructing shadows. Let

$$\mathcal{S}_C : \overline{\sigma_C} = \overline{C}^T \nabla\overline{\sigma} = 0, \tag{5.11}$$

in homogeneous coordinates, be the first polar of $\mathcal{S}$ with respect to C, and with

$$\sigma_C = 0 \tag{5.12}$$

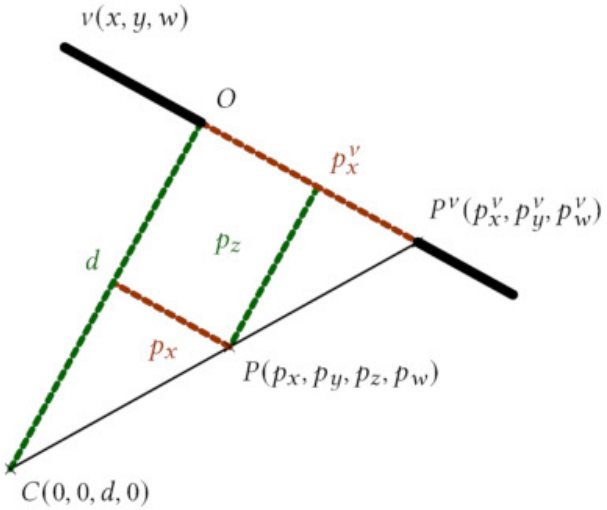

Figure 5.15: The principle of a 4-D perspective projection from a center C onto a modeling 3-space $\nu(x, y, w)$. 2-D orthogonal projection view on the 4-D perspective shows the homothety between the pre-image in a 4-space and its perspective image in the modeling 3-space from the center of projection.

being its dehomogenized equation. Since we are projecting to a 3-space instead of an arbitrary hypersurface, we can use the derived rules of the 4-D perspective mapping (Equations 5.9). In the next step, we set up a system of polynomials prepared for elimination using Gröbner basis or Dixon resultant such that the final image will be in the coordinates (x, y, w) of the modeling space.

Let $Q(q_x, q_y, q_z, q_w)$ be a point on a contour generator

$$c_C : \sigma = 0 \wedge \sigma_C = 0. \tag{5.13}$$

First, we substitute variables $X(x, y, z, w)$ by $Q(q_x, q_y, q_z, q_w)$ in (5.13) such that $\sigma(X) \to \sigma(Q)$ and $\sigma_C(X) \to \sigma_C(Q)$. The rules of the mapping (5.9) are represented by the system of linear equations:

$$\begin{aligned} x - d\frac{q_x}{d - q_z} &= 0, \\ y - d\frac{q_y}{d - q_z} &= 0, \\ w - d\frac{q_w}{d - q_z} &= 0. \end{aligned} \tag{5.14}$$

Elimination of q_x, q_y, q_z, and q_w from the system of polynomials

$$\left\{\sigma(Q), \sigma_C(Q), x - d\frac{q_x}{d - q_z}, y - d\frac{q_y}{d - q_z}, w - d\frac{q_w}{d - q_z}\right\}$$

leads to a polynomial σ^ν in (x, y, w) such that its zero set represents the 4-D perspective image $\mathcal{S}^\nu$ of the surface $\mathcal{S}$.

Assuming a point light source L, the terminator c^ν is, in this case, a 2-surface, obtained by the intersection of $\mathcal{S}$ and $\mathcal{S}_L$, given by Equations 5.3 and projected

into modeling space ν through Equations 5.9. The images of terminator 2-surfaces are derived from the system of polynomials

$$\left\{\sigma(Q), \sigma_L(Q), x - d\frac{q_x}{d-q_z}, y - d\frac{q_y}{d-q_z}, w - d\frac{q_w}{d-q_z}\right\},$$

similarly as above.

For the sake of better understanding, we also visualize the tangent hypercones $\mathcal{T}$ of $\mathcal{S}$ from L, when possible (cf. Subsections 5.2.3 and 5.2.3). The tangent hypercones $\mathcal{T}$ are 3-surfaces given by Equation 5.6, and the contours of their images $\mathcal{T}^\nu$ are created by the same procedure as images $\mathcal{S}^\nu$ of $\mathcal{S}$.

The final shadows are three-dimensional regions bounded by 2-spaces in the 4-space. Conveniently, in a 4-D perspective, we can find implicit equations of the 2-surface boundaries in the modeling 3-space. To do so, we need to find the zero set of the system of polynomials

$$\left\{\sigma(Q), \theta(Q), x - d\frac{q_x}{d-q_z}, y - d\frac{q_y}{d-q_z}, w - d\frac{q_w}{d-q_z}\right\},$$

representing the perspective image of the intersection of the surface $\mathcal{S}$ and the tangent cone $\mathcal{T}$. The last step is to select the regions according to Section 5.2.1. In a 4-D perspective, we only highlight shadow boundaries so that we can see through 3-D images.

5.2.3 Experimental results and technical details

In this section, we review several examples and comment on technical details.

3-D scene

"Implicit Bakery", Figure 5.14

See the video in Appendix B.2.

The 3-D scenario from Section 5.2.1 shows a surface $\mathcal{Z}$ composed of three implicitly given factor surfaces: sphere $\mathcal{S}_1$, torus $\mathcal{S}_2$, and ellipsoid $\mathcal{S}_3$

$$\mathcal{S}_1 : (x-1)^2 + (y+4)^2 + (z-5)^2 - 4 = 0, \tag{5.15}$$

$$\begin{aligned}\mathcal{S}_2 : \Big((x-1)^2 + (y-1)^2 + (z-2)^2 + 3\Big)^2 \\ -16(x-1)^2 + 16(y-1)^2 = 0,\end{aligned} \tag{5.16}$$

$$\mathcal{S}_3 : 4(x-3)^2 + (y+1)^2 + 4(z+2)^2 - 12 = 0. \tag{5.17}$$

We describe constructions of shadows cast between them and their shadows cast on a hyperbolic paraboloid $\mathcal{P}$

$$\mathcal{P} : 2(y+3)^2 - 2(x-5)^2 - 25(z+7) = 0 \tag{5.18}$$

from the light source $L\,[-1, -2, 10]$.

The polynomial of $\mathcal{Z}$ has degree 8, but we treat its decomposition into factors (factor surfaces $\mathcal{S}_1, \mathcal{S}_2, \mathcal{S}_3$). In this case, the factor surface of the highest degree, 4, is the torus.

A terminator line of each "factor surface" is its intersection with the first polar with respect to L. Explicitly, terminators are the four sets of points that satisfy the following pairs of equations:

factor surface		first polar	
$\mathcal{S}_1$: Eq. 5.15	$\wedge$	$19 + 2x - 2y - 5z = 0$	(5.19)
$\mathcal{S}_2$: Eq. 5.16	$\wedge$	$\begin{aligned} &128 - 30x + 12x^2 \\ &+2x^3 - 29y - 10xy \\ &+3x^2y + 10y^2 + 2xy^2 \\ &+3y^3 - 104z + 8xz \\ &-8x^2z + 4yz - 8y^2z \\ &+40z^2 + 2xz^2 + 3yz^2 \\ &-8z^3 = 0 \end{aligned}$	(5.20)
$\mathcal{S}_3$: Eq. 5.17	$\wedge$	$16x + y - 48z - 131 = 0$	(5.21)
$\mathcal{P}$: Eq. 5.18	$\wedge$	$24x + 4y - 25z - 708 = 0$	(5.22)

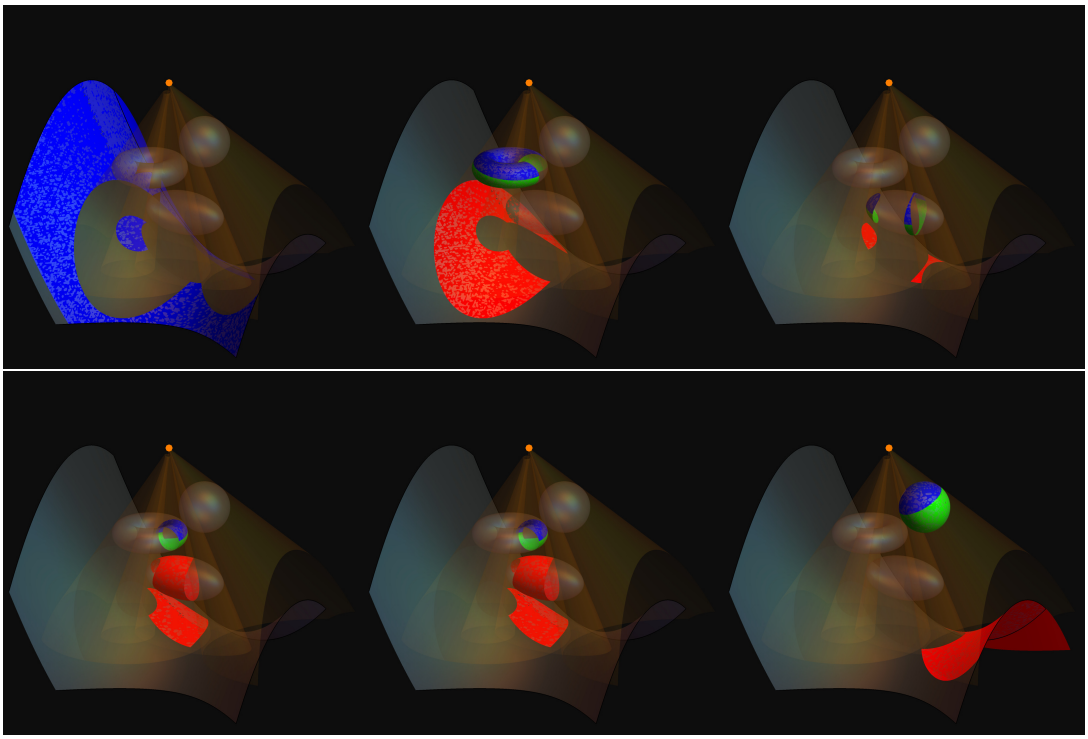

Figure 5.16: A selection of the regions contained in subcones. Each picture shows a different subcone of the scene $\mathcal{Z}$ consisting of a sphere $\mathcal{S}_1$, torus $\mathcal{S}_2$, and ellipsoid $\mathcal{S}_3$. The blue regions are illuminated, the green regions are excluded by the first polars, and the red regions are in the shade of the blue regions with a shorter distance to the light source. The top left figure shows the complement of the union of all subcones in the 3-space; hence it distinguishes the shadow of the scene on the hyperbolic paraboloid $\mathcal{P}$. The rest of the empty regions are not shown.

If a surface has a degree n, its first polar has a degree $(n-1)$, and the degree of the terminator line is due to Bézout's theorem $n(n-1)$. Therefore, the terminator line of the entire scene $\mathcal{Z}$ would have the degree $8 \cdot 7 = 56$. However, after factorization, the factor surfaces will have degrees 2 for the quadrics and 12 for the torus. The same holds for degrees of tangent cones (Bydžovský [1948]).

Next, we omit the shaded subspaces divided by the first polar. In this case, the points on illuminated regions have non-negative values in the equations of the first polars.

Tangent cones are also treated separately for each factor surface. For example, for the torus $\mathcal{S}_2$, we have the following system of polynomial equations:

$$\begin{aligned} &\text{Eq. (5.16)},\\ &\text{Eq. (5.20)},\\ aq_1 - (a-1) - x &= 0,\\ aq_2 - 2(a-1) - y &= 0,\\ aq_3 + 10(1-a) - z &= 0. \end{aligned} \tag{5.23}$$

Eliminating q_1, q_2, q_3, and a leads to an 8th-degree polynomial of the tangent cone. Similarly, we find the rest of the tangent cones of the surfaces in the scene.

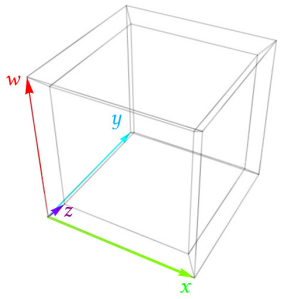

Figure 5.17: A reference hypercube in the 4-D perspective. The colors of the arrows mark the directions of the coordinate axes: Green $\to x$, Blue $\to y$, Purple $\to z$, Red $\to w$.

Next, we decompose the regions bounded by the system of tangent cones into all subcones and obtain five nonempty and three empty intersecting regions in this case (Figure 5.16). The subcones are represented by implicit equations and inequalities.

In the last step, we trace subspaces separated by the first polars over each subcone and choose the region nearest to the light source.

4-D scenes

Understanding the 4-D visualizations

Let us give a few remarks on how to understand the 4-D visualizations below:

- The visualizations are 3-D models (occluding contours), and the figures in the paper are only 2-D images of the 3-D scenes.
- Standing in a gallery in front of an actual 2-D painting in the 3-D linear perspective, we can find the position of our eye such that the picture makes

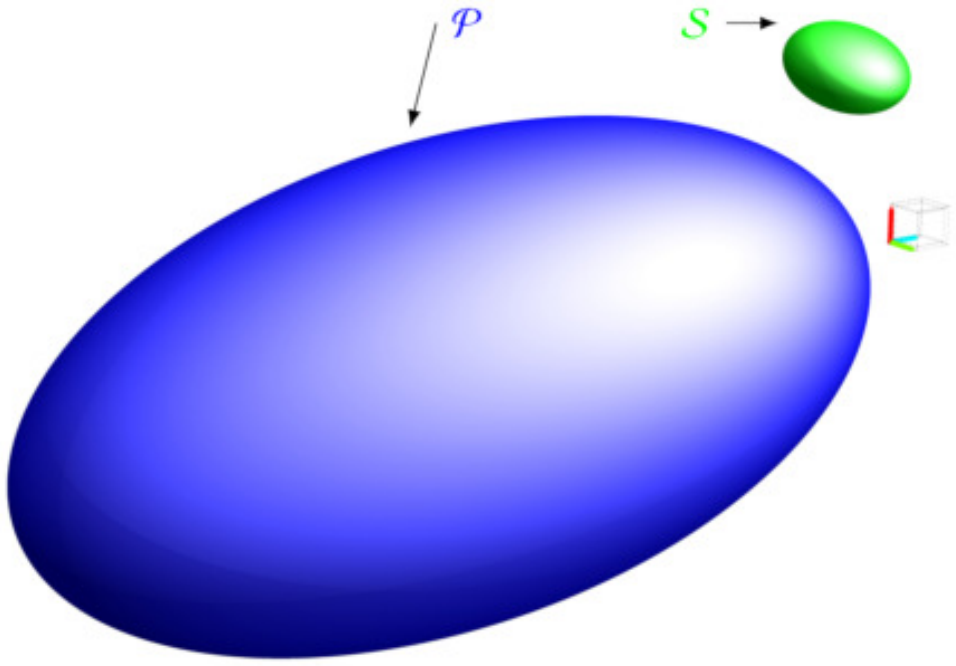

Figure 5.18: A 4-D scene with a 3-sphere $\mathcal{P}$ and a 3-ellipsoid $\mathcal{S}$ in a 4-D perspective.

an illusion of 3-D space. This is unreachable in the 4-D perspective because we cannot leave the 3-D space of the 3-D image (of a 4-D object).

- One could think of observing the picture from the inside, i.e., we can reach any location in the 3-D static image. On the contrary, the change of the 4-D eye/camera position would change the contours of the objects.
- For better orientation, we always attach an image of a reference hypercube with the center in $[0, 0, 0, 0]$ (Figure 5.17).
- The default value of the oriented eye distance in figures is $d = -6$, and its coordinates are $[0, 0, d, 0]$.
- To understand the (3-D) spatial properties of the modeling 3-space, we keep the software lighting properties of the 3-D graphics.

Technical notes on the implementation of the 4-D perspective

Let us reflect on some pros and cons of the 4-D perspective:

+ Intersections of 3-surfaces in a 4-space are 2-surfaces; hence, we can visualize them using only one implicit equation in the modeling 3-space. The equation can be obtained directly from the corresponding polynomial system.

– 4-D perspective images should include "inner points" of hypersurfaces, but we only show their occluding contours. Otherwise, we would not see images

that overlap in the modeling 3-space. An analogous problem occurs in 3-D perspective, where we can imagine a smaller object in front of a bigger object, so the perspective image of the smaller object would lie inside the image of the bigger object. Although we can easily decompose figures in the picture plane, we would not see much in the modeling 3-space. The understanding becomes very unclear with non-closed surfaces, where parts of hypersurfaces might seem to go through their contours (see Section 5.2.3).

– The algorithm to find and fill the unshaded and shaded parts of surfaces inside tangent cones works well in theory and is successfully applied in 3-D scenes. However, it meets technical difficulties in 4-D. In our experiments, the computation time to find points on the hypersurface (polynomial equation in four variables) and inside the subcone (system of polynomial inequalities in four variables) was beyond reasonable limits. For this purpose, a parametric representation might be more appropriate.

4-D scene: "HyperQuadrics" Figure 5.20

See the video in Appendix C.3.

In the first 4-D case (Figure 5.18), we have a 3-ellipsoid

$$\mathcal{S} : \frac{(x+2)^2}{4} + \frac{(y+1)^2}{2} + z^2 + (w-4)^2 - 1 = 0 \tag{5.24}$$

casting a shadow on a 3-sphere

$$\mathcal{P} : (x+5)^2 + (y+6)^2 + (z-2)^2 + (w+3)^2 - 36 = 0 \tag{5.25}$$

from the light source $L = [1, 1, -1.5, 5]$.

In this scene, the given 3-surfaces and their tangent hypercones have degrees 2. The highest degree, 4, has the two-dimensional boundary of the shadow cast by the 3-ellipsoid on the 3-sphere. The occluding contours $\mathcal{S}^\nu$ and $\mathcal{P}^\nu$ of $\mathcal{S}$ and $\mathcal{P}$ are ellipsoids, and the same holds for their terminator 2-surfaces $c_\mathcal{S}, c_\mathcal{P}$ and their images $c^\nu_\mathcal{S}, c^\nu_\mathcal{P}$.

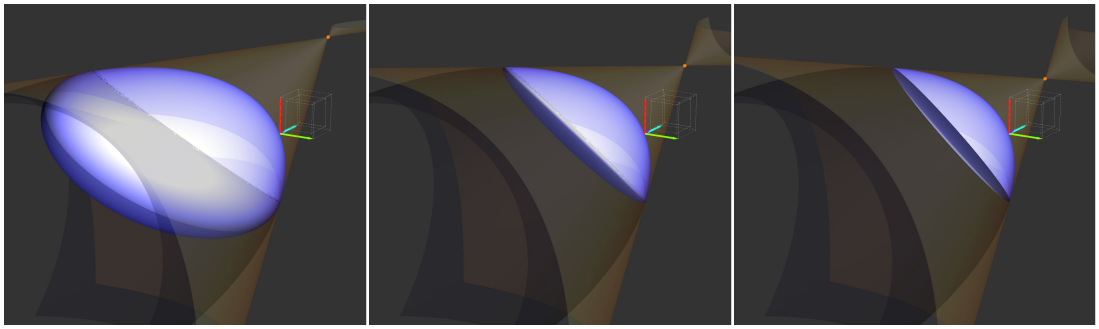

Figure 5.19: Transitions of the illuminated part of the 3-sphere $\mathcal{P}$ from the point light source $L = [1, 1, z_L, 5]$ moving in the z-direction: (left) $z_L = 2.5$, (center) $z_L = 7.5$, (right) $z_L = 12.5$. The point L lies in the first polar 3-space for $z_L = 9.5$. The illuminated part is bounded by the occluding contours of the 3-sphere and terminator 2-surface with respect to L.

In the case of hyperquadrics, we can easily deduce the transition of the visible illuminated parts with respect to the given 4-D perspective (Figure 5.19). The first polar of the 3-sphere $\mathcal{P}$ with respect to the perspective center C is a 3-space, dividing the 4-space into two half-4-spaces. Thus, we have the following three cases:

1. The shape of the illuminated part is in a special position when the light source L is in the polar 3-space (with respect to C), i.e., the terminator 2-surface of the 3-sphere with respect to L degenerates to an ellipse including inner points.
2. When L is in the same half-4-space as the center C, the visible illuminated part includes the inner points of the terminator 2-surface.
3. If the light source L and the center C lie in the opposite half-4-spaces, we must exclude the inner points of the terminator 2-surface.

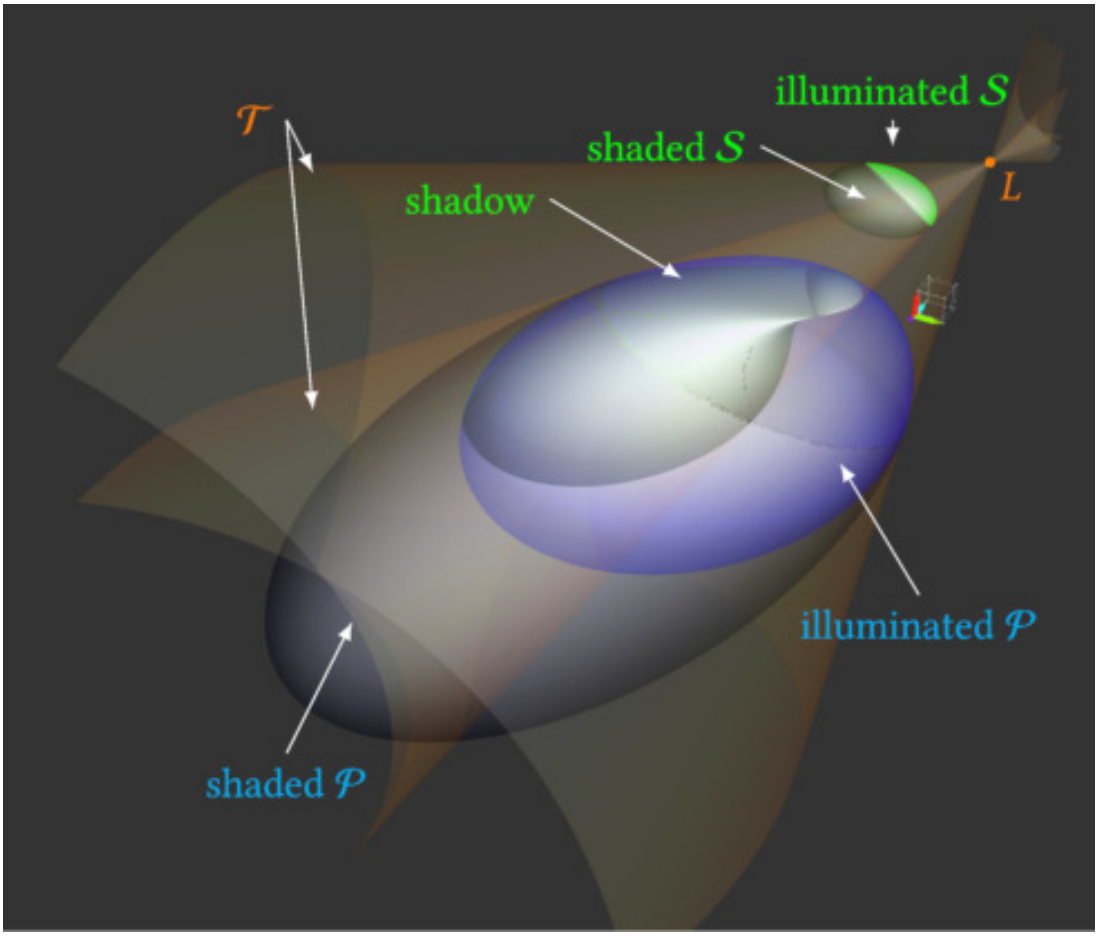

Figure 5.20: A 4-D scene with the shadow of a 3-ellipsoid $\mathcal{S}$ on a 3-sphere.

4-D scene: "Full HyperMoon Between HyperMountains", Figure 5.22

The second 4-D scene (Figure 5.21) shows a more complicated situation. Let us have a 3-sphere

$$\mathcal{S} : w^2 + (x+1)^2 + y^2 + (z+1)^2 - \frac{1}{4} = 0 \tag{5.26}$$

casting a shadow on a 3-surface of degree 3

$$\mathcal{P} : (x-1)(x+2)x + y^2 + z^2 + w = 0 \tag{5.27}$$

from the light source $L = [5, 1, 1, 2]$.

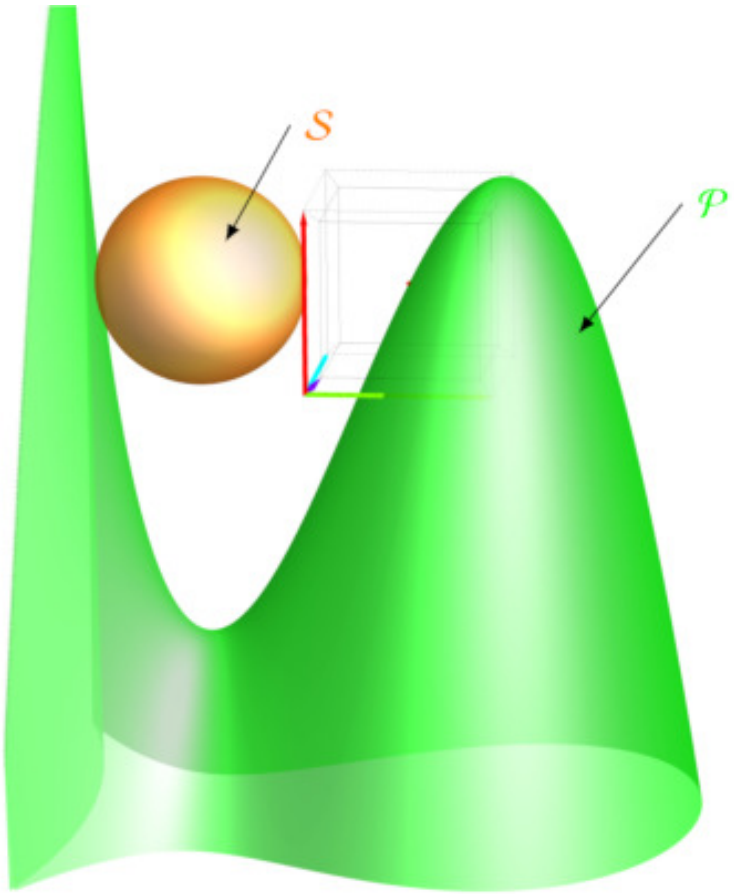

Figure 5.21: A 4-D scene with a 3-sphere $\mathcal{S}$ and a 3-surface $\mathcal{P}$ of degree 3 in a 4-D perspective.

The contours of the occlusion are 2-surfaces of degree 2 for $\mathcal{S}^\nu$ and degree 6 for $\mathcal{P}^\nu$. In this case, it is hard to perceive the 4-D spatial properties of the scene from the contours. In particular, we cannot intuitively grasp the infinite 3-surface $\mathcal{P}$.

Let us bring more light to this scene. After finding the terminator 2-surfaces and tangent hypercones[6] to the 3-surfaces through the vertex L, we can create shadows between the 3-surfaces. The 3-sphere casts a shadow on $\mathcal{P}$. The contour of the intersection of the tangent hypercone to $\mathcal{S}$ with $\mathcal{P}$ is a 2-surface of degree 6. It consists of two disjoint parts, and the part closer to L is omitted in Figure 5.22. The image of the 2-surface boundary of the shadow of $\mathcal{P}$ cast on $\mathcal{S}$ is given by a polynomial of degree 14 and the contour of the shadow of $\mathcal{P}$ on itself is a surface of degree 18.

[6]The computations of the projection of the tangent hypercone to $\mathcal{P}$ was terminated after too long ($5 - 10$h).

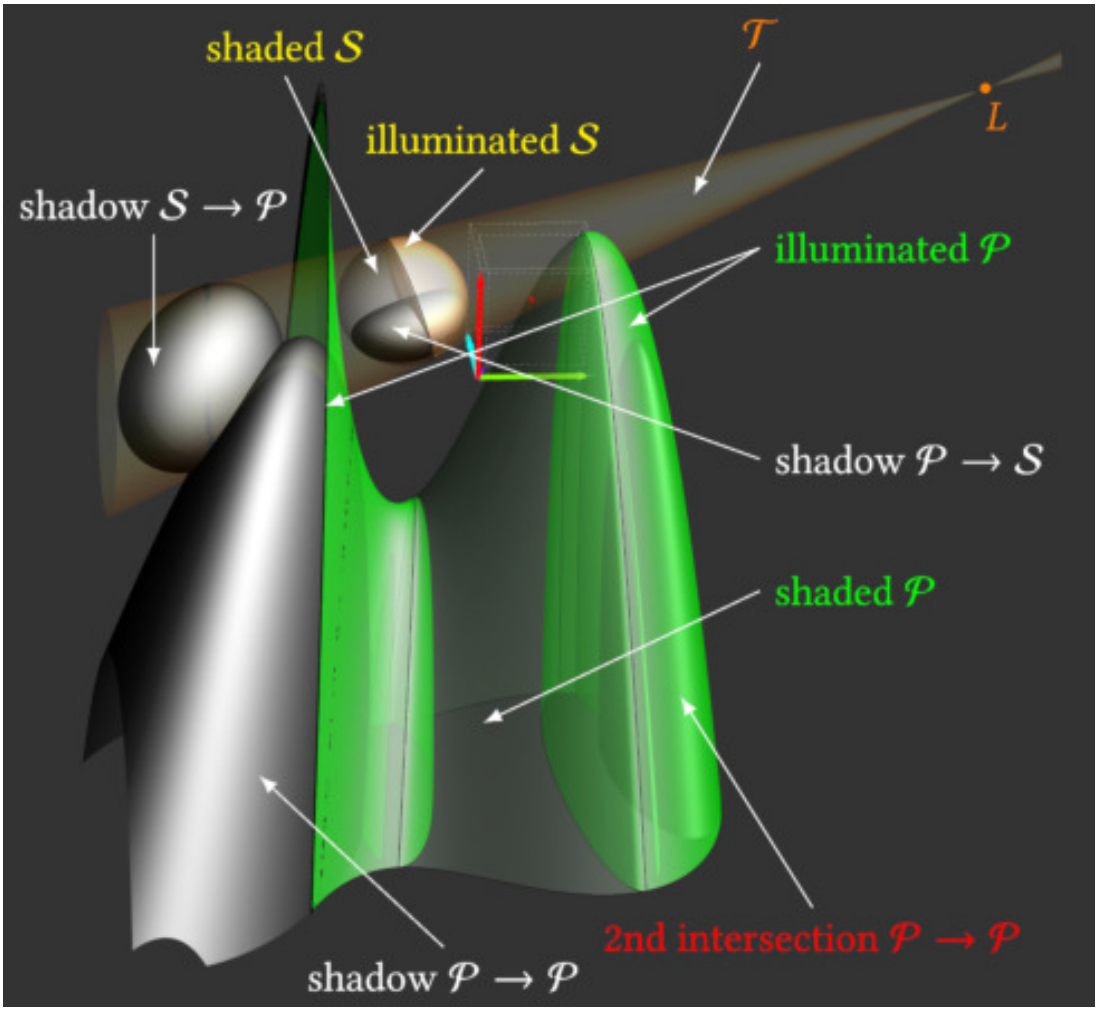

Figure 5.22: An illumination of a 3-sphere $\mathcal{S}$ and its shadow on a 3-surface $\mathcal{P}$ of degree 3 from a point light source L in a 4-D perspective. The figure contains the excess intersection of the tangent cone (not visualized) of $\mathcal{P}$, and the self-shaded region of $\mathcal{P}$ is not excluded from the illuminated part.

4-D scene: "HyperRing", Figure 5.24

See the video in Appendix D.4.

The last 3-surface (Figure 5.21) is given by a polynomial of degree 4:

$$\mathcal{S} : (x-1)^2 + ((w-2)^2 + y^2 - 4)^2 + z^2 - 1 = 0. \tag{5.28}$$

The first polar $\mathcal{S}_L$ with respect to the light source $L[0, 2, -2, 4]$ is:

$$\begin{aligned} \mathcal{S}_L : 4w^3 - 3x + x^2 + 4w^2(-8+y) - 16y^2 \\ +4y^3 + 4w(16 - 4y + y^2) - 2z + z^2 = 0. \end{aligned} \tag{5.29}$$

Let us have a 3-space

$$\mathcal{P} : w + 2 = 0. \tag{5.30}$$

The occluding contour $\mathcal{S}^\nu$ is after elimination given by a polynomial of degree 8 in 72 terms (in variables x, y, z). After elimination, the terminator surface c^ν is given by a polynomial of degree 8 in 146 terms (in variables x, y, z). The tangent cone $\mathcal{T}$

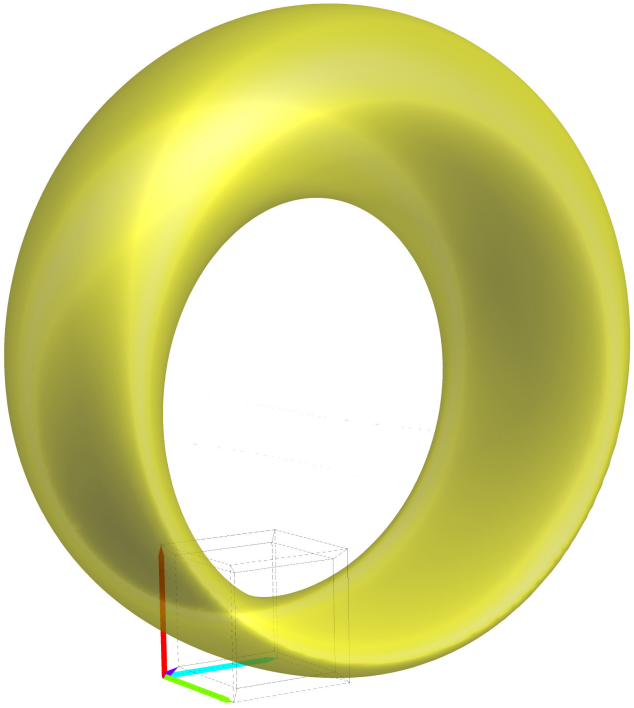

Figure 5.23: A surface $\mathcal{S}$ of degree 4 in a 4-D perspective.

generated by the terminator c (intersection of $\mathcal{S}$ and $\mathcal{S}_L$) is after elimination given by a polynomial of degree 8 in 483 terms (in variables x, y, z, w). The occluding contour of the shadow of $\mathcal{S}$ on $\mathcal{P}$ is a 2-surface of degree 8 (Figure 5.24).

5.2.4 Discussion and future work

Throughout the paper, we tried to bring the "most universal" solution to visualizing shadows of algebraic hypersurfaces. In this sense, the method presented in Section 5.2.1 works in a general dimension; the key point is to construct tangent cones with Equations 5.5. Illumination of a scene, both in 3-D and 4-D, is a complex process, and we should always consider the properties and positions of objects in the scene. The critical features of objects in our approach are the finiteness, orientability, and degree of a hypersurface and its terminator. Additionally, the position of the point light source and the projection center is crucial to define the inside and outside of a hypersurface or its part and, consequently, its visibility. The degree of a hypersurface opens up problems of computational complexity. Evidently, the appropriate setting and the choice of elimination method (Gröbner basis or the Dixon resultant) plays a crucial role in the computation time for higher-degree polynomial systems. The computational complexity also depends on the form of the polynomial, i.e., transformations of the hypersurface. The computations with hypersurfaces of degree four and higher easily failed after minor adjustments in our experiments. Furthermore, the diversion between dimensions became important in the final visualizations of the inner points of shadows. While in 3-D, we could cover the regions with a satisfying number

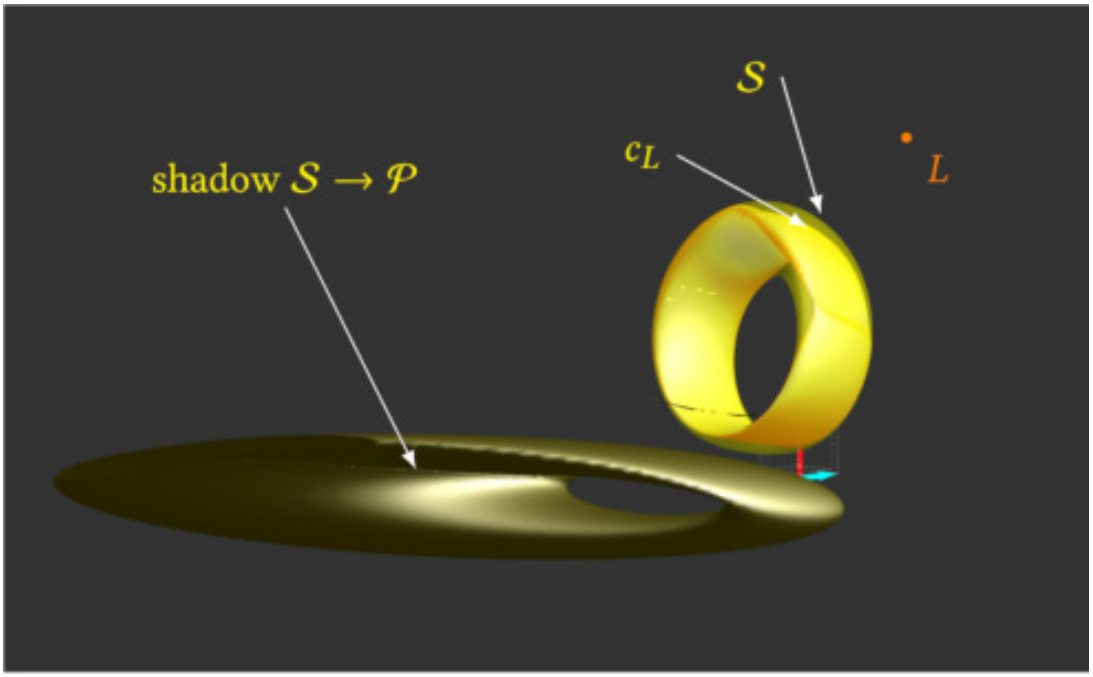

Figure 5.24: The shadow cast by a 3-surface $\mathcal{S}$ on a 3-space $\mathcal{P}$. Since the terminator overlaps itself, we cannot properly distinguish the illuminated visible part of $\mathcal{S}$.

of points, our solution in 4-D was defeated by time to solve a system of equations and inequalities in four variables. We dropped this case because filling the 3-dimensional volumes would not clarify our visualizations in any way.

The question of perceiving four- and more-dimensional spaces is very challenging. We only added one more "perspective" open for further investigation. One of the possibilities is to study the properties of 3-surfaces through their projections. Since we developed our method on implicit surfaces, it is convenient for mathematical visualization. Second, we can pursue more "natural" illumination details, including 4-dimensional light intensity, specularity, reflections, etc. Polynomial systems that create tangent cones and occluding contours always contain first-degree polynomials. Hence, there might be possibilities for improving the algorithms tailored to our situation and consequently reducing the computation time. Last but not least, illuminated four-dimensional scenes might be used to study, understand, and train four-dimensional spatial ability (if possible).

5.2.5 Conclusion

This paper focuses on a four-dimensional visualization based on implicit representations of hypersurfaces. We have described a general method to find shadow boundaries in an arbitrary dimension and applied it in a three- and four-dimensional space. Furthermore, we have designed a system of polynomial equations to construct occluding contours of hypersurfaces in a 4-D perspective. The method was presented on a composed 3-D scene and three 4-D cases with gradual complexity. Our experimental journey was extensively commented on throughout the article.

In this section, we discussed shadows in 4D geometry. In my opinion, shadows in higher dimensions do not improve clarity and depth as much as shadows in 3D. In the next section, we will try to improve the clarity of 4D images using 3D printing.

5.3 3D printed models of a tesseract in the double orthogonal projection and 4D perspective

Introduction

3D models and 3D printing are becoming commonplace all around us. Many companies print their prototypes on a 3D printer before going into production. 3D models have been with us for a long time (Volkert [2017]). Even in mathematics, we find many ways to use the possibilities of 3D models (Kupčáková [2002]). 3D printing can describe reality or be used to understand 4D space.

In descriptive geometry, space is usually drawn on paper (3D is projected into 2D). 4D objects are also usually drawn on paper or a computer screen (4D is projected into 2D), but keeping them in 3D space is possible. Thanks to modern technology, 3D printing can skip the last projection and show 4D objects projected in 3D (Segerman [2016]). For this reason, a 3D-printed model was created for this work. This 3D printed model was created in Geogebra. This part describes the projections mentioned before and shows problems with the preparation of the 3D printing and the 3D printing itself.

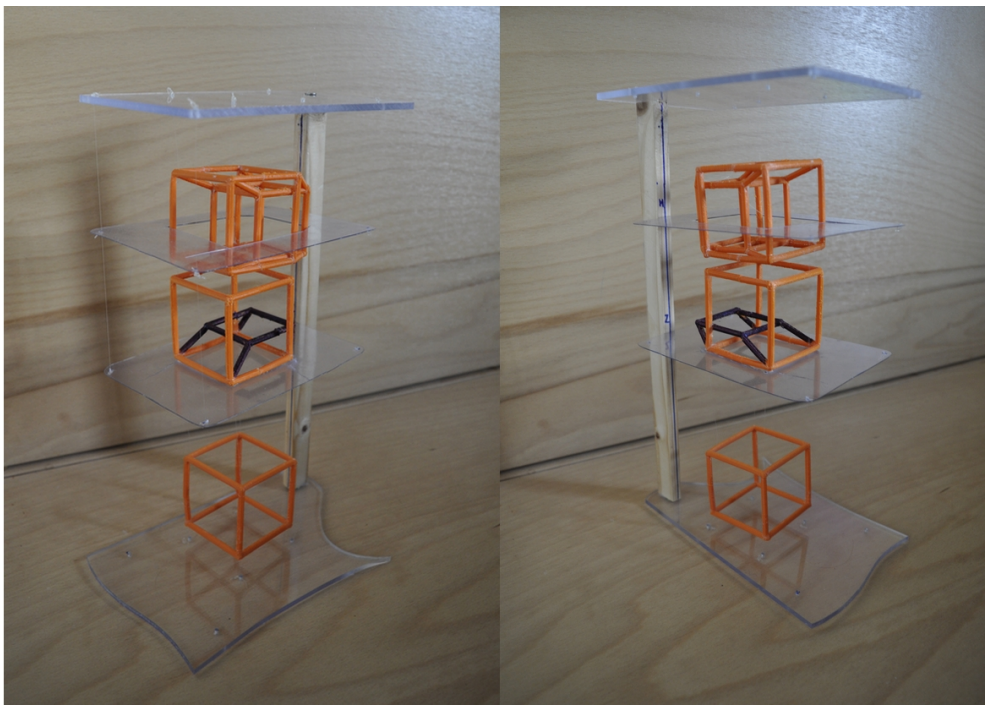

Figure 5.25: 3D printed models of a tesseract in the double orthogonal projection and 4D perspective.

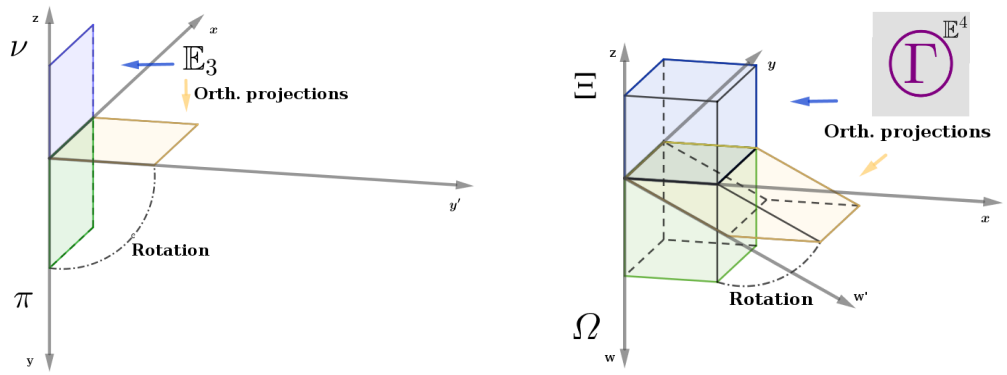

(a) Monge's projection (b) Double orthogonal projection

Figure 5.26: Visualization of the main principles of above mentioned projections.

Preparation and 3D printing

Projections

The first step is to create a 3D model for 3D printing. The 3D printed model of a tesseract consists of a tesseract in double orthogonal projection and a tesseract in 4D perspective. The 3D model is created in Geogebra (figure 5.27). The interactive Geogebra model can be found at this link:
https://www.geogebra.org/m/xbp8ucgj

Geogebra 3D print export

If we have created model in GeoGebra, it remains to export the model from the programme for 3D printing. The first problem is continuity. The image (figure 5.28) shows each layer of the 3D print in progress, and mostly, there is a corner of a cube (one point and two lines). Unfortunately, the lines are not connected to the point. GeoGebra exports lines and points separately. Maybe GeoGebra will fix this bug soon, but today, we must use for example the free web browser program Tinkercad *(www.tinkercad.com)* to fix this bug. We upload the model to Tinkercad and export it again. Tinkercad recalculates the continuity itself and fixes the problem nicely. Another disadvantage of the Geogebra export for 3D printing is that all lines have the same thickness. The primary and auxiliary lines cannot be distinguished by their thickness. For this reason, the auxiliary lines in this model are replaced by a fishing line.

3D printing preparation

The next step is to prepare the 3D model for printing. The first thing we need to do is resolve the overhanging lines. Overhanging lines are any lines that have an angle greater than 45 degrees. These lines need support; otherwise, they would fall under gravity during 3D printing. It is better to keep the number of these lines to a minimum. Firstly, it is better to change the horizon's position and other essential elements to eliminate overhanging lines; in this case, it is also necessary to rotate with the object, but the horizontal lines remain. For this reason, it is

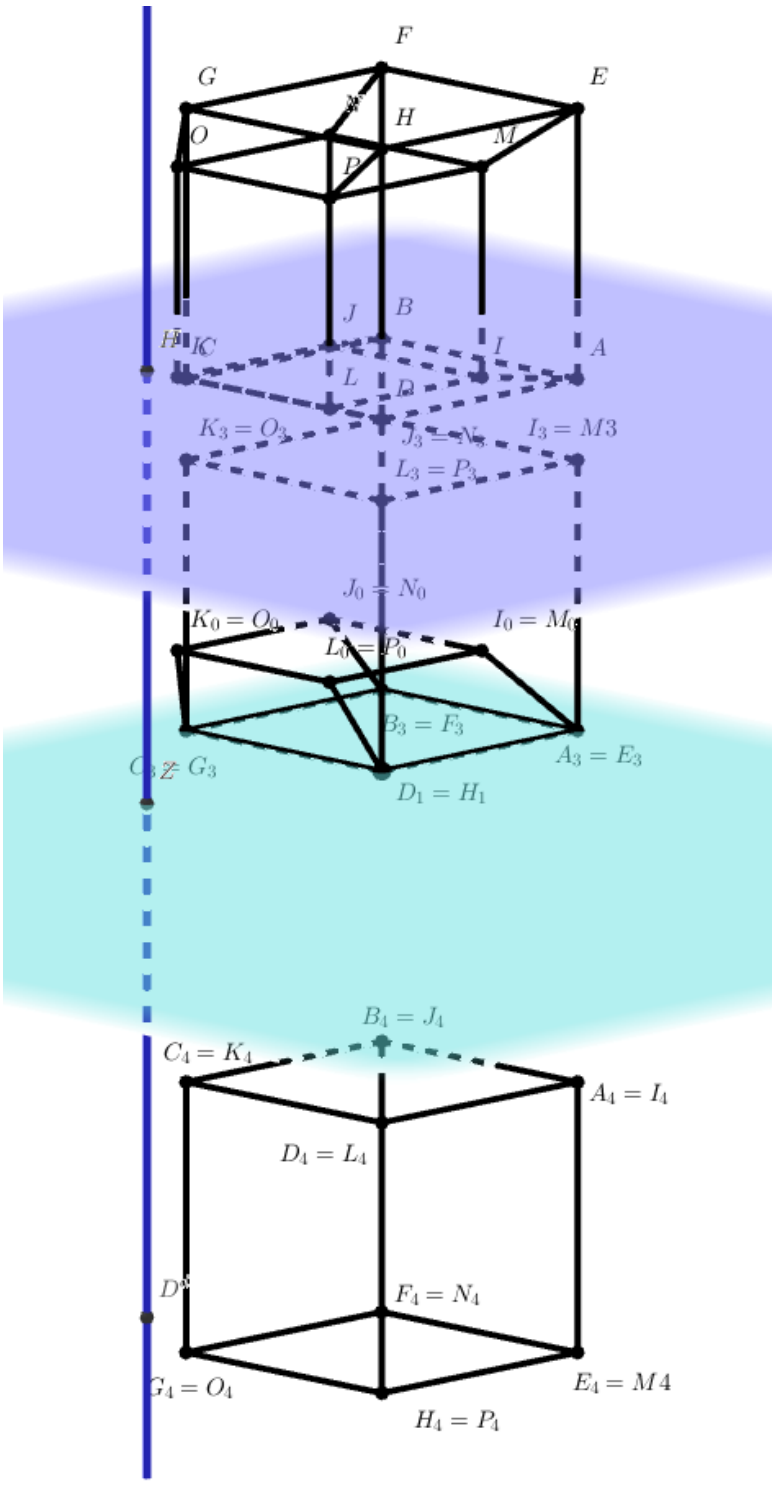

Figure 5.27: Models of a tesseract in the double orthogonal projection and 4D perspective made in Geogebra.

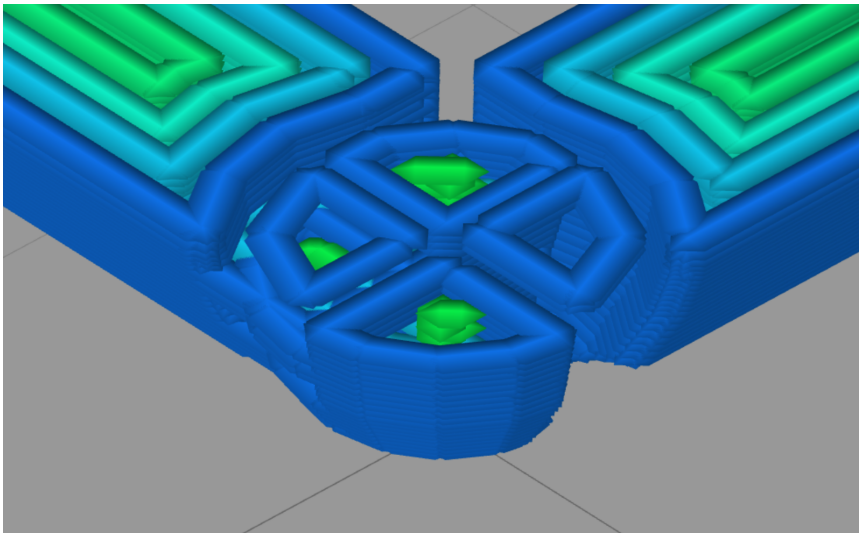

Figure 5.28: Detail of printed layers in Geogebra export.

also necessary to print support from the filament. The support is removed in the resulting 3D print, and the model is finished. Many printers do a poor job of separating the support, and the result does not look good. For this reason, this model is printed in parts and then glued together to eliminate the amount of support. Therefore the 3D print is divided into parts before each horizontal line (figure 5.29).

Conclusion

In this part, a tesseract was projected on a computer screen in double orthogonal projection and 4D perspective and then transferred from the screen to an accurate 3D model printed on a 3D printer. Some of the pitfalls of 3D printing were described, from problems with GeoGebra export to the correct positioning of objects.

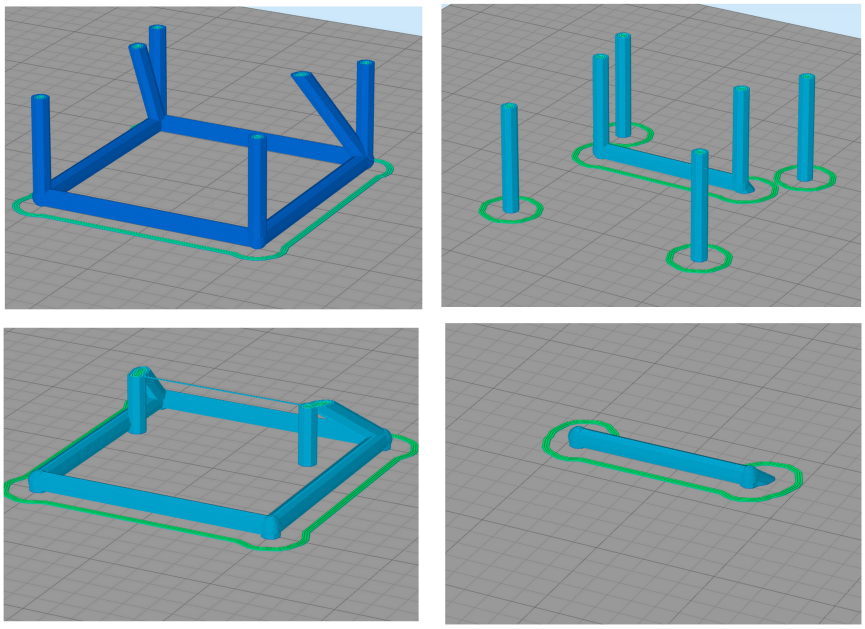

Figure 5.29: Visualisation of one printed part of the models. Each part of the model has horizonatl line only on the heatbed.

Conclusion

This thesis is divided into five chapters. The first chapter of this thesis deals with plane geometry. There are many geometric theorems which are usually proved algebraically. Therefore, we take some theorems and show geometrical proofs of them. We aimed to show that, in many cases, geometric theorems can be proved with geometric proofs. This work focuses on synthetic geometry in different dimensions, so the second chapter is focused on dimensions. In the second chapter of this thesis, we introduce n-dimensional geometry and how to visualise n-dimensional geometry, focusing mainly on four-dimensional geometry. For this, we use two typical geometrical generalisations of how to describe higher dimensions. The third part of this thesis aims to generalise Monge's projection to double orthogonal projection onto two mutually perpendicular 3-spaces. We explain the basic principles of how to draw a point, a line, a plane and a shape. This part of the thesis also briefly introduces the next section. The fourth part aims to generalise linear perspective to 4D perspective using double orthogonal projection. After a brief introduction to the historical development of perspective, the basic principles of 4D perspective are explained. The principles of visualising basic shapes are described. The final part of this thesis uses double orthogonal projection and 4D perspective in practice. This section shows several methods of using 4D visualisation. The first is to visualise and solve problems in the complex number plane. The complex number plane is visualised as a four-dimensional space. The central part is devoted to an intersection of a real circle with sets of lines. In other words, we visualise the circle with its complex parts. The second part describes shadows in 4D algebraically. We describe how shadows work algebraically in 3D space and then generalise this approach to 4D space. The last part describes how we can better understand and visualise 4D space through 3D printing. There has been a huge development in 3D printers in recent years. Therefore, 3D printers are a good and cheap way to look at 4D space from any angle and to touch it ourselves using the methods of double orthogonal projection and 4D perspective.

Appendices

A. Attachment: 3D Shadows of 4D Algebraic Hypersurfaces in a 4D Perspective

A.1 Computation times

Table A.1 (Computation times: 4D Scene: "Full HyperMoon Between Hyper-Mountains" 5.2.3)

Table A.2 (Computation times: 4D Scene: "HyperRing" 5.2.3)

Notation:
deg – degrees of polynomials
WM-GB – Wolfram Mathematica implementation of the function GroebnerBasis with the attributes:

LO: default lexicographic monomial order

MO (BEO):
MonomialOrder → EliminationOrder,
Method → "Buchberger"

MO (EE):
MonomialOrder → EliminationOrder,
Method → {"GroebnerWalk",
"EarlyElimination→True"}

MO (GWEE):
MonomialOrder → EliminationOrder,
Method → {"GroebnerWalk",
"EarlyElimination→True"}

WM-Dix – function DixonResultant in Wolfram Mathematica
Fer-Dix-EDF – Dixon resultant implementation in Fermat
T – terminated after 5 hours or more
F – failed

Table A.1: Computation times: 4D Scene: "Full HyperMoon Between HyperMountains" 5.2.3

object	deg	WM-GB LO	WM-GB MO	WM-Dix	Fer-Dix-EDF
occ. cont. $\mathcal{S}^\nu, \mathcal{P}^\nu$	3, 6	0.03s	0.01s (EO)	0.14s	—
terminators $c^\nu_\mathcal{S}, c^\nu_\mathcal{P}$	2, 6	0.26s	0.01s (EO)	0.19s	—
tang. hypcon. τ_S, τ_P	2, 6	0.1s	0.03s (GWEE)	F	—
shadow $\mathcal{S} \to \mathcal{P}$	6	25s	0.03s (GWEE)	0.33s	—
shadow $\mathcal{P} \to \mathcal{P}$	18	T	F	11s	26s
shadow $\mathcal{P} \to \mathcal{S}$	14	T	0.24s (BEO)	15966s	79s

Table A.2: Computation times: 4D Scene: "HyperRing" 5.2.3

object	deg	WM-GB LO	WM-GB MO	WM-Dix	Fer-Dix-EDF
occ. cont. $\mathcal{S}^\nu$	8	1.2s	0.02s (EO)	0.27s	—
terminator $c^\nu_\mathcal{S}$	8	516s	0.06s (EO)	0.40s	—
tang. hypcon. $\mathcal{T}$	8	2701s	0.20s (EO)	75s	3.08s
shadow $\mathcal{S} \to \mathcal{P}$	8	0.06s	0.05s (BEO)	8.6s	—

B.2 3D Implicit bakery

- Video: https://youtu.be/tKqZn7tzAQE

C.3 4D HyperQuadrics

- Video: https://youtu.be/01kYwSblPEY

D.4 4D HyperRing

- Video: https://youtu.be/6ZdwJ-P18Gw

B. Attachment: GeoGebra Tools for Drawing in Double Orthogonal Projection and 4D Perspective

Introduction

Every author who writes a text on synthetic geometry has experienced a situation where inserting some drawn pictures into the written text is necessary. In the past, figures were drawn by hand and inserted into a book. Nowadays, the figures are drawn on the computer, and the question is which software should be used to solve the problem and which software will do it with the least effort. The pictures can theoretically be drawn in Microsoft Paint (Davison [2014]), but it will be hard work without the help of tools. A better option is to use special software designed for projections. A Sketch 360, described in Řada [2021b], is a program for drawing equirectangular spherical perspectives, but unfortunately, the program is narrowly focused. For Monge's projection, it is possible to use the program *Deskriptivní geometrie* by Petr Plavjanik (Plavjanik [2017]). This program won first place in the national round of the Czech Republic Student's Professional Activities (SPA) in mathematics and mathematical informatics. It was also exhibited at INVEX '99 in the Creative Hall. Several hundred licences of the program were sold, and it was used by twenty secondary schools and six universities in the Czech Republic and at three universities in the USA, Brazil and Egypt (Plavjanik [2017]). No new program version was released after 2006 (Plavjanik [2021]).

Every user has the choice to choose a specific software (like the one mentioned above) and learn how to use it or to use a universal graphical software like Geogebra (Hohenwarter and Hohenwarter [2002]). In addition, GeoGebra offers the possibility of making drawing easier with its own custom tools. Then, any projection can be drawn in an easier way (Poincaré disc model (Manthey et al. [2016]), immersive perspective (Araújo [2020]), Monge's projection (Ferdiánová et al. [2021]). We do not yet know of any software that can display objects in the double orthogonal projection of a 4-space onto two mutually perpendicular 3-space and 4-perspective. For this reason, we have chosen GeoGebra, which allows you to draw line by line with basic tools as if you were drawing by hand, or it is possible to create your own custom tools and save the work locally.

Custom GeoGebra tools

To construct some objects in the 4D perspective is necessary to find the object in 4DDOP and then project the object into a 4-perspective using the associated 4DDOP. This is similar to viewing a Monge projection in a linear perspective. Recently, it was necessary to visualise a 3-sphere in 4-perspective (figure B.1) (step-by-step construction Řada [2021b]).

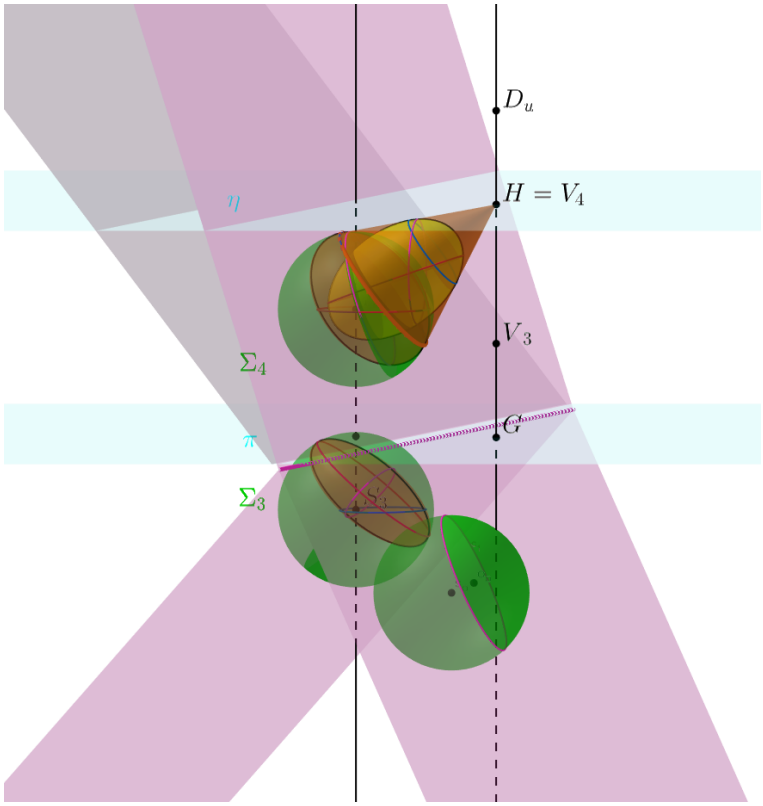

Figure B.1: 3-sphere in 4-perspective and 4DDOP

To visualise such an object, there is a need to use about 500 construction steps or make it easier/faster using a command line or custom tools. In GeoGebra, it is possible to visualise objects by clicking on tools or constructing the object via the command line. The user can click through if there are already many lines in the image (especially in 3D). For this reason, it is safer to use the command line for the right construction. The user can use simple commands. For example:

$$Line(< Point >, < Point >)$$

$$Circle(< Point >, < RadiusNumber >)$$

$$Intersect(< Object >, < Object >)$$

Alternatively, multiple commands composed from simple commands:

$$Intersect(Line(< Point >, < Point >), Circle(< Point >, < RadiusNumber >)).$$

Commands inserted through the command line make work easier, and for frequently repeated commands, you often only need to change the variables inside the command:

$$Intersect(Line(S_1, S_2), Circle(S, r))$$

$$Intersect(Line(O_1, O_2), Circle(O, r))$$

$$Intersect(Line(K_1, K_2), Circle(K, r)).$$

If there is a need to use a structure frequently or in other projects, it is better to create a GeoGebra tool. After drawing the desired construction from which the tool is to be made or downloaded as a GeoGebra applet, the user must click on Tools =>

Create New Tool. Then, select the input and output objects. The tool is successfully created and can be used or exported. Select custom tools in Manage Tools and click on Save as... to export custom tools. The tool will then be saved as a .ggt file and can be opened in any GeoGebra by dragging it with the mouse. It is recommended that a folder on the computer with tools is placed where the user can drag and drop into GeoGebra as needed. This way, the tools are always at hand.

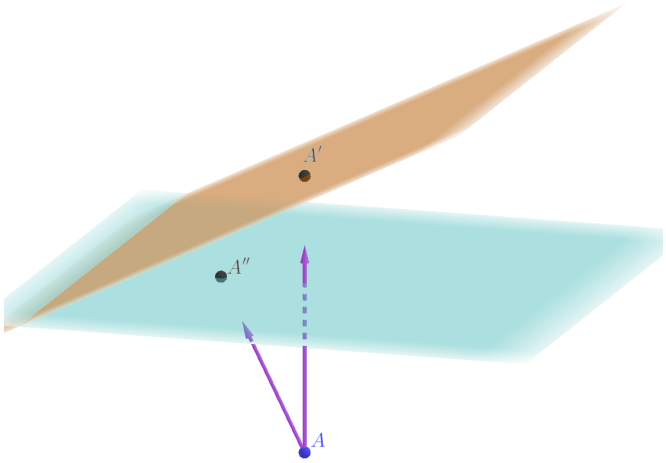

Figure B.2: Projection of a point onto a plane in a direction perpendicular to another plane

It is usually a good idea to keep your distance when creating tools. The user will not use an incorrectly named tool. It will not be used if the tool has no proper name because no one will know what it does. Consider constructing a tool that projects a point into a plane perpendicular to another plane (figure B.2). If the user does not distinguish in the label which plane is which and in which order they are arranged in the tool, the result of the construction will be completely different. Point A'' will be created instead of point A' (figure B.2). Moreover, the user will not even notice the wrong solution if the whole construction is messy because of all the lines and points.

Sometimes, the user needs a tool to construct, for example, a quadric through 9 points. Unfortunately, there is no database of custom GeoGebra tools. On the other hand, there is a database of GeoGebra applets (Hohenwarter [2021]) where it is possible to find an applet that constructs a quadric through 9 points (Blossier [2019]). There is a way to download the applet from the website (at the top right in the menu) and create your tool from the applet. In this case, the output will be a quadric, and the input will be the required 9 points.

Sometimes it is worthwhile and convenient to find the appropriate applet on the Geogebra portal and create the tool from it. Sometimes it is difficult to find the required applet, or the applet is often imperfect or incomprehensible. It is up to each user to decide whether it is faster and easier for them to use the command line, create their own tools, or create them from the GeoGebra applet. This is a question that everyone has to answer for themselves. The author of this article combined all three methods as needed.

Geogebra tools used for visualize 3-sphere in 4-perspective

The author planned to use nine custom tools to simplify the construction of the 3D sphere in 4D perspective (figure B.1). This number was reduced to five as the remaining four were entered via commands on the command line. As mentioned above, creating a custom tool for everything is unnecessary. The individual constructions used can be found in the properties of the objects in the GeoGebra applet (Řada [2021b]) after downloading. The most commonly used custom tool in this construction is the orthogonal projection of a point onto a plane in a given direction. Another tool finds the corresponding orthogonal projection of a point on the 4-sphere. This tool is specifically designed to solve this problem. The other tools are for general use. Another tool is used to display the perspective projection of an object from the corresponding projection of a point in 4DDOP and the given 4D perspective (H, G, D_u). The author uses this custom tool in every project with a 4D perspective. The last tool used is to display a quadric of 9 points. This tool uses GeoGebra's analytical capability, and the quadric is calculated analytically, after which only the calculated surface is visualised.

Conclusion

The author of this article describes the need to accompany texts on geometry with images. This part mentions the possibility of using special software, which often does not exist, or using GeoGebra. The article's author describes the possibility of drawing almost anything in GeoGebra. The simplest method is to click on all the constructions with the mouse. This method is time-consuming, and the picture sometimes becomes labyrinthine and unclear. The second method is to use the command line. The user does not have the possibility of clicking in the wrong way; the commands can be grouped, and in the case of a repetitive construction, there is the possibility of changing only the variables. The last option mentioned in the article is to create your own GeoGebra tool. The advantages of this approach are the possibility of transferring the tool between projects and the possibility of creating the tool from GeoGebra applets available online. Finally, the author describes the tools used to construct the sphere in 4D perspective.

Bibliography

E. Abbott. *Flatland, A Romance of Many Dimensions*. Princeton University Press, 2015. ISBN 9780486272634.

A. V. Akopyan. *Geometry in figures*. Createspace, 2017. ISBN 9781548710781.

A. B. Araújo. A GeoGebra tool for drawing immersive perspectives. *ARTe-FACTo2020. International Conference on Digital Creation in Arts and Communication, pp. 155-160, Edições Centro de Investigação em Artes e Comunicação*, 2020.

R. Avitzur. Functions of a complex variable, 20.2. 2022a. URL http://www.nucalc.com/ComplexFunctions.html.

R. Avitzur. Pacific tech graphing calculator for iOS, 20.2. 2022b. URL https://apps.apple.com/us/app/pacific-tech-graphing-calculator/id1135478998?ls=1.

T. F. Banchoff. *Beyond the third dimension: geometry, computer graphics, and higher dimensions*. Scientific American Library; W. H. Freeman and Company, New York, 1990. ISBN 9780716750253.

T. F. Banchoff. Complex function graphs., 20.2. 2022. URL http://www.tombanchoff.com/complex-function-graphs.html.

D. Banks. Interactive manipulation and display of two-dimensional surfaces in four-dimensional space. *Proceedings of the Symposium on Interactive 3D Graphics*, Part F1296:197–207, 1992. doi: 10.1145/147156.147205.

I. Bars, J. Terning, and F. Nekoogar. *Extra dimensions in space and time*, volume 66. Springer, 2010.

N. L. Biggs. T. P. Kirkman, mathematician. *Bulletin of the London Mathematical Society*, 13(2):97–120, 1981.

D. V. Black. Computational techniques to enable visualizing shapes of objects of extra spatial dimensions. *University of California, Irvine*, 2010.

M. Blossier. Quadric through 9 points, 1.7. 2019. URL https://www.geogebra.org/m/xqkwgcan.

S. Bogdan and A. Serbanoiu. Multidimensional descriptive geometry. 2021.

A. Bogomolny and N. Taleb. *Cut the knot: Probability riddles*. Wolfram Media, Champaign, IL, 2020. ISBN 978-1579550417.

M. T Bosch. N-dimensional rigid body dynamics. *ACM Transactions on Graphics (TOG), 39(4), 55-1.*, 2020.

S. Bozlee and S. V. Amethyst. Visualizing complex points of elliptic curves, 20.2. 2022. URL https://im.icerm.brown.edu/portfolio/visualizing-complex-points-of-elliptic-curves/.

G. Braun and J. Narboux. A synthetic proof of Pappus' theorem in Tarski's geometry. *Journal of Automated Reasoning*, 58:209–230, 2017.

L. Buse, D. Cox, and C. D'andrea. Implicitization of surfaces in $\mathbb{P}^3$ in the presence of base points. *Journal of Algebra and Its Applications*, 02(02):189–214, jun 2003. ISSN 0219-4988. doi: 10.1142/S0219498803000489.

D. Butler. Where the complex points are., 20.2. 2022. URL https://blogs.adelaide.edu.au/maths-learning/2016/08/05/where-the-complex-points-are.

B. Bydžovský. *Úvod do algebraické geometrie*. Prometheus, Praha, 1948.

M. Cavallo. Higher dimensional graphics: Conceiving worlds in four spatial dimensions and beyond. *Computer Graphics Forum*, 40(2):51–63, 2021. doi: https://doi.org/10.1111/cgf.142614. URL https://onlinelibrary.wiley.com/doi/abs/10.1111/cgf.142614.

J. Charvát, L. Boček, and J. Zhouf. *Matematika pro gymnázia–Rovnice a nerovnice*. Prometheus, 1999.

A. Chu, C. Fu, A.J. Hanson, and P. A. Heng. A GPU-based architecture for interactive 4D visualization. *IEEE transactions on visualization and computer graphics, 15(6), 1587-1594*, 2009.

P. Davison. Because of the pixels: On the history, form, and influence of MS Paint. *Journal of Visual Culture 13.3, pp. 275-297*, 2014.

R. Descartes. *Discourse on method, optics, geometry, and meteorology*. Hackett Publishing, 2001. ISBN 978-0872205673.

Descartes (translated by: J. Fiala), R. . *La géométrie*. OIKOYMENH, 2010.

A. Dürer. *Underweysung der Messung mit dem Zirckel und Richtscheyt, in Linien Ebnen unnd gantzen corporen*. H. Andreae, 1966.

H. W. Eves. An introduction to the history of mathematics. *(No Title)*, 1964.

V. Ferdiánová, J. Poruba, and M. Procházková. GeoGebra tools in creating materials for teaching Monge projection. *13th International Conference on Education and New Learning Technologies, pp. 5669-5678,*, 2021.

P. A. Florenskij. Obrácená perspektiva. *Ortodox revue*, pages 4–5, 2001.

A. R. Forsyth. Geometry of four dimensions. *The Mathematical Gazette*, (217): 46–49, 1930. doi: 10.2307/3608137.

G. Glaeser, H. Stachel, and B. Odehnal. *The Universe of Conics: From the ancient Greeks to 21st century developments*. Springer, 2016.

A Gray. Osculating circles to plane curves. *Modern differential geometry of curves and surfaces with mathematica, 2nd edn. CRC Press, Boca Raton*, pages 111–115, 1997.

A. J. Hanson and R. A. Cross. Interactive visualization methods for four dimensions. *In Proceedings Visualization'93 (pp. 196-203). IEEE.*, 1993.

A. J. Hanson and P. A. Heng. Visualizing the Fourth Dimension Using Geometry and Light. In *Proceedings of the 2nd conference on Visualization '91*, pages 321–328, San Diego, 1991. IEEE. doi: 10.1109/VISUAL.1991.175821.

J.L.S. Hatton. The Theory of the imaginary in geometry. *Cambridge university press*, 1, 1920.

L. D. Henderson. The fourth dimension and non-euclidean geometry in modern art (revised edition). *Leonardo*, 2013.

Ch. H. Hinton. What is the fourth dimension? *The University magazine, 1878-1880*, 1(1):15–34, 1880.

Ch. M. Hoffmann and J. Zhou. Some techniques for visualizing surfaces in four-dimensional space. *Computer-Aided Design*, 23(1):83–91, 1991. doi: 10.1016/0010-4485(91)90083-9.

J. Hohenwarter and M. Hohenwarter. Geogebra. 2002. URL http://www.geogebra.org.

M. Hohenwarter. GeoGebra applets, 8. 2021. URL https://www.geogebra.org/materials.

V. Honnecourt. *The medieval sketchbook of Villard de Honnecourt*. Courier Corporation, 2012.

O. A. C. Hypsicles and G Mocenigo. *Euclid's Elements*. Venice: Ratdolt, E., 1482.

J. Janson. The history of perspective, 3.5. 2023. URL http://www.essentialvermeer.com/technique/perspective/history.html.

A. Jones. *Pappus of Alexandria Book 7 of the Collection: Part 1. Introduction, Text, and Translation and Part 2. Commentary Index, And Figures*, volume 8. Springer Science & Business Media, 2013.

F. Kadeřávek. *Perspektiva: příručka pro architekty, malíře a přátele umění*. Jan Štenc, 1922.

F. Kadeřávek. *Úvod do dějin rýsování a zobrazovacích nauk*, volume 6. Nakl. Československé akademie věd, 1954.

F. Kadeřávek. *Geometrie a umění v dobách minulých*. Půdorys, 1997. ISBN 8090079156.

M. Kaku. *Hyperspace: A scientific odyssey through parallel universes, time warps, and the tenth dimension*. OUP Oxford, 1995.

D. Kapur and Y. N. Lakshman. Elimination methods: An introduction. In Bruce Randall Donald, Deepak Kapur, and Joseph L. Mundy, editors, *Symbolic and Numerical Computation for Artificial Intelligence*, pages 45–89. Academic Press, 1992.

N. Khan. *Silhouette-Based 2D-3D Pose Estimation Using Implicit Algebraic Surfaces*. Master's thesis, Saarland University, 2007. URL http://faculty.pucit.edu.pk/nazarkhan/work/pose_estimation/masterThesisNazar.pdf.

N. Khan, B. Rosenhahn, R. H. Lewis, and J. Weickert. Silhouette-based 2D-3D Pose Estimation Using Algebraic Surfaces, 2014. URL https://www.researchgate.net/publication/255455984_Silhouette-based_2D-3D_Pose_Estimation_Using_Algebraic_Surfaces.

M. Kline. *Mathematical Thought from Ancient to Modern Times*, volume 1. Oxford university press, 1990. ISBN 9780195061352.

V. A. Korotkiy. Construction of a Nine-Point Quadric Surface. *Journal for Geometry and Graphics, 22(2), 183-193*, 2018.

M. Kupčáková. Základní úlohy deskriptivní geometrie v modelech. *Prometheus*, 2002.

L. Kvasz. *Prostor mezi geometrií a malířstvím: vývj pojetí prostoru v geometrii a jeho zobrazování v malířství od renesance po 20. století*. Nakladatelství Slovart, 2020.

J. Lehrer. *A Physicist [solves] the City*. New York Times, 2010.

R. H. Lewis. Example of Dixon-EDF, 2008a. URL http://home.bway.net/lewis/dixon.

R. H. Lewis. Fermat computer algebra system, 2008b. URL http://home.bway.net/lewis/.

R. H. Lewis. Heuristics to accelerate the Dixon resultant. *Mathematics and Computers in Simulation*, 77(4):400–407, apr 2008c. doi: 10.1016/j.matcom.2007.04.007.

R. H Lewis. Resultants, Implicit Parameterizations, and Intersections of Surfaces BT – Mathematical Software – ICMS 2018. pages 310–318, Cham, 2018. Springer International Publishing.

Q. Li, S. Zhang, and X. Ye. Algebraic Algorithms for Computing Intersections between Torus and Natural Quadrics. *Computer-Aided Design and Applications*, 1(1-4):459–467, jan 2004. ISSN 1686-4360. doi: 10.1080/16864360.2004.10738288.

D. Lichtblau. DixonResultant, Wolfram Function Repository, version 1.1.0, 2023. URL https://resources.wolframcloud.com/FunctionRepository/resources/DixonResultant/.

C. E. Lindgren and S. M. Slaby. *Four dimensional descriptive geometry*. McGraw-Hill, 1968.

T. Liu. Geometric, Kinematic and Radiometric Aspects of Image-Based Measurements. In *22nd AIAA Aerodynamic Measurement Technology and Ground Testing Conference*, Reston, V., jun 2002. American Institute of Aeronautics and Astronautics. ISBN 978-1-62410-112-0. doi: 10.2514/6.2002-3239.

A. Manetti, H. Saalman, and C. Enggass. *The life of Brunelleschi*. The Pennsylvania State University Press, 1970. ISBN 978-0271000756.

H. P. Manning. Geometry of four dimensions. *The Mathematics Teacher*, 7(2): 49–58, 1914.

J. Manthey, K. Ward, E. Lioutikova, and H. Zhou. Geogebra Tools For The Poincaré Disk. *North American GeoGebra Journal 5.2*, 2016.

Mathcam. Proof of Pappus's theorem, 2013. URL https://planetmath.org/proofofpappusstheorem.

K. Matsumoto, N. Ogawa, H. Inou, S. Kaji, Y. Ishii, and M. Hirose. Polyvision: 4D Space Manipulation through Multiple Projections. *SIGGRAPH ASIA Emerging Technologies (pp. 36-37)*, 2019.

T. Miwa, Y. Sakai, and S. Hashimoto. Four-dimensional viewing direction control by principal vanishing points operation and its application to four-dimensional fly-through experience. In *Proceedings of the 25th Australian Computer-Human Interaction Conference: Augmentation, Application, Innovation, Collaboration*, pages 95–104, New York, NY, USA, nov 2013. ACM. ISBN 9781450325257. doi: 10.1145/2541016.2541029.

T. Miwa, Y. Sakai, and S. Hashimoto. Learning 4-D spatial representations through perceptual experience with hypercubes. *IEEE Transactions on Cognitive and Developmental Systems, 10(2), 250-266.*, 2017.

J. Molnár. *Rozvíjení prostorové představivosti (nejen) ve stereometrii*. Univerzita Palackého v Olomouci, 2009. ISBN 9788024422541.

G. Monge. *Géométrie descriptive*. Bachelier, 1847.

V. Moravcová. *Výuka deskriptivní geometrie v našich zemích*. PhD thesis, Univerzita Karlova, Matematicko-fyzikální fakulta, 2016.

A. M. Noll. A computer technique for displaying n-dimensional hyperobjects. *Communications of the ACM, 10(8), 469-473*, 1967.

P. Plavjanik. Deskriptivní geometrie, 3.4. 2017. URL dg.vidivici.cz.

P. Plavjanik. "Instaluj":, 8. 2021. URL https://www.instaluj.cz/deskriptivni-geometrie.

M. V. Pollio, A. Otoupalík, J. Bouzek, and M. Honzík. *Deset knih o architektuře*. Arista, 2001.

E. Pomykalová, K. Horák, and A. Kalcovský. *Matematika pro gymnázia: Planimetrie*. Jednota českých matematiků a fyziků, 1993.

J. V. Poncelet. *Traité des propriétés projectives des figures: ouvrage utile á ceux qui s'occupent des applications de la géométrie descriptive et d'opérations géométriques sur le terrain (Tome 2)*. Gauthier-Villars, 1866.

J. Řada. *Projektivní pohled na rovinnou euklidovskou geometrii*. Univerzita Karlova, Matematicko-fyzikální fakulta, 2019.

J. Řada. Geogebra book: 3-sphere in a 4-perspective, 1.7. 2021a. URL https://www.geogebra.org/m/qw297dfd.

J. Řada. 3-sphere in 4-perspective, 8. 2021b. URL https://www.geogebra.org/m/xv3evzyh.

J. Řada. Řešení kvadratické rovnice graficky, 6.2. 2022a. URL https://www.geogebra.org/m/ny9hwpdb.

J. Řada. Řešení kvadratické rovnice graficky. *Rozhledy matematicko-fyzikální*, 97 (3):14–18, 2022b.

J. Řada. Selected geometric constructions and proofs. *Proceedings of Slovak-Czech Conference on Geometry and Graphics 2023, volume 43, pp 177-184*, 2023.

J. Řada and M. Zamboj. 3D printed models of a tesseract in the double orthogonal projection and 4D perspective. *Proceedings of Slovak-Czech Conference on Geometry and Graphics 2020, volume 40, pp 153-158*, 2020.

J. Řada and M. Zamboj. 3-Sphere in a 4-Perspective. In Z. Jeli, B. Popkonstantinović, S. Mišić, R. Obradović, editor, *Proceedings moNGeometrija 2021*, pages 52–61, Belgrade, 2021. Planeta Print.

J. Řada and M. Zamboj. Four-Dimensional Visual Exploration of the Complex Number Plane. In L.-Y. Cheng, editor, *ICGG 2022 - Proceedings of the 20th International Conference on Geometry and Graphics*, pages 138–149, ICGG 2022. Lecture Notes on Data Engineering and Communications Technologies, vol 146, 2023. Springer International Publishing. ISBN 978-3-031-13588-0. doi: 10.1007/978-3-031-13588-0_12.

W. Research. GroebnerBasis, Wolfram Language function, 1991. URL https://reference.wolfram.com/language/ref/GroebnerBasis.html.

J. Richter-Gebert. *Perspectives on projective geometry: A guided tour through real and complex geometry*. Springer Science Business Media, 2011. ISBN 9783642172854.

A. Roscoe. Pappus' theorem and 7 proofs. *Mathematics REU*, 8, 2021.

R. Rucker. *The fourth dimension: Toward a geometry of higher reality*. Courier Corporation, 2014.

A. Šarounová. Geometrie a malířství. Zrození lineární perspektivy. *Pokroky matematiky, fyziky a astronomie*, 30.3:130–150, 1995.

Ch. J. Scriba and P. Schreiber. *5000 years of geometry: Mathematics in history and culture*. Birkhäuser, 2015. ISBN 9783034808989. doi: 10.1007/978-3-0348-0898-9.

T. W. Sederberg, D.C Anderson, and R.N Goldman. Implicit representation of parametric curves and surfaces. *Computer Vision, Graphics, and Image Processing*, 28(1):72–84, oct 1984. doi: 10.1016/0734-189X(84)90140-3.

M. Segerman. Visualizing Mathematics with 3D Printing. *JHU Press*, 2016.

H. Stachel. The right-angle-theorem in four dimensions. *Journal of Theoretical Graphics and Computing*, 3(1):4–13, 1990.

A. Strzebonski. Cylindrical algebraic decomposition, 2023. URL https://mathworld.wolfram.com/CylindricalAlgebraicDecomposition.html.

M. K Tomić, B. Aberšek, and I. Pesek. Geogebra as a spatial skills training tool among science, technology engineering and mathematics students. *Computer Applications in Engineering Education*, 27(6):1506–1517, 2019.

K. Volkert. On Models for Visualizing Four-Dimensional Figures. *Mathematical Intelligencer*, 2017.

S. Weinberg. *The first three minutes: a modern view of the origin of the universe.* basic books, 2022.

G. Weiss. (n,2)-axonometries and the contour of hyperspheres. *Journal for Geometry and Graphics*, 1(1):157–167, 1997. ISSN 14338157.

S. Wolfram. *The MATHEMATICA® book.* Cambridge university press, 1999. URL https://www.wolfram.com/mathematica.

S. Zachariáš and D. Velichov'a. Projection from 4d to 3d. *Journal for Geometry and Graphics, 4(1), 55-69*, 2000.

M. Zamboj. Sections and Shadows of Four-Dimensional Objects. *Nexus Network Journal, 21. pp. 475–487*, 2018a.

M. Zamboj. Double orthogonal projection of four-dimensional objects onto two perpendicular three-dimensional spaces. *Nexus Network Journal*, 20(1):267–281, 2018b.

M. Zamboj. 1-2-3-sphere in the 4-Space. *In Proceedings of Slovak-Czech Conference on Geometry and Graphics, pp. 217-222*, 2019.

M. Zamboj. Visualizing Objects of Four-Dimensional Space: From Flatland to the Hopf Fibration. In *19th Conference on Applied Mathematics, APLIMAT*, pages 1140–1164, 2020.

H. Zhang and A. Hanson. Shadow-driven 4d haptic visualization. *IEEE Transactions on Visualization and Computer Graphics, 13(6), 1688-1695*, 2007.

J. Zhou. *Visualization of Four Dimensional Space and Its Applications.* PhD thesis, Purdue University, 1991.

FD ČVUT. Lineární perspektiva, 31.5. 2022. URL https://www.fd.cvut.cz/department/k611/pedagog/K611GM_soubory/webskriptum/perspektiva/linearni_perspektiva.html.

List of publications

J. Řada and M. Zamboj. Graphical models of the projective extension of the real 3-space. Proceedings of Slovak-Czech Conference on Geometry and Graphics 2020, volume 40, 2020.

J. Řada and M. Zamboj. 3D printed models of a tesseract in the double orthogonal projection and 4D perspective. Proceedings of Slovak-Czech Conference on Geometry and Graphics 2020, volume 40, pp 153-158, 2020.

J. Řada. GeoGebra Tools for Drawing in Double Orthogonal Projection and 4D Per- spective. Proceedings of Slovak-Czech Conference on Geometry and Graphics 2021, volume 41, pp 137-142, 2021.

J. Řada. Matematická hra: Kurýr. Rozhledy matematicko-fyzikální. Volume 96 (2), pp 16-23, 2021

J. Řada and M. Zamboj. 3-sphere in a 4-perspective. Proceedings of the 8rd International Scientific Conference MoNGeometrija 2021. Novi Sad: Faculty of Technical Sciences, University of Novi Sad, 2021.

J. Řada and M. Zamboj. Four-Dimensional Visual Exploration of the Complex Number Plane. ICGG 2022 - Proceedings of the 20th International Conference on Geometry and Graphics. Springer International Publishing, pp 138-149, DOI: $10.1007/978-3-031-13588-0-122023$.

J. Řada. Selected geometric constructions and proofs. Proceedings of Slovak-Czech Conference on Geometry and Graphics 2023, volume 43, pp 177-184, 2023.

J. Řada and M. Zamboj. 3-D Shadows of 4-D Algebraic Hypersurfaces in a 4-D Perspective. arXiv preprint arXiv:2307.12986, 2023.

J. Řada and M. Zamboj. Geometric Illumination of Implicit Surfaces. arXiv preprint arXiv:2403.19679, 2024.